Alma Mater Studiorum – Università di Bologna

DOTTORATO DI RICERCA IN

Ingegneria Biomedica, Elettrica e dei Sistemi (IBES) –

Curriculum in Bioingegneria

Ciclo XXXVI

Settore Concorsuale: 09/G2

Settore Scientifico Disciplinare: ING-INF/06

A FRAMEWORK TO QUANTIFY THE 3D LEFT ATRIUM WALL MOTION MODEL ON A PATIENT SPECIFIC BASIS, IN ATRIAL FIBRILLATION PATIENTS

Presentata da: Sachal Hussain

Coordinatore Dottorato

Prof. Michele Monaci

Supervisore

Prof.ssa Cristiana Corsi

Co-Supervisore

Prof. Stefano Severi

Esame finale anno 2024

To my affectionate parents,

supportive wife and beloved son, Saleh.

Acronyms

AF	Atrial fibrillation
LA	Left atrium
LAA	Left atrial appendage
CFD	Computational fluid dynamic
CT	Computed tomography
LV	Left ventricle
PVs	Pulmonary veins
ESRs	Early-stage researchers
WP	Work packages
SR	Sinus rhythm
MV	Mitral valve
CTRL	Control
ECG	Electrocardiogram
LS	Left superior
RS	Right superior
LI	Left inferior
RI	Right inferior
EF	Ejection fraction
REF	Regional ejection fraction
SD	Standard deviation
IA	Index of LA asynchrony
LS	Longitudinal strain
RS	Radial strain
RRD	Regional radial dimension
RRS	Regional radial strain
CS	Circumferential strain
RWM	Regional wall motion
RSF	Regional shortening fraction
CFEs	Complex fractionated electrograms
3DSTE	3D speckle tracking echocardiography
2DSTE	2D speckle tracking echocardiography
IQR	Inter-quartile range
PVI	Pulmonary vein isolation
CFAEs	Complex fractionated atrial electrograms
DFs	Dominant frequencies
ROI	Region of interest

STL	Stereolithography
LSPV	Left superior pulmonary vein
LIPV	Left inferior pulmonary vein
RSPV	Right superior pulmonary vein
RIPV	Right inferior pulmonary vein

List of figures

List of tables

Table of contents

Abstract

Atrial fibrillation (AF) is the most common, clinically significant cardiac arrhythmia. This disorder is a major cause of morbidity, mortality, and health care expenditure. It is associated with a five-fold risk for stroke and is estimated to cause 15% of all strokes. AF causes structural remodeling to the left atrium (LA) chamber and reduces the contractility of the walls of the LA which ultimately impairs the physiological LA function and disrupts the normal blood flow within the LA chamber and consequently gives rise to thrombogenic events. However, it has been observed that there is a lack of emphasis placed on the analysis and quantification of the global and regional contractility of the left atrium.

Therefore, the primary goal of this study is to propose a step-by-step workflow on a patient-specific basis, which can potentially assess and quantify the global and regional impact of AF on the contractility of LA and left atrial appendage (LAA) as 90% of the clot formation happens within the LAA. The outcome of this analysis can further be used as a boundary condition to perform patient-specific realistic computational fluid dynamic (CFD) simulations to provide better understanding of the probability of thrombi formation.

To conduct this study, the analysis was performed separately for the LA and LAA. However, for both the analysis, same cohort of computed tomography (CT) dynamic imaging dataset was utilized. In the case of the LA, a standardized regionalization approach was proposed to define distinct LA regions and then in the next step, global and regional contraction parameters for the LA were defined and computed to characterize LA function. Moreover, for the LAA, a semi-automatic LAA centerline extraction technique was developed and by considering the centerline as reference, LAA global and regional parameters were assessed. In both the cases, the proposed methodologies were tested and validated on LA and LAA morphologies also including anatomic variations.

Results showed the potential of the proposed methods to assess and quantify the dysfunctional global and regional LA and LAA mechanical contraction in AF patients. By computing the contraction parameters, a

global contraction impairment, significant dilation and regional heterogeneity in contraction were noticed in AF patients as compared to the healthy subjects. Additionally, irregular and asynchronous contraction between different LA regions was also noticed in AF patients. Also for LAA, statistically significant disparities were noticed in the length [(4.0 vs 2.5) cm, $p = 0.005$], orifice [(5.4 vs 2.9) cm^2, $p = 0.005$], and tortuosity [(1.4 vs 1.2), $p = 0.005$] of AF affected LAA group when compared with healthy group. While on a regional basis, LAA regions closest and farthest to the LA chamber exhibited deviation from normal functionality in certain contraction parameters.

In conclusion, the computed patient-specific contraction indices of LA and LAA were found to have the capabilities to identify and quantify global and regional contraction dysfunctionalities in AF patients. Furthermore, in addition to the mechanistic implications of these new knowledge, these parameters can be helpful to explore the role of AF in blood stasis when integrated in CFD simulations as boundary conditions.

Keywords: atrial fibrillation, left atrial regionalization, left atrial appendage, atrial mechanical contraction, patient-specific, global and regional analysis.

1 Introduction

The main aim of this thesis is to explore and devise a framework which can potentially assess and quantify the impact of atrial fibrillation on the mechanical contractility of left atrium (LA) and left atrial appendage (LAA) on a patient-specific basis.

In this chapter, we introduce the context in which this work was developed, including the clinical scenario and the state of the art about left atrium contraction assessment also in presence of atrial fibrillation. We present atrial fibrillation and discuss the impact of atrial fibrillation on the left atrium and left atrial appendage. We also highlight the importance and relevance of the challenge we faced within the broader field by presenting the existing left atrium regionalization approaches and previously performed contraction analysis on left atrium as well as left atrial appendage. Finally, we highlight the primary contributions and the workflow of this thesis work for the intention of providing better understanding of the conducted investigation.

1.1 Atrial fibrillation

Atrial fibrillation (AF) is the most common sustained cardiac arrythmia worldwide [1], [2], [3], [4] with rapidly increasing prevalence due to the aging of the population. People suffering with AF have shown higher morbidity and mortality rates than those without this disorder due to an increased risk of stroke [5], [6], [7]. The occurrence of stroke has increased nearly five-fold in AF patients [8]. In the last two decades, it has emerged as one of the most crucial health issues and an important cause of health care expenditure in western countries. Healthcare expenses related to the management and treatment of AF just in the US, has been estimated over $28 billion yearly [9].

Even though AF is not regarded as a potentially fatal cardiac arrhythmia, it significantly influences an individual's quality of life due to its impact on the anatomy, hemodynamics, and functionality of cardiac chambers. Prominent studies on the epidemiology of AF, conducted in developed nations and published between the late 20th century and the early 21st century, have estimated that the prevalence of AF in the general population ranged from 0.5% to 1% [1][10]. Nevertheless, in recent years, there has been a prevailing belief that the prevalence of AF, as indicated by hospitalizations, emergency room visits, and the burden of outpatient visits for AF, must be considerably higher [11][12].

The most recent research has validated this perception and demonstrated that the occurrence of AF in the general adult population of Europe is more than double that reported just one decade earlier, varying from 1.9% in Italy, Iceland, and England to 2.3% in Germany and 2.9% in Sweden. (Figure 1-1).

AF is characterized by high-frequency excitation of the atria that results in both dyssynchronous atrial contraction and irregularity of ventricular excitation. Persistent or long-standing AF can result in alterations in the electrical properties of atrial tissue, promoting a pro-arrhythmic substrate. A prolonged AF can lead to the development of fibrosis, which is the formation of excess fibrous tissue in the atria. Fibrosis alters the normal architecture of the heart tissue, impairs electrical conduction, and

contributes to the maintenance of AF. It creates areas of scar tissue that disrupt the normal electrical pathways in the atria.

The irregular and rapid contraction in AF can cause blood to stagnate in the left atrium (LA) chamber, particularly in the left atrial appendage (LAA). Stagnant blood is more prone to the formation of blood clots. Clots that form in the LA, especially within the LAA, can embolize or break loose. If a clot travels from the heart to the brain, it can obstruct a blood vessel, leading to a stroke. The risk of stroke in individuals with AF is primarily associated with the formation of atrial thrombi.

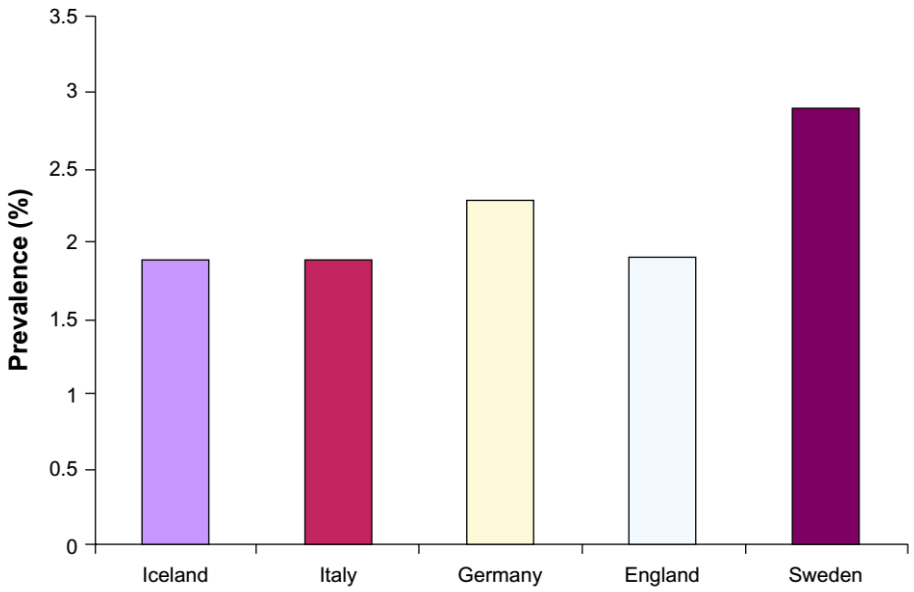

Figure 1-1: Prevalence of atrial fibrillation in European countries. [108]

For better understanding, AF has been variously classified over the years, and the American College of Cardiology/American Heart Association/European Society of Cardiology (ACC/AHA/ESC) international guidelines distinguish three forms of AF: paroxysmal, persistent, and permanent [13].

- **Paroxysmal –** Paroxysmal AF refers to AF that comes and goes on its own. The AF may last for seconds, minutes, hours, or even several days before the heart returns to its normal rhythm. People with this type of AF may have more symptoms than others. As the

heart goes in and out of AF, the pulse rate may change from slow to fast and back again in short periods of time.

- **Persistent –** Persistent AF is when the AF does not stop by itself and lasts for more than 7 days. Medications or medical therapies are needed to help the heart return to a normal rhythm. If no treatment is given, the heart will stay in AF. If the persistent AF lasts for more than 1 year, this type of AF is called long-standing persistent AF.
- **Permanent –** Permanent AF is when a normal heart rhythm cannot be restored. Medications, procedures, and controlled electrical shocks do not help return the heart to a normal rhythm.

1.2 Left atrium

Left atrium (LA) is one of the four chambers of the heart and its involvement in AF has significant clinical implications. Understanding the role of the LA in AF is crucial for both diagnosis and treatment decisions in individuals with this common arrhythmia. LA receives oxygen rich blood from the pulmonary system and pumps this blood into the left ventricle (LV) which then returns it to the systemic circulation. It has a cuboidal shape, located at the base of the heart and is the most posterior among all the chambers of the heart [14] (Figure 1-2).

The left atrial body is characterized by a venous component which receives the pulmonary veins and a vestibule which surrounds the mitral valve orifice, and it has a blind-ending pouch-like appendage. It shares the septum with the right atrium. All these components are without obvious demarcations except for the appendage which has an opening from the atrial body. The pulmonary veins enter the posterior part of the left atrial body with the orifices of left veins located more superiorly than the right veins.

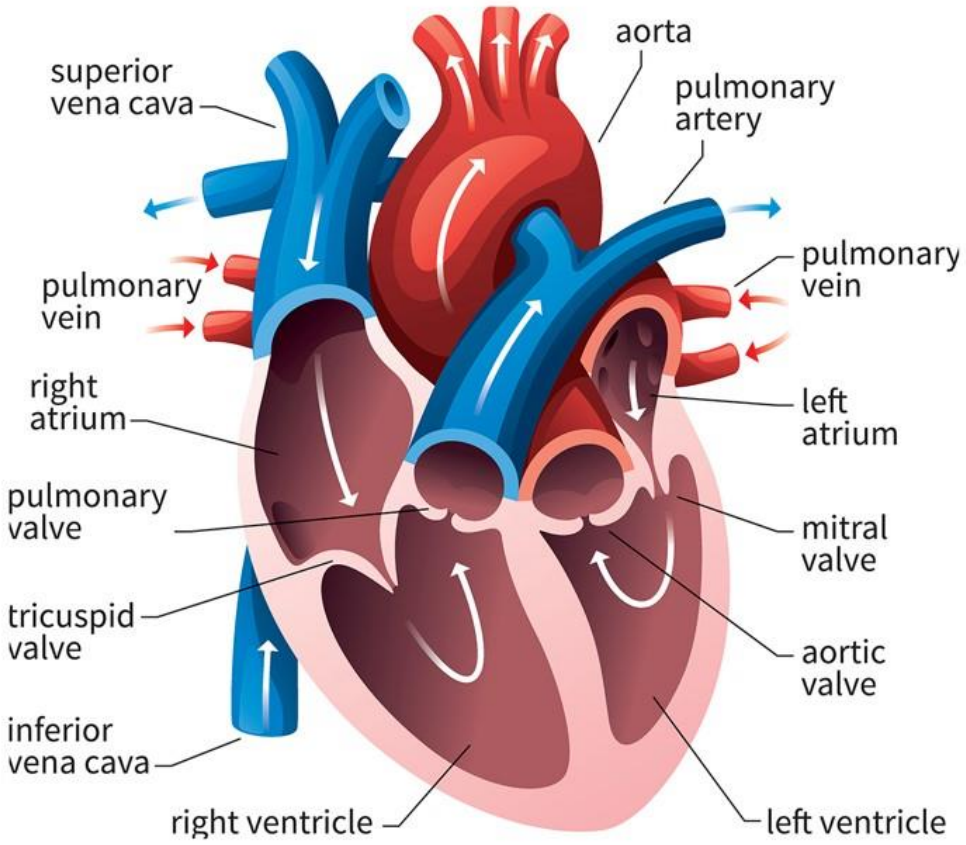

Figure 1-2: Anatomy of the heart.

1.2.1 Impact of AF on LA

Chronic AF is often associated with the enlargement and dilation of the LA [15]. The irregular and rapid electrical impulses in AF cause LA to contract inefficiently, leading to stretching and enlargement over time. Additionally, the prolonged episodes of AF may contribute to the development of fibrosis in the LA and fibrosis alters the normal tissue structure which further impairs atrial functionality.

Furthermore, the normal coordinated contraction of the atria is replaced by rapid and irregular electrical signals, resulting in chaotic and dysfunctional atrial contractions. This leads to a loss of the atrial booster pump function, which is responsible for contributing to the final filling of the ventricles. The reduced contraction of LA can result in blood stasis

and is more prone to clot formation, particularly in the LAA. This poses an increased risk of stroke as clots may travel to the brain. Therefore, it has been a topic of interest to assess and quantify the global and regional dysfunctional contraction of LA in AF patients, which has significant contribution in the thrombogenic events, happening within LA.

1.2.2 Variable left atrial morphologies

The assessment of regional contraction requires a clear understanding of LA morphology. Differently from the other cardiac chamber, the LA presents several anatomical variations due to the occurrence of variable pulmonary veins (PVs) which makes the standardization of LA regions a challenging task. PVs play a pivotal role as triggers of AF, and anatomic variants of PV have been described as having high arrhythmogenic potential [16], [17]. Multiple imaging investigations employing computed tomography and magnetic resonance imaging have documented anatomical variations in the anatomy of the PVs in a range of 18% to 45% of individuals afflicted with AF [18]. In addition, it has been observed that even populations without AF exhibit a substantial proportion of pulmonary vein variants, with estimates as high as 30% [19].

Depending on the variable pulmonary venous anatomy, LA has been classified into variable morphologies as shown in Figure 1-3 [20].

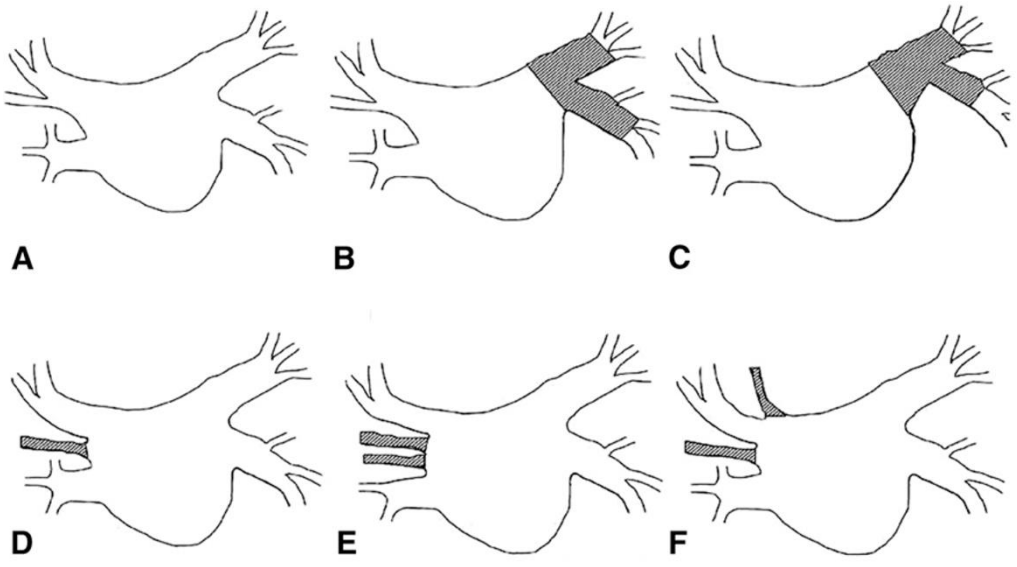

Figure 1-3: LA anatomies with variant pulmonary venous anatomy.
A, Normal. B and C, Short and long left pulmonary trunks, respectively. D and E, Variant right middle PVs. F, Top (roof) PV.

1.2.3 Left atrial regionalization

To conduct a comprehensive regional analysis of LA, the need for standardized LA regions that encompass the previously described anatomical diversity of PVs, has a paramount importance.

McAlpine, was the first person to describe the muscular walls of LA as superior, posterior, left lateral, septal (or medial), and anterior [21]. But unlike the LV, the LA does not have standardized regions which is basically because of the complex structural nature of the LA and the existence of connected structures such as PVs and LAA. However, by reviewing existing literature, it has been noticed that several studies have been conducted to define regions of LA and those LA regions have been utilized to perform several analyses which shows the significance and the need of a validated approach for LA regionalization.

Subsequently, the existing work on LA regionalization has been enlisted in Table 1-1 with the desired aim of utilizing the LA regions as well as the number of defined regions.

The most common approach to execute atrial regionalization was found to be a surface flattening methodology which is essentially the transformation of 3D LA surface into a 2D domain to define regions [28],[41],[37]. But due to the existence of PVs, LAA and MV structures, there is a possibility of distortion while defining region. Furthermore, LA anatomical variations are yet to be tested which can be a challenging task (Figure 1-4).

The most descriptive method found in the literature is demonstrated by Benito et al. in which they subdivide some LA regions for analysis purposes [31]. But the execution highly depends on the user as it requires multiple biomarkers to initiate the regionalization which may affect the reproducibility of the proposed approach. At the same time, testing has been performed on standard LA anatomies, the variable LA anatomies are yet to be tested (Figure 1-5).

Several studies have been conducted to analyze and assess the electrophysiological abnormalities [26-27], [32], [34-35], [38-39], AF

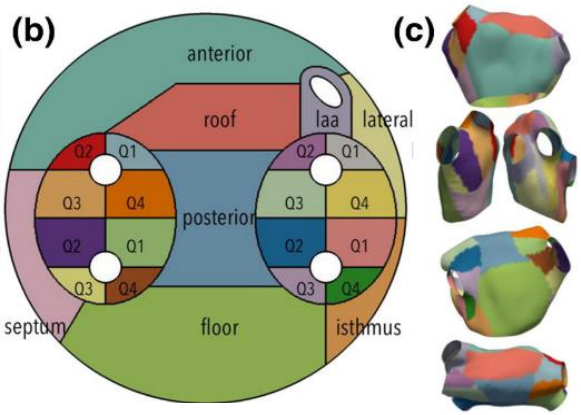

Williams et al. (2017) [28]

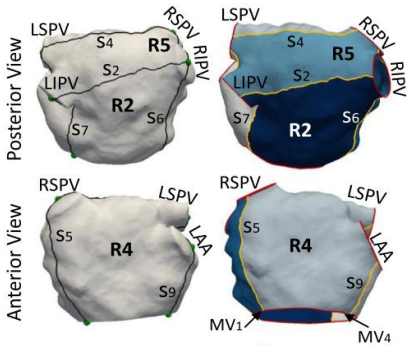

Nunez-Garcia et al. (2020) [41]

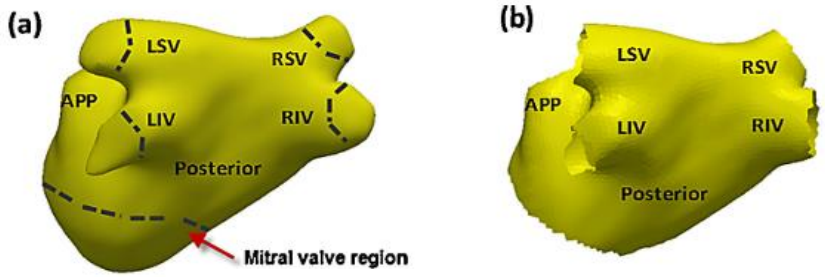

R. Karim et al. (2014) [37]

Figure 1- 4: Surface flattening LA regionalizations.

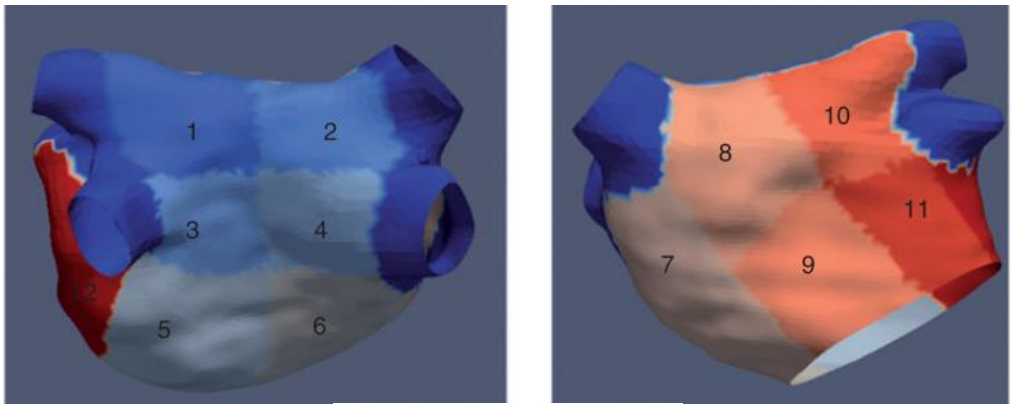

Benito et al. (2018) [31]

Figure 1-5: Visualization of Benito's LA regions.

termination sites and AF drivers on regional basis [29], [33], [36]. But without providing a clear definition of regions and even the number of regions are variable among them. This poses a challenge when attempting to compare assessments of the same nature (Figure 1-6 & 1-7)

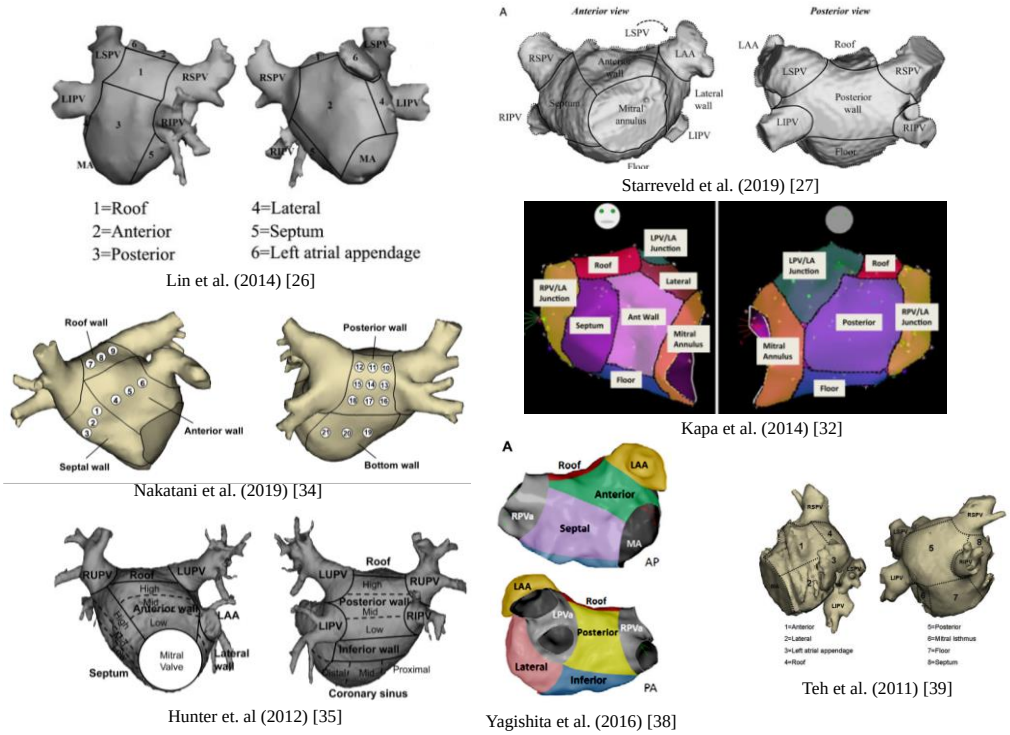

Lin et al. (2014) [26]

Starreveld et al. (2019) [27]

Nakatani et al. (2019) [34]

Kapa et al. (2014) [32]

Hunter et. al (2012) [35]

Yagishita et al. (2016) [38]

Teh et al. (2011) [39]

Figure 1-6: LA regions used to asses regional electrical disparities.

Apart from above mentioned studies, there have been few studies in which regional mechanics of LA have been evaluated [30], [40]. However, in some studies PVs and MV are also considered as LA regions which are in fact non-atrial structures. Furthermore, like most of the

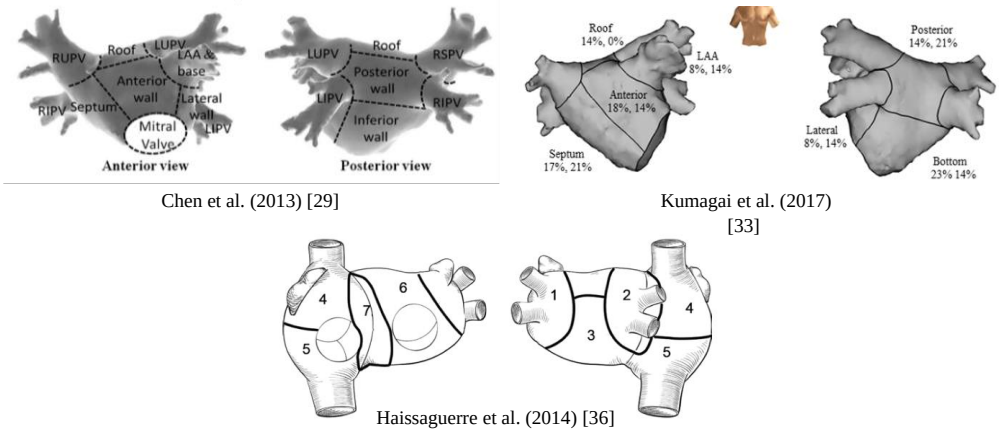

Chen et al. (2013) [29]

Kumagai et al. (2017) [33]

Haissaguerre et al. (2014) [36]

Figure 1-7: LA regions utilized to assess AF termination sites

previous studies there was a lack of explicitly defined regions and validation on variable LA anatomies (Figure 1-8).

Overall, it can be seen that there is a lack of consensus not only on the definition of regions but also on the number of regions.

In addition, there are several studies in which LA regions have been considered but without the definition of regions and without classifying the boundaries between LA regions [22][23][24][25]. Due to the lack of universally accepted standardized LA regions, the comparison between diverse LA regional investigations and quantified results has become a highly challenging task.

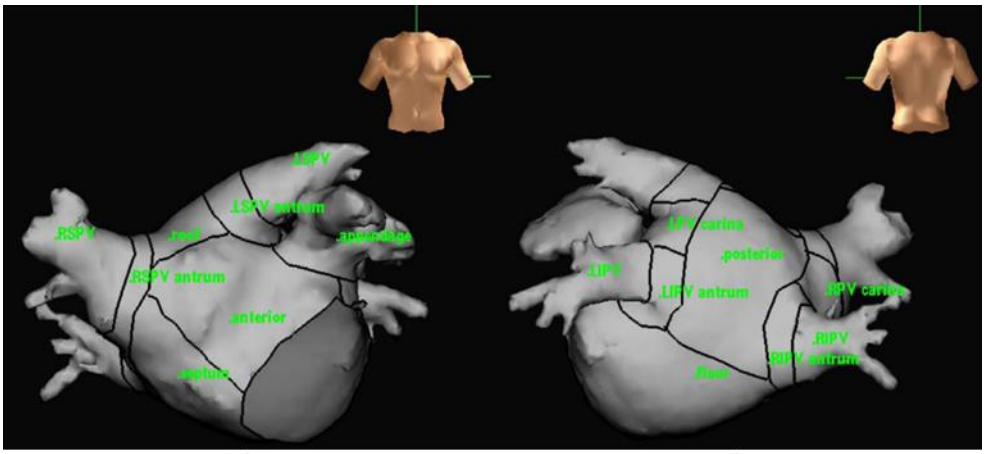

R. Kogawa,et al. (2017) [30]

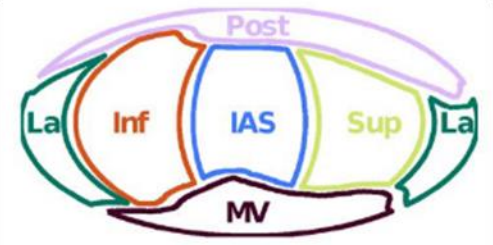

Moyer et al. (2013) [40]

Figure 1-4: LA regions used in the assessment of regional mechanics

As a result, in this thesis, we have dedicated one part of our work to develop an automatic approach for the regionalization of LA and validated this methodology by testing it on variable LA morphologies. Afterwards, the defined LA regions have been used to perform regional

contraction analysis of LA. This work has been addressed and explained further in chapter 2 of this thesis.

Table 1-1: List of existing LA regionalization implementations.

Sr. #	Author's name	Primary goal of defining LA regions	Automatic/Semi automatic/Manual	Definition of regions	# of regions	# of subjects
1.	Lin et al. [26]	To explore electrophysiological abnormalities in AF patients	Not reported	Not defined explicitly	06	100
2.	Starreveld et al. [27]	To study the hotspots of complex fractionated electrograms	Not reported	Not defined explicitly	09	N/A
3.	Tobon-Gomez et al. [28]	To standardize LA regions	Automatic	Not defined explicitly	24	10
4.	Y. Chen et al. [29]	To study spatial distribution of termination sites in AF patients	Not reported	Not defined explicitly	07	97
5.	R. Kogawa et al. [30]	To analyze regional remodeling in AF patients	Not reported	Not defined explicitly	16	36
6.	Benito et al. [31]	To study regional distribution of fibrosis in AF patients	Semi-automatic	explained	12	113
7.	S. Kapa et al. [32]	To characterize regional left atrial voltages in AF patients	Not reported	Not defined explicitly	08	20
8.	K. Kumagai et al. [33]	To study the distribution of high - dominant frequency sites in AF patients	Not reported	Not defined explicitly	09	32
9.	Y Nakatani et al. [34]	To evaluate the association between left atrial wall thickness and low voltage areas in AF patients	Not reported	Not defined explicitly	05	43
10.	Hunter et al. [35]	To characterize fractionated atrial electrograms in AF patients	Not reported	Not defined explicitly	22	20

11.	Haissaguerre et al. [36]	To study drivers in AF patients	Not reported	Not defined explicitly	07	103
12.	Karim et al. [37]	To propose surface flattening of LA	Semi-automatic	Not defined explicitly	05	14
13.	Yagishita et al. [38]	To study left atrial voltage distribution in AF patients	Not reported	Not defined explicitly	09	33
14.	Teh et al. [39]	To study regional electro-anatomical substrate in AF patients	Not reported	Not defined explicitly	08	46
15.	Moyer et al. [40]	To analyze regional mechanics of LA in AF patients	Not reported	Not defined explicitly	04	23
16.	Nunez-Garcia et al. [41]	To propose regional flattening technique for LA	Semi-automatic	explained	05	N/A

1.2.4 LA contraction analysis

The main source to investigate LA global mechanical functionality is by using several imaging modalities such as computed tomography, magnetic resonance imaging and echocardiography [42], [43]. However regional mechanical quantification has been performed by means of echocardiography, with color doppler tissue imaging and speckle tracking [44]. Despite being low cost and non-invasive in nature, they have certain limitations, mainly poor reproducibility between different users.

Furthermore, multiple investigations have been conducted to assess and quantify global and regional atrial mechanics in AF patients with the hypothesis that different regions of LA may be affected differently and may contribute to a varying extent to global LA contractile function [45], [46], [47]. Although, these studies were able to explore regional mechanics of LA in AF, a clear explanation of the methods applied for regionalization and their validation on variable LA morphologies have not been illustrated, which made the comparison between different regional assessments a challenging task.

Therefore, by considering the above-mentioned research outcomes, we formulated a new approach which can potentially quantify the global and regional contractility of LA in AF patients and can help to address the previously described aspects. This topic has been thoroughly discussed in chapter 02 of this thesis.

1.3 Left atrial appendage

A connected structure which has a significant importance in AF is the left atrial appendage (LAA), a hook shape, tubular anatomy [48] originating from LA chamber [49]. The LAA holds high variability in size, shape, and volume. It is a most primary site for thrombus formation in non-valvular AF due to the reduced contraction functionality which leads to the drastic drop of blood flow velocity and causes blood stagnation in the LAA [50].

LAA carries variable morphologies which seem crucial in assessing the risk of thromboembolism in AF. Therefore, in a research study employing cardiac imaging data, the shape configurations of the LAA in AF patients were categorized into 4 morphological types (Figure 1-9), with “chicken-wing” being the most common (48%), followed by “cactus” (30%), “windsock” (19%), and “cauliflower” (3%) [51].

- **Chicken-wing morphology:** has a dominant lobe that presents with an obvious bend in its proximal or middle part, folding back on itself at some distance from the orifice, and it may have secondary lobes.
- **Cauliflower morphology:** most often associated with an embolic event. It is described as having a short overall length, more complex internal characteristics, a variable number of lobes with the lack of a dominant lobe, and a more irregular shape of the orifice.
- **Cactus morphology:** has a dominant central lobe and secondary lobes arise from it superiorly and inferiorly.
- **Windsock morphology:** has a dominant lobe as the primary structure and there are variations in the location and number of secondary or even tertiary lobes.

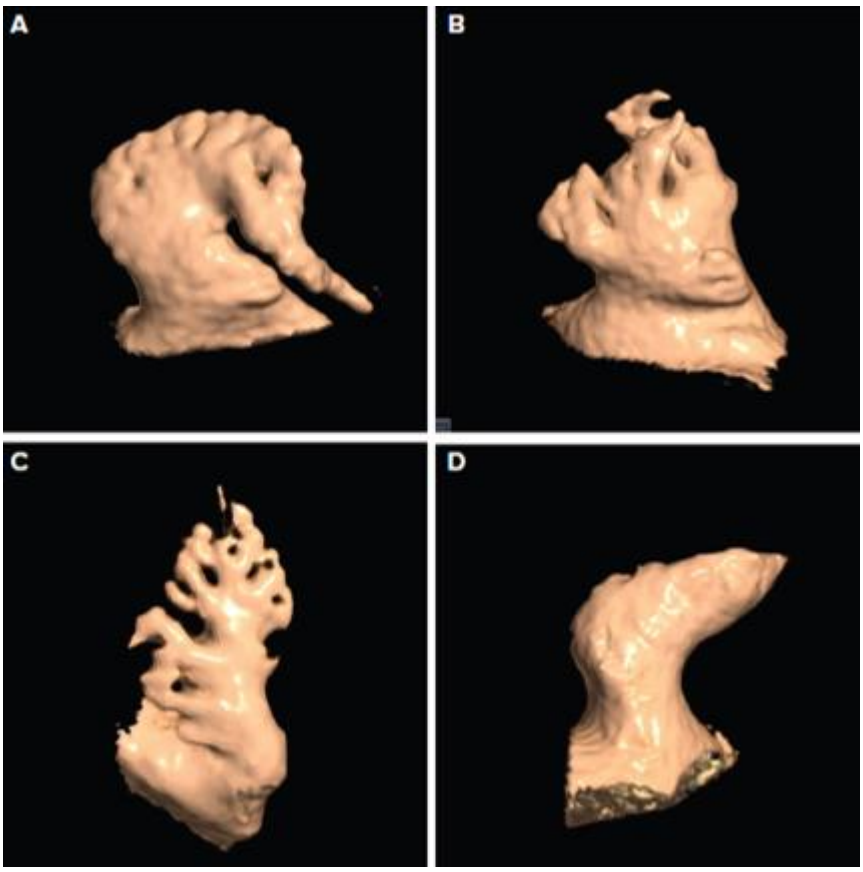

Figure 1-5: Variable standard LAA morphologies
A: Chicken-wing, B: Cauliflower, C: Cactus, D: Windsock.

Despite the high probability of thrombus formation within LAA due to the disturbed contraction, the impact of AF on the contractility of LAA in terms of global and regional analysis has not been explored deeply. Previously, some quantitative indices based on the LAA orifice such as its area, minimum/maximum diameter as well as LAA volume, width, height, and number of lobes have been used to assess thrombogenic risk.

However, to derive global and regional LAA contraction parameters, there is a need for a common reference system which can be fulfilled by computing LAA centerline. But, to define a common framework to compute LAA centerline is challenging due to the highly variable, complex, and curvy anatomy of LAA. Therefore, in a recent study[52], synthetic LAA anatomies were considered to study and investigate the alterations in contractility due to AF. Apart from this, advance imaging systems have been utilized to study global and

regional disparities as well as to perform strain analysis on LV and LA [53]. Furthermore, quite recently this technique has been implemented on LAA to study regional characteristics of LAA [54]. But these advanced imaging systems are not easily available and to perform regional analysis, there is a lack of common reference system to define regions. To address this aspect, we have introduced a framework in chapter 03 to quantify the global and regional contractility of AF on LAA.

1.4 Main contributions

This thesis work presents following primary contributions:

- a well-tested workflow to quantify global and regional contractility of LA in healthy subjects and AF patients. To perform this analysis, we reconstruct LA including LAA using CT dataset throughout the cardiac cycle and then exclude LAA as we proceed with only LA geometries to propose a new automatic standardized LA regionalization approach which is tested and validated on variable LA morphologies, regardless of the size and number of pulmonary veins. This approach has the capability to provide well defined anatomical regions of LA, without requiring manual seeds from the user which minimizes the probability of human error. Furthermore, based on the LA regions, we identify global and regional contraction parameters of LA which can potentially assess and quantify the dysfunctional contraction of LA due to AF. This proposed regionalization methodology and the contraction analysis workflow have been verified on patient-specific LA surfaces, acquired from CT imaging (Figure 1-10).

- a new workflow to perform the global and regional contraction analysis of LAA. In this process, we start with the excluded LAA geometries, generated in the previous workflow and we develop an algorithm which can semi-automatically compute the centerline of LAA, irrespective of morphological variations in LAA. With respect to the centerline, we define LAA regions and global and regional contraction parameters. Previously, LAA regional contraction analysis had been performed either on synthetic LAA

surfaces or directly on images without standardizing regions. However, our proposed framework has been tested on patient-specific LAA surfaces, reconstructed from CT dataset and acquired from healthy subjects as well as AF patients (Figure 1-10).

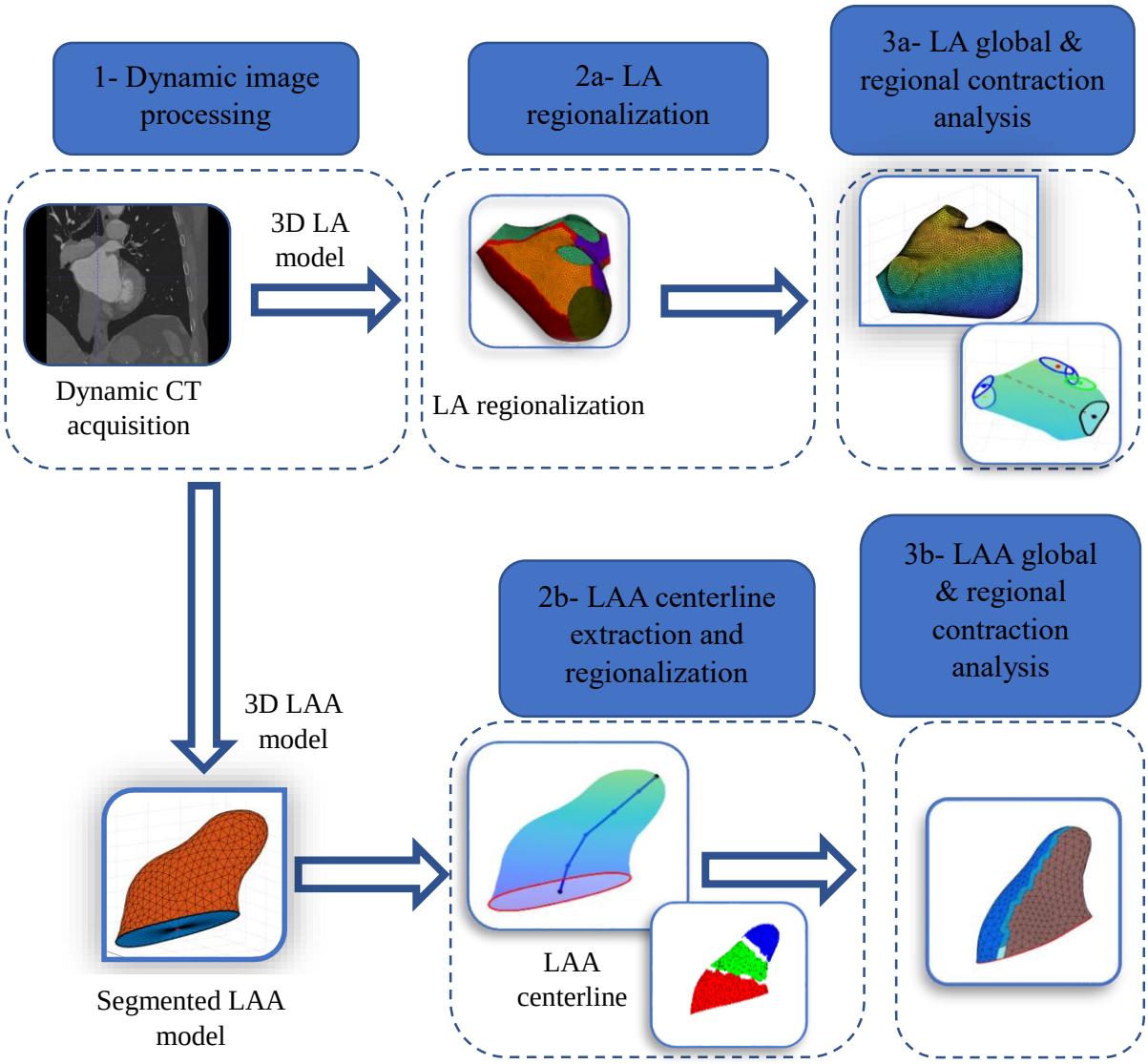

Figure 1-10: Workflow of LA and LAA contraction analysis.

1.5 Outline of the thesis

After this introductory chapter, the rest of the thesis has been organized as follows:

- **Chapter 2:** in this chapter, we propose a workflow to quantify and assess the dysfunctional global and regional contractility of LA in AF patients. We also introduce a standardized left atrial regionalization approach which is tested on healthy subjects and atrial fibrillation patients having typical variable left atrium morphologies. Additionally, we define and discuss LA contraction parameters which have the capability to identify and quantify the compromised mechanical functionality in atrial fibrillation patients.

- **Chapter 3:** this chapter presents a patient-specific step-by-step approach to assess the global and regional mechanical contraction of LAA in AF patients. In the process of implementing the proposed workflow, we also introduced a semi-automatic methodology to define, and extract left atrial appendage centerline and tested this methodology on classical structural morphologies of LAA. Lastly, we discuss the statistically significant contraction parameters which can potentially recognize and quantify the differences between healthy subjects and AF patients.

- **Chapter 4:** this chapter summarizes the most important ideas and contributions of this thesis. To conclude, we propose future research directions.

1.6 MSCA PersonalizeAF project

This PhD thesis work is a part of Marie Skłodowska-Curie Actions (MSCA) project namely ‘PersonalizeAF’. The primary goals and main intentions of this overall project have been briefly explained below.

1.6.1 Vision

PersonalizeAF aims to change the paradigm of classification and diagnosis of AF delivering a precision medicine strategy based on the personalized characterization of each atrial substrate and disease manifestation.

1.6.2 Objectives

The primary goal of PersonalizeAF is to create an innovative multinational, multi-sectorial, multidisciplinary, and excellent doctoral training network program to train 15 Early-stage researchers (ESRs) in cardiac genetics, cardiac ion channel mapping, stem cell experimentation, novel drug testing, signal and image processing, computer modelling and patient management.

The specific research objective of PersonalizeAF program is to improve the success rate of therapies applied to patients with atrial fibrillation through the individual characterization of the disease through different diagnostic techniques. For this purpose, several items will be addressed:

- improve atrial state characterization and its progression during AF remodeling addressing the individual characterization of the electrophysiological mechanisms provoking the initiation and maintenance of the cardiac arrhythmia, and the study and classification of the genetic and biological markers able to differentiate between different basic mechanisms.
- develop new diagnostic methods to identify, both invasively and non-invasively, patient-specific markers describing the individual manifestation of the cardiac disease and its progression.
- develop novel technologies to test the effect and success of current and novel therapies on the different atrial substrates and help in patient-specific treatment assignment based on the previous phenotype description.

- improve AF patient management by the creation of a decision-making platform to help clinicians to individualize the therapy based on the specific disease manifestation. This platform will combine patient characterization with the different described technologies to predict the success rate of the therapy options.

1.6.3 Overview of the Research Program

AF patient's treatment needs to be based on the synergistic interaction between novel knowledge on AF's pathophysiological mechanisms, new stratification methodologies and the most effective and efficient treatment technology for each individual patient. To enable this interaction, PersonalizeAF has been structured in three scientific interdependent work packages WPs (1-3) corresponding to the three main research objectives: Substrate characterization, Therapies and Stratification. WP1 will be focused on the development of new technologies, and improving the existing ones, to describe the atrial substrate which is promoting the onset and maintenance of AF. WP1 will carefully consider the tools able to characterize AF progression, in terms of anatomic, electrophysiological, and functional changes present during the disease progression, creating a profile of the AF individual manifestation. This will be carried out through novel technologies, such as impedance mapping catheters, image algorithms for fibrotic infiltration detection, non-invasive tools for electric activity characterization and atrial mechanics assessment. All this patient-specific information will be summarized in terms of biomarkers associated with the different disease profiles.

Our project entitled 'A framework to quantify the 3D left atrium wall motion model on a patient specific basis, in atrial fibrillation patients' comes under WP1. The main aim of this project is to develop and design a novel approach which can automatically compute and quantify the patient-specific LA and LAA deformation throughout the cardiac cycle in AF patients.

2 Patient-specific left atrium contraction quantification associated with atrial fibrillation: a region-based approach

This chapter introduces the workflow that can potentially assess the impact of atrial fibrillation on the contractility of the left atrium. To perform this assessment, a left atrium regionalization approach has also been implemented using patient-specific left atrium models acquired from CT images. Furthermore, global and regional contraction parameters have been defined and computed to quantify the dysfunctional contractility of the left atrium in atrial fibrillation patients. Finally, statistical analysis has been performed to evaluate the significant differences between healthy subjects and atrial fibrillation patients and to further discuss the acquired results.

2.1 Abstract

Background and objectives: Atrial fibrillation (AF) is a widespread cardiac arrhythmia that significantly impacts heart function. AF disrupts atrial mechanical contraction, leading to irregular, uncoordinated, and slow blood flow inside the atria which favors the formation of clots, primarily within the left atrium (LA). A standardized region-based analysis of the LA is missing, and even any consensus about how to define the regions of the LA has yet to be made. In this study we propose an automatic approach for regionalizing the LA into segments and provide a comprehensive 3D region-based LA contraction assessment. LA global and regional contraction were quantified in control subjects and in AF patients to describe mechanical abnormalities associated with AF.

Methods: The proposed automatic approach for LA regionalization has been tested in thirteen control subjects and seventeen AF patients. After dividing LA into standard regions, we evaluated the global and regional mechanical function by measuring LA contraction parameters, such as regional volume, global and regional strains, regional wall motion and regional shortening fraction.

Results: LA regionalization was successful in all study subjects. In the AF group compared with control subjects, results showed: a global impairment of LA contraction which appeared more pronounced along radial and circumferential direction; a regional impairment of radial strain which was more pronounced in septal, inferior, and lateral regions suggesting a greater reduction in mechanical efficiency in these regions in comparison to the posterior and anterior ones.

Conclusion: An automatic approach for LA regionalization has been proposed. The regionalization method has been proved to be robust with several LA anatomical variations and able to characterize contraction changes associated with AF.

Keywords:

Atrial fibrillation, left atrium, atrial regionalization, atrial mechanical function, regional analysis.

This chapter has been adapted from: S. Hussain, M. Falanga, A. Chiaravalloti, C. Tomasi, C. Corsi, “Patient-specific left atrium contraction quantification associated with atrial fibrillation: a region-based approach.” Computer Methods and Programs in Biomedicine 249 (2024) 108138.

2.2 Introduction

Left atrium (LA), throughout a complex structure, plays a crucial mechanical role in modulating left ventricle (LV) filling by diverse actions, acting as a reservoir during systolic phase, as a conduit during early diastolic phase, and as a booster pump during late diastolic phase [55]. It is well known that abnormalities in LA mechanical function favours clot formation due to inadequate contraction, disturbed blood flow and incomplete blood washout in the left atrial appendage (LAA) [48]. Among various important cardiac disorders, atrial fibrillation (AF) is considered the epidemic of our century [56]. Prominent studies on the epidemiology of AF, conducted in developed nations and published between the late 20th century and the early 21st century, have estimated that the prevalence of AF in the general population ranged from 0.5% to 1% [1], [10]. Nevertheless, in recent years, there has been a prevailing belief that the prevalence of AF, as indicated by hospitalizations, emergency room visits, and the burden of outpatient visits for AF, must be considerably higher [11], [12]. AF basically disrupts LA and LAA mechanics, leading to LA dilation, electrical and tissue modifications and long-term structural abnormalities often lasting well over sinus rhythm (SR) restoration. Atrial dilation per se, which appears at an early stage during AF, has been demonstrated to be associated with an increased cardiovascular morbidity and mortality [57], [58].

Significant impairment of the LA strains has been described in several disorders [59], [60], and in AF patients several reports have shown a decreased left atrial ejection fraction [61]. However, a standardized region-based analysis able to (1) maintain consistency with accepted anatomic data, (2) utilize accepted approaches to LA segmentation and nomenclature and (3) allow precise localization by using anatomic landmarks, is still missing, and even any consensus about how to define the regions of the LA has yet to be made. The first consequence of this lack is the inability to compare results from different studies applying different approaches for region-based LA segmentation. The current method used for region definition is the surface flattening method [41], seems to have some limitations; as reported by the authors some LA intrinsic structures such as the pulmonary veins (PVs), mitral valve (MV) and LAA may cause a distorting effect on the flattening process of the LA surface [37]. Moreover, other fairly common anatomical variations, for

instance in the number and size of PVs [62], can make the implementation of this method more challenging.

Indeed, a shared and standardized method for regional assessment of LA may support studying the impact of AF on several functional issues such as: the detection of more subtle AF related damages in different regions; the regional contributions to the global LA contractile impairment; the correlation between propagation and amplitude of EGM abnormalities and regional contraction; the assessment of regional impacts of medical and catheter-based therapies on mechanics, both in SR and during AF. Finally, by means of a quantitative approach it would be possible to continuously monitor regional function and remodelling, following catheter ablation [40]. For research purposes, the quantification of AF contraction on a patient-specific basis could provide realistic boundary conditions for computational fluid-dynamics simulations which represent a promising tool for the study of blood flow and for investigating and quantifying stroke risk associated with AF.

In this study, we propose an automatic approach for regionalizing the LA into segments and provide a comprehensive 3D region-based LA contraction assessment, which is nowadays available only through echo imaging in 2D. To this aim, we analysed LA global and regional contraction in control subjects and in AF patients and described mechanical abnormalities associated with AF.

2.3 Materials and methods

2.3.1 Selection of patients and CT imaging

Data used in this study were acquired within the FATA project, approved by the Ethics IRST, IRCCS AVR Committee (CEIIAV n. 1456 prot.6076/2015 I.5/220). All subjects gave written informed consent in accordance with the Declaration of Helsinki.

To conduct this study, twelve patients with paroxysmal atrial fibrillation (10 males, mean age: 58.7 ± 10.5 yrs and 2 females, mean age: 74 ± 3.0 yrs) and five patients with persistent atrial fibrillation (3 males, mean age: 60.6 ± 4.0 yrs and 2 females, mean age: 73.5 ± 1.5 yrs) were retrospectively enrolled with a control (CTRL) group of thirteen healthy

subjects (10 males, mean age: 60 ± 10.2 yrs and 3 females, mean age: 61.5 ± 0.5 yrs) having average size of heart structures and no previous history of AF.

CT dynamic acquisitions of the heart after injection of contrast medium were obtained applying retrospective electrocardiogram (ECG) gating during normal SR using a 64-slice multi-detector CT scanner (Philips Brilliance 64 CT scanner) in each patient.

Volumetric CT images were reconstructed for a total of 10 phases from ventricular end diastole (from 0%RR to 90%RR, where RR indicates the interval between two consecutive electrocardiographic R wave peaks). Each reconstructed CT volume was 512x512x200 pixels. The voxel resolution was not isotropic: in-plane resolution was 0.39 mm, and through-plane resolution was 1 mm, resulting in a voxel size of 0.39x0.39x1 mm^3.

2.3.2 Data analysis

The workflow for the analysis of CT data is shown in Figure 2-1 and requires several steps detailed in the following subsections.

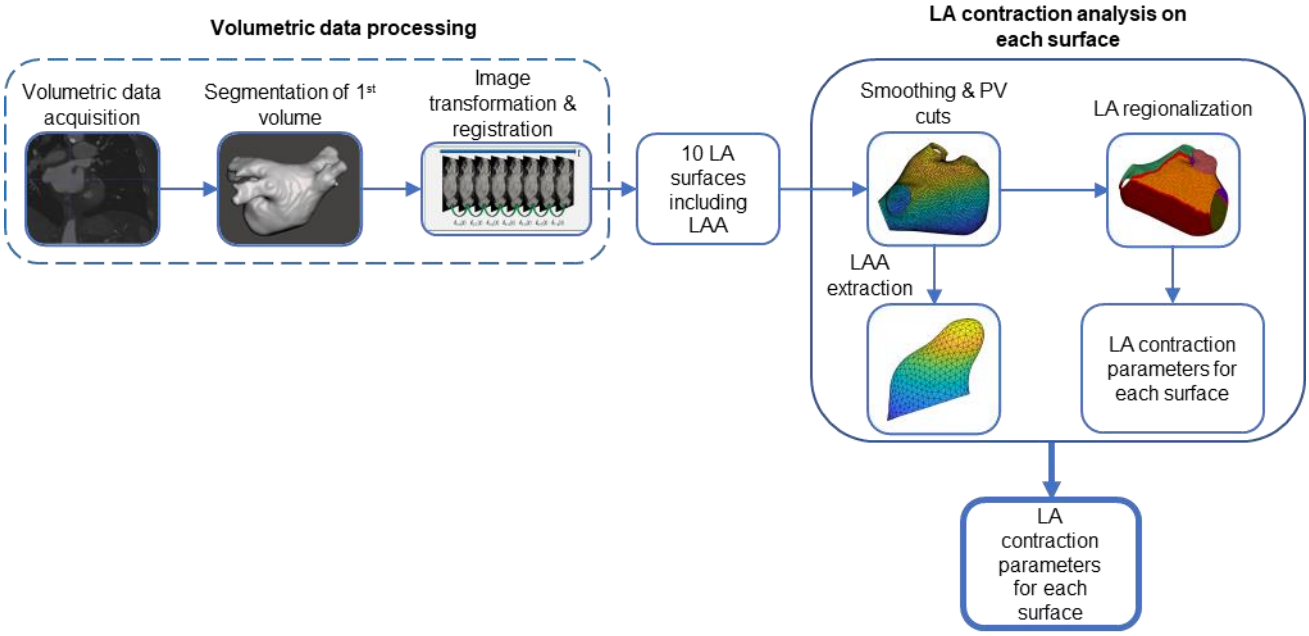

Figure 2-1: Schematic diagram of the implementation of LA regionalization and evaluation of contraction parameters on a complete cardiac cycle.

2.3.2.1 Image segmentation and post-processing

For LA segmentation in our cohort, the active contour algorithm proposed by Luminita Vese and Tony Chan [63] was implemented in MATLAB (MATLAB R2023a, The Mathworks Inc.). The active contour model we applied is based on Mumford-Shah segmentation techniques and level set models: an energy-based functional taking into account mean gray level intensity inside and outside the evolving contour and a regularization term is minimized partitioning the image in the two most different regions in term of average gray level. After the selection of a volume of interest within the CT scan and the manual positioning of a seed point inside the LA, the algorithm was applied to the first CT volume. To run this algorithm, we weighted differently the two terms compositing the functional to be minimized; and in some cases, depending on the quality of the imaging data, it was necessary to optimize these values on a patient-specific basis. The LA surface resulting from segmentation included proximal regions of the PVs, MV and part of the basal region of the left ventricle and the LAA.

After finalizing the segmentation process, the deformation of the LA surface throughout the cardiac cycle was computed by applying a 3D image registration step to the CT volumes. Indeed, registration of CT volumes required two steps: a preliminary rigid transformation followed by a non-rigid transformation based on B-spline [103] using the mean square difference as similarity measure. Following the registration procedure, the displacements between frames were then applied to the vertices of the LA surface allowing the reconstruction of the LA surfaces for the remaining phases [104].

Before regionalization, a Laplacian smoothing was applied to the LA surfaces and cutting planes were defined on the surface extracted from the first volume, to detect the four PVs ostia, the MV and the LAA (taking into account the curvature of the surface and including the ridge within the LA chamber). For this purpose, open-source Autodesk Meshmixer software [64] was utilized. The cut planes were then propagated to all the surfaces throughout the cardiac cycle.

2.3.2.2 LA regionalization

To initiate the process of regionalization, the annulus of MV, LAA, and PVs ostia were automatically recognized based on their respective location and area. Then the barycenter of each ostium was computed by using the coordinates of the points on the ostia (Figure 2-2(a)). Subsequently, the weighted barycenter of the four PVs was calculated by taking into consideration the area of the ostium of each PV and their corresponding barycenter. In case of more than four PVs, the extra PV(s) was identified by considering it's the smaller size of its ostium and neglected.

In the next step, the long axis of LA was defined by connecting the weighted barycenter of the PVs and MV barycenter with a straight line (Figure 2-2(b)). In our approach, the long axis was considered as a reference to compute contraction parameters and for the projection of boundary lines onto the LA body.

Following the detection of the LA long axis, a line was drawn to connect the left superior (LS) pulmonary vein and the right superior (RS) pulmonary vein barycenter: this line intersects the two ostia and consequently one point on LS and on the RSPV ostium were detected; these two points were rotated 90° towards the MV (P1 and P2 in Figure 2-2(c)). Finally, by connecting P1 and P2 onto the surface of LA, the roof line was generated, which constitutes a borderline between anterior and posterior regions (roof line, Figure 2-2(c)). Similarly, the left inferior (LI) pulmonary vein barycenter was linked with the LS pulmonary vein barycenter; and the right inferior (RI) pulmonary vein barycenter was linked with the RS barycenter. These lines were projected onto the LA surface in the direction of midpoint of long axis and used as boundaries between lateral and posterior regions and between septal and posterior regions, respectively.

In the next step, the MV anulus was divided into four segments: the MV barycenter was linked with P2; this segment was projected on the LA surface to detect point P3 on the MV annulus (Figure 2-2(d)); P3 was then rotated three times at 90° in the clockwise direction to get three more points, namely P4, P5 and P6 (Figure 2-2(e)). Then, P4 was joined with P1 and P3 with P2 (Figure 2-2(f)); then P5 and P6 were joined with the barycenter of LI and RI respectively (Figure 2-2(f)). By connecting P5

and P6 with the barycenter of LI and RI respectively, another point was generated on each PV, namely P7 and P8 (Figure 2-2(g)). The boundary between inferior and posterior zones was defined by linking P7 and P8 at the ostium of LI and RI, respectively. The complete suffice regionalization of LA yielded five regions: anterior, posterior, lateral, septal, and inferior (Figure 2-2(h)).

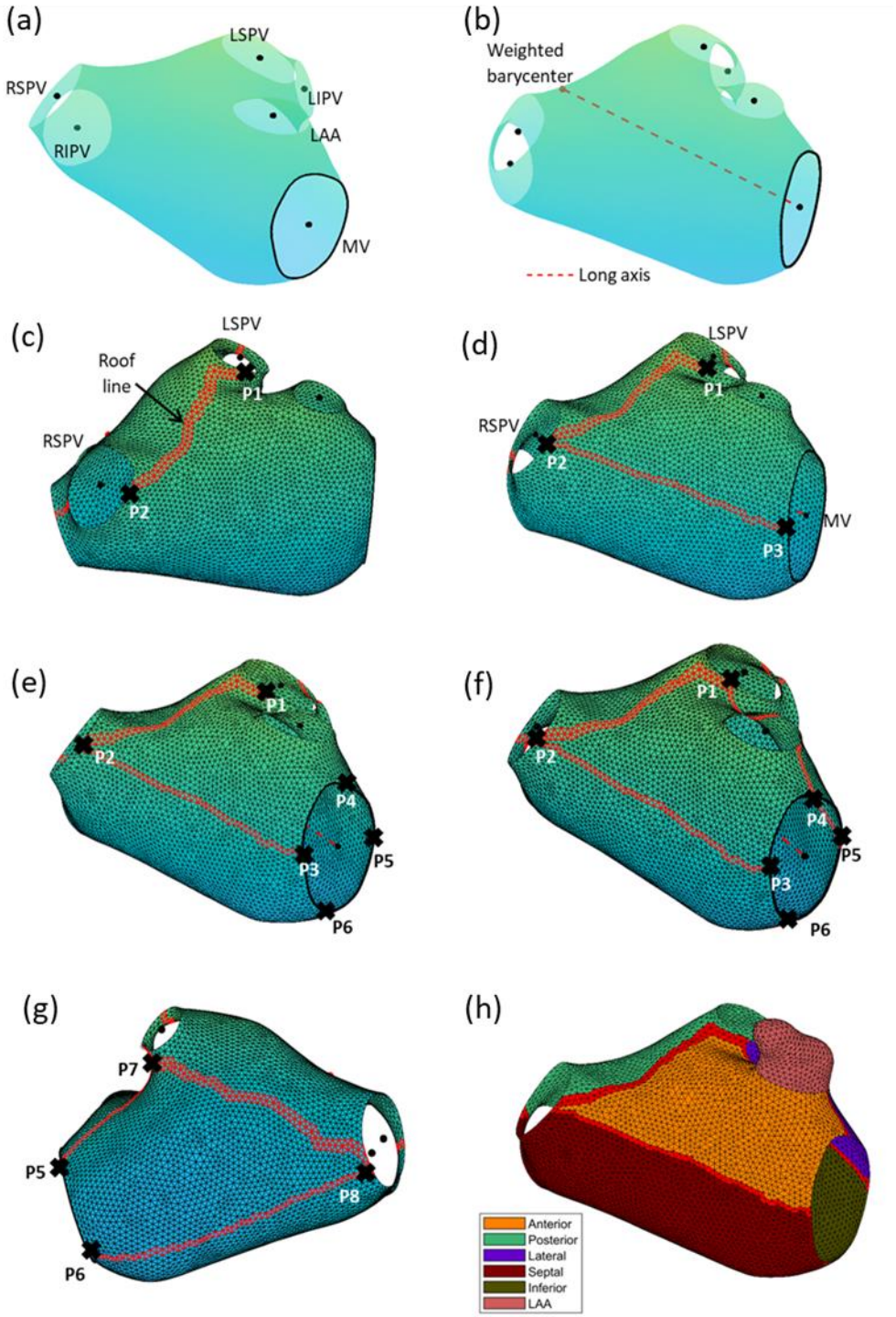

Figure 2-2: Graphical description of the LA regionalization approach.
(a) LA surface showing the 4 PVs and the MV and the respective barycenters; (b) long axis detection obtained connecting the barycenter of the MV and the weighted barycenter of the PVs; (c) detection of the roof boundary line between the superior PVs; (d) detection of the starting point on the mitral annulus by linking the MV barycenter and the point on the RSPV ostium previously computed; (e) the four points on MV annulus obtained by 90° rotation of the starting point; (f) connection of all the four points with the nearby PVs; (g) boundaries of the posterior and inferior regions generated by connecting the points on the MV and the inferior PVs; (h) final LA segmentation in regions.

Once the surface regionalization was obtained, to detect volumetric regions the posterior region and the long axis were selected (Figure 2-3(a)). By using the barycenter of each PV, the best fitting plane was computed. This best fitting plane intersected the long axis at one point, named as intersecting point (Figure 2-3(b)). To close posterior region, all the boundary points of posterior region were projected towards the intersecting point (Figure 2-3(c)); this closing was repeated for each surface in the cardiac cycle to compute posterior regional volumetric curve. For all the other regions, all the boundary points were projected onto the long axis (Figure 2-3(d)). This complete implementation is graphically described in Figure 2-3.

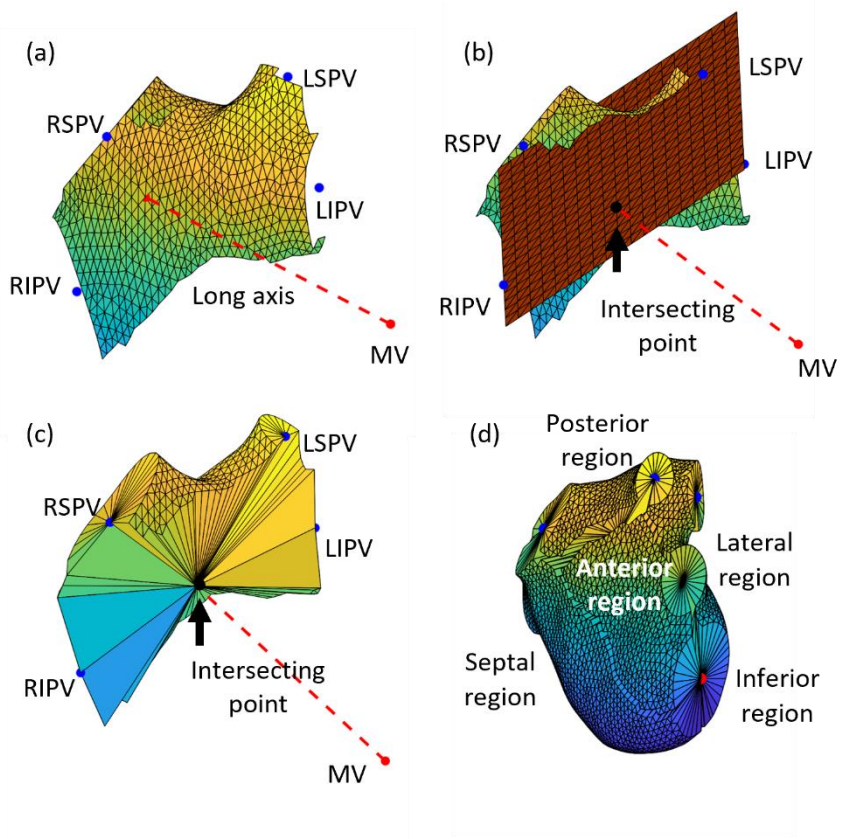

Figure 2-3: Graphical description of the LA volumetric regions.
(a) the posterior surface and long axis of LA; (b) best fitting cutting plane used to detect the intersecting point with LA long axis; (c) closed posterior region obtained by connecting all the posterior boundary points with the intersecting point; (d) final five closed regions of LA.

This entire regionalization analysis was repeated for each of the 10 surfaces throughout the cardiac cycle resulting in posterior, lateral, inferior, anterior, and septal dynamic volumetric regions (Figure 2-1).

2.3.3 Testing and statistics

2.3.3.1 LA regionalization in presence of anatomical variations

To prove that the proposed LA regionalization approach has the capability to work on different anatomical variations of LA, it was tested on existing well-established variations of LA [20], [65]. The most common anatomy was with four PVs, the regionalization of which is presented in Figure 2-2(h). Then there were anatomies with ipsilateral superior and inferior PVs very close to each other to form either short or long trunks. For these special cases, the trunk part was manually excluded and then regionalization approach was applied. Thirty CT volumes presenting a wide range of anatomical variations (short trunk, long trunk, middle PV, double mid PVs, and top-middle PV) were tested. Since in our dataset middle PVs, double middle PVs and top-middle PV were not represented, we virtually generated those cases.

The performance of our regionalization results was evaluated qualitatively by an expert electrophysiologist assigning a grade to each regionalization result (good - fair - poor - unacceptable) based on his experience. Only one surface, corresponding to the first CT volume for each enrolled subject was evaluated, for a total of 30 evaluations.

2.3.3.2 LA contraction parameters computation

Parameters to assess LA function were computed, including LA volume-time curve and LA ejection fraction (EF).

To study regional changes, region-based contraction parameters were defined. Regional volume throughout the cardiac cycle and regional EF (REF) for each region were computed. From regional volumetric curves, REF was computed by considering end-diastolic and end-systolic atrial phases from LA volumetric curve. For each region, the standard deviation (SD) of the time intervals at which regional volumes reached the peak

value was computed and was used as an index of LA asynchrony (IA) in each patient [66].

Furthermore, to conduct strain analysis, longitudinal strain (LS) was computed by tracing the variation in the length of long axis with reference to the end-diastolic ventricular frame throughout the cardiac cycle, using this formula:

$$LS(x)=\frac{LA_{len}(x)-LA_{len\_ED}}{LA_{len\_ED}}\cdot 100$$

where $LA_{len}(x)$ is the length of long axis at current frame x and LA_{len_ED} is the length of long axis at end-diastolic ventricular frame.

To analyze radial strain (RS), regional radial dimension (RRD) was evaluated for each region, as the average of the Euclidean distance of each vertex of that specific region from the long axis and then regional radial strain (RRS) was calculated as:

$$RRS(x) = \frac{RRD(x) - RRD_{ED}}{RRD_{ED}} \cdot 100$$

where RRD(x) is the current regional radial dimension of any region and RRD_{ED} is the regional radial dimension at ventricular end-diastole of that same region. Ultimately, RS is the average of all RRS values at each frame.

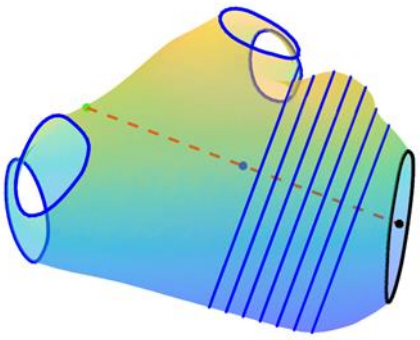

Figure 2-4: Six equally distributed circumferential curves on LA surface starting from midpoint of long axis to MV barycenter.

To calculate circumferential strain (CS), six circumferential curves (Figure 2-4) were considered between the midpoint of long axis and the MV barycenter. These curves were equidistantly distributed and for each curve [67], the percentage strain was computed using the formula:

$$CS(x) = \frac{L(x) - L_{ED}}{L_{ED}} \cdot 100$$

where L(x) is the length of the curve at frame x and L_{ED} is the length of the curve at end-diastolic ventricular frame. The circumferential strain of LA was calculated as the average strain of those six curves.

Once global strains were computed, contraction of each region was assessed in terms of regional wall motion (RWM), calculated as the difference between current RRD and RRD at ventricular end diastole for each region:

$$RWM(x) = RRD(x) - RRD_{ED}$$

According to this definition, regional wall motion equals zero at ventricular end diastole. The index of LA asynchrony (IA_{RWM}) for each region was computed also for the regional wall motion curves as the standard deviation (SD) of the time intervals at which RWM curves reached the peak value.

To calculate regional shortening fraction (RSF) for each surface region, the corresponding regional peak wall motion was divided by the corresponding peak radial dimension. RSF values were then averaged for each subject.

2.3.3.3 Global and regional assessment in controls and AF patients

The procedure developed for LA regionalization and for the computation of the proposed indices was tested in 17 patients with AF and 13 control subjects. All surfaces are available in the Zenodo repository (Left atrial geometries).

Global and regional average LA volume-time curves were compared between AF and CTRL groups, as well as EF and REF. Average IA in the two groups was computed and compared between them.

The same comparison was performed between longitudinal, radial, and circumferential strains computed for the LA chamber and for RRS in each region in the two groups in terms of peak strains. Peak RWM and RSF were also compared.

2.3.3.4 Statistical analysis

Data are expressed as mean ± standard deviation. T-test was applied to verify the statistically significant difference between the two groups with $p<0.05$.

2.4 Results

2.4.1 Anatomical variations

In Figure 2-5, we show the LA regionalization obtained, by applying the proposed approach, in five samples of anatomies characterized by anatomical variations in PVs (long trunk, short trunk, double middle PVs, middle PV, top-middle PV).

The expert electrophysiologist qualitatively graded the regional segmentation as good in 20 cases, fair in 7 and poor in 3 cases, based on his clinical experience.

One example of a poor regional segmentation is shown in Figure 2-6.

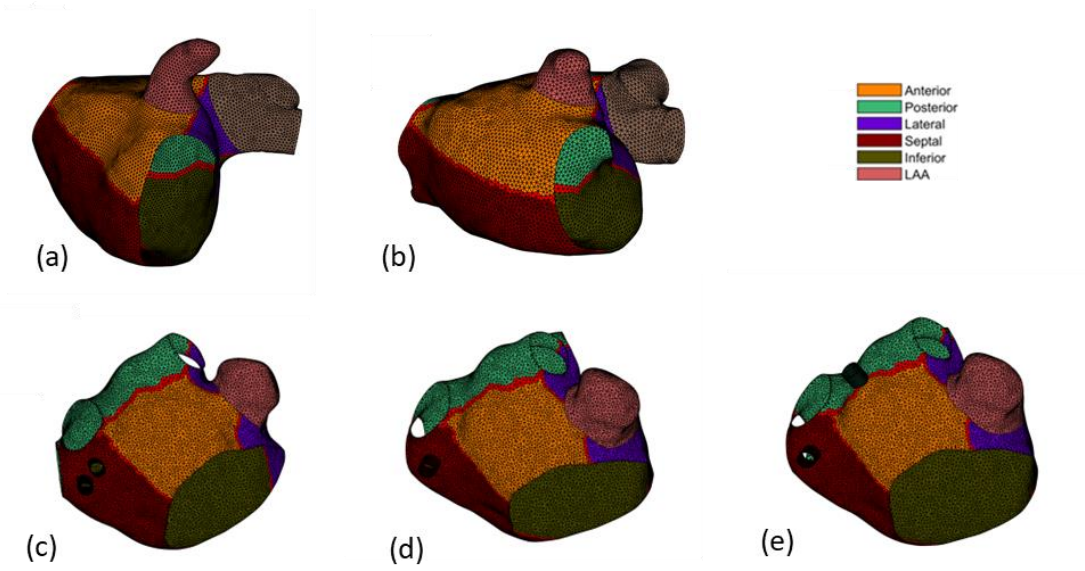

Figure 2-5: Regionalization results on anatomically variable LA geometries: (a) long trunk; (b) short trunk; (c) double middle PVs; (d) middle PV; (e) top-middle PV.

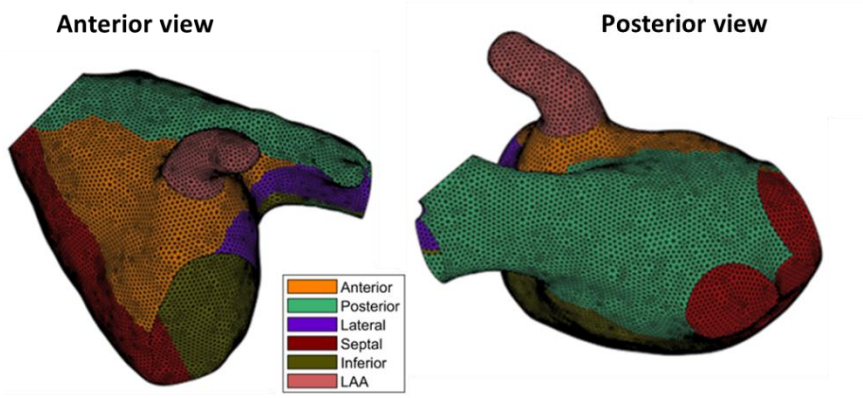

Figure 2-6: Regionalization result of one anatomy in which the performance of the proposed approach was considered poor.

2.4.2 Contraction in control subjects and AF patients

Dynamic detection of regions in one sample patient is shown in Figure 2-7.

Average LA global and regional volume-time curves for CTRL group and AF group are shown in Figure 2-8. All these volumetric curves presented higher magnitude of volume in AF as compared to CTRL group. However, IA did not show significant differences between the two groups (see Table 2-1).

When the LA EF and REFs were computed, it was seen that in the AF group, the values of these parameters both for the entire LA and in each region were considerably lower than in the CTRL group (see Figure 2-9(a)).

Overall, global and regional strain values were higher in CTRL group as compared to AF group, a fact which accounts for the expected normal functionality of LA throughout the cardiac cycle in CTRL group (see Table 2-1 for mean strain values at global and regional level, and Figure 2-9(b) for mean peak global strain and mean peak radial strain at distinct regions in the two populations). Global LA strain variation was more evident in the circumferential and radial directions ($p < 0.005$). As regards regional strains, the differences were more prominent in RS in inferior, lateral, and septal regions ($p < 0.005$).

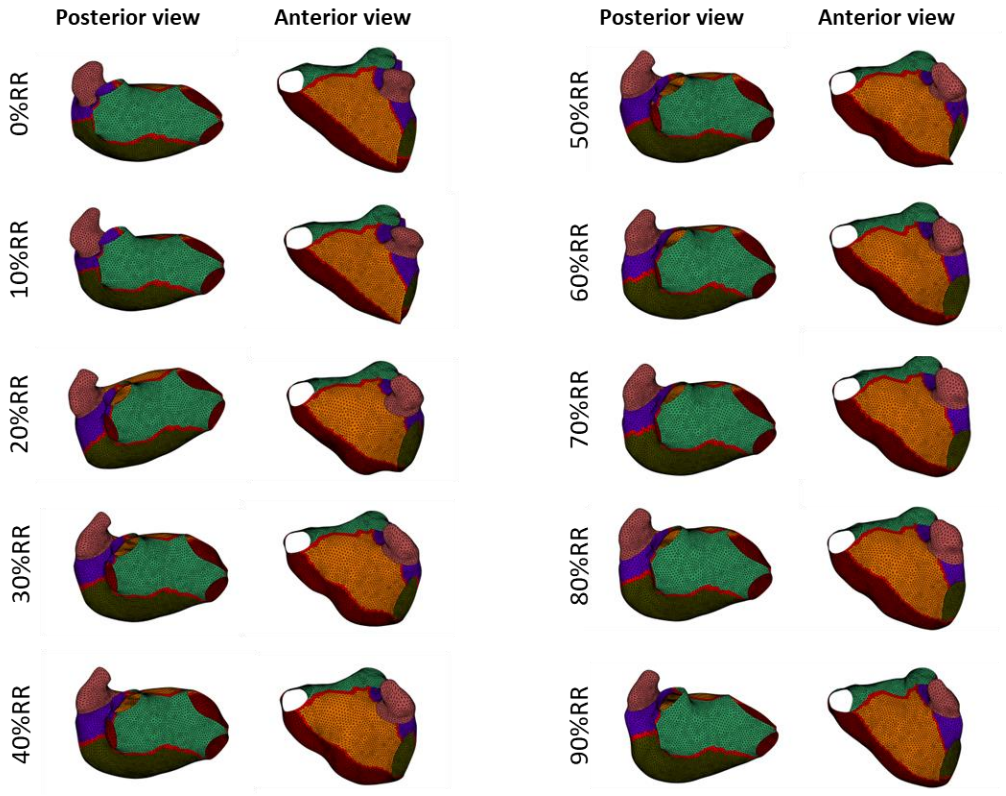

Figure 2-7: Regionalization results applied to the ten surfaces throughout the cardiac cycle (from 0%RR to 90%RR, where RR indicates the interval between two consecutive electrocardiographic R wave peaks) in one sample patient.

This same behaviour was noticed in mean peak RWM (Figure 2-9(c)) where, apart from posterior region, every other region presented higher mean peak RWM values in CTRL group as compared to AF group (Table 2-1). However, this difference in variation was more evident in septal region ($p < 0.005$).

On the other hand, mean RSF values were close to each other in both the groups, but statistical test was able to identify significant variations in anterior, inferior, lateral, and septal regions ($p < 0.005$) as shown in the Table 2-1.

Among all the regions, posterior region showed non-significant differences between CTRL group and AF group (Table 2-1).

Although IA_{RWM} did not show statistically different values ($p = 0.08$) between CTRL and AF groups, RWM curves revealed noticeable

irregularities and random regional contractions in some AF patients. To illustrate this finding, in Figure 2-10 we show RWM curves of an AF patient alongside a CTRL subject. In CTRL, the peak RWM occurred simultaneously in all regions except the posterior, whereas in the AF patient, a lack of synchronicity in the contraction is evident across all regions.

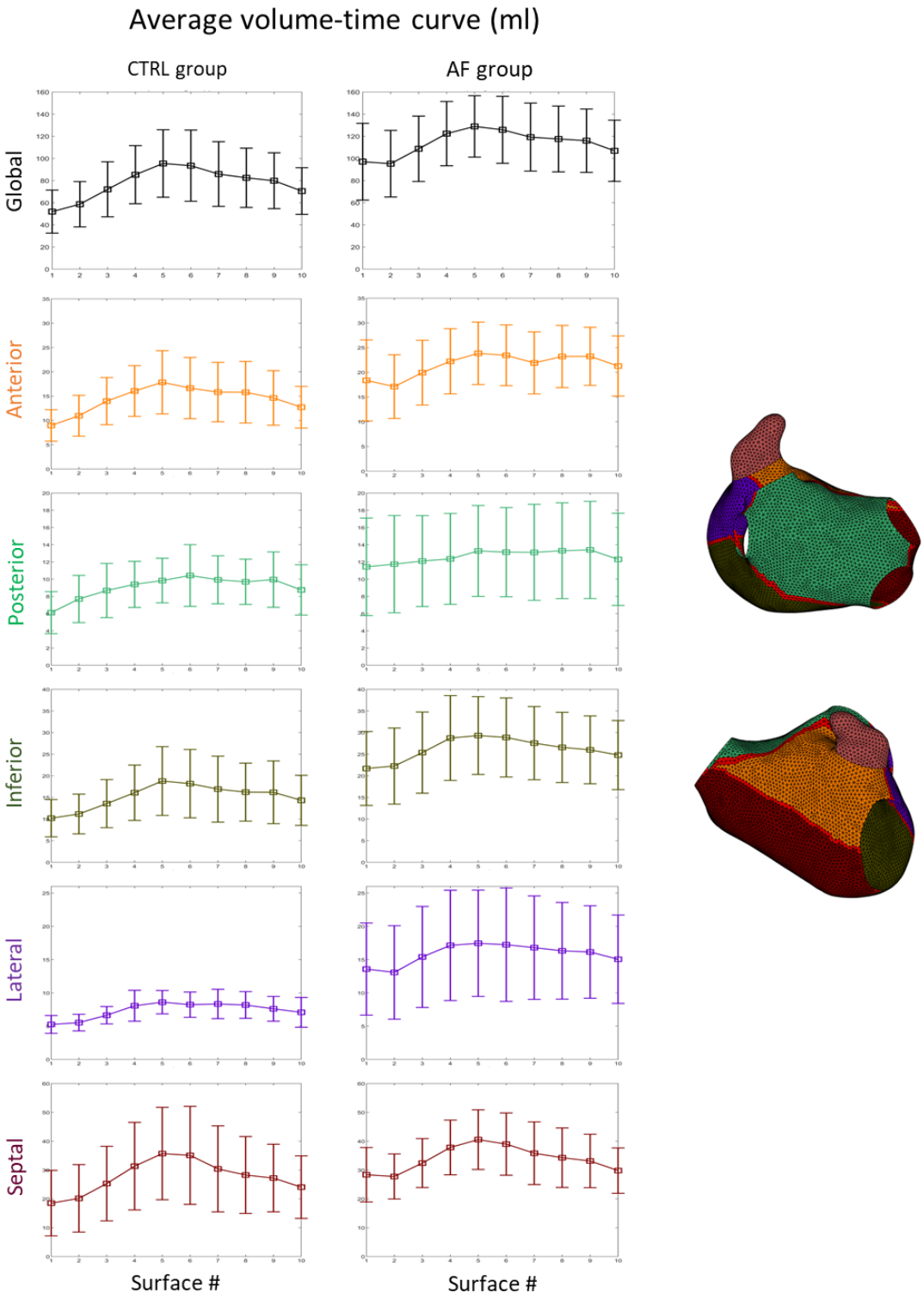

Figure 2-8: Mean LA and regional volumetric curves throughout the cardiac cycle in CTRL (left panels) and AF (right panels) groups with standard deviation.

Table 2-1: Computed parameters in CTRL and AF groups.

Parameters		CTRL group (*n*=13)		AF group (*n*=17)		*p*-value
		Mean +/- SD	Range	Mean +/- SD	Range	
Mean volume (ml)	LA	77.6 +/- 13.5	[52, 95.5]	113.8 +/- 10.9	[95.3, 129]	*P < 0.005*
	Anterior	14.3 +/- 2.6	[9.0, 17.8]	21.5 +/- 2.2	[17.1, 23.8]	*P < 0.005*
	Posterior	9.1 +/- 1.2	[6.1. 10.4]	12.6 +/- 0.7	[11.4, 13.4]	*P < 0.005*
	Inferior	15.2 +/- 2.7	[10.2, 18.8]	26.1 +/- 2.5	[21.7, 29.3]	*P < 0.005*
	Lateral	7.4 +/- 1.1	[5.3, 8.6]	15.9 +/- 1.5	[13.1, 17.5]	*P < 0.005*
	Septal	27.6 +/- 5.5	[18.5, 35.7]	33.9 +/- 4.2	[27.8, 40.5]	*P = 0.01*
IA regional volume		1.2	[0.5, 2.8]	1.5	[0.5, 2.8]	*P = 0.20*
Peak LS (%)		22 +/- 7.9	[11.0, 44.3]	13.7 +/- 7.8	[3.6, 29.2]	*P = 0.01*
Peak RS (%)		25.2 +/- 11	[13.9, 60.5]	11.7 +/- 7.7	[2.0, 26.1]	*P < 0.005*
Peak CS (%)		30.1 +/- 11	[12.8, 55.2]	13.1 +/- 7.6	[2.7, 28.7]	*P < 0.005*
Peak RRS (%)	Anterior	32.8 +/- 19.6	[10.8, 92.2]	14.6 +/- 12.3	[0, 34.1]	*P = 0.01*
	Posterior	20.2 +/- 15.7	[3.1, 68.2]	14.5 +/- 8.3	[0.8, 26.4]	*P = 0.26*
	Inferior	28.2 +/- 9.1	[15.2, 51.6]	15.8 +/- 8.4	[3.2, 31.0]	*P < 0.005*
	Lateral	24.3 +/- 7.9	[11, 36.9]	13.7 +/- 8.1	[3.3, 30.5]	*P < 0.005*
	Septal	29.0 +/- 13.5	[13, 69.4]	13.1 +/- 8.6	[0.3, 28.5]	*P < 0.005*
Peak RWM (mm)	Anterior	5.2 +/- 2.5	[2.1, 13.0]	2.8 +/- 2.2	[0, 6.2]	*P = 0.01*
	Posterior	2.6 +/- 1.6	[0.5, 7.2]	2.3 +/- 1.3	[0.2, 4.3]	*P = 0.69*
	Inferior	5.0 +/- 1.7	[2.3, 8.6]	3.5 +/- 1.7	[0.9, 7.0]	*P = 0.02*
	Lateral	4.0 +/- 1.3	[2.0, 6.1]	2.9 +/- 1.5	[0.9, 6.2]	*P = 0.04*
	Septal	6.5 +/- 2.6	[3.1, 14.3]	3.5 +/- 2.3	[0.08, 6.6]	*P < 0.005*
IA_{RWM}		1.1	[0, 2.1]	1.6	[0, 3.1]	*P = 0.08*
RSF	Anterior	0.2 +/- 0.09	[0.1, 0.5]	0.1 +/- 0.09	[0, 0.3]	*P < 0.005*
	Posterior	0.2 +/- 0.09	[0.03, 0.4]	0.1 +/- 0.06	[0.01, 0.2]	*p = 0.27*
	Inferior	0.2 +/- 0.05	[0.1, 0.3]	0.1 +/- 0.06	[0.03, 0.2]	*P < 0.005*
	Lateral	0.2 +/- 0.05	[0.1, 0.3]	0.1 +/- 0.06	[0.03, 0.2]	*P < 0.005*
	Septal	0.2 +/- 0.07	[0.1, 0.4]	0.1 +/- 0.07	[0, 0.2]	*P < 0.005*

2.5 Discussion

Our study presents several points of originality. First, we have proposed an automatic approach for regional segmentation of the LA which, as far as we know, appears to be the most comprehensive 3D model available nowadays. Whereas regional segmentation of the LV in 17 segments according to a widely accepted guideline [68] is a standard in clinical practice, nothing similar exists as regards LA. In previous studies the proposed methodologies were solely evaluated on conventional LA anatomies having four PVs [69]. Electrogram-based methods for subdividing LA in regions, like those aimed at analysing complex fractionated electrograms (CFEs) [29], [35], [39], [70] have led to an excess of heterogeneity in defining the boundaries of the LA regions [27], which overall have never been tested on variable anatomies nor, most importantly, correlated with the corresponding regional mechanical behaviour.

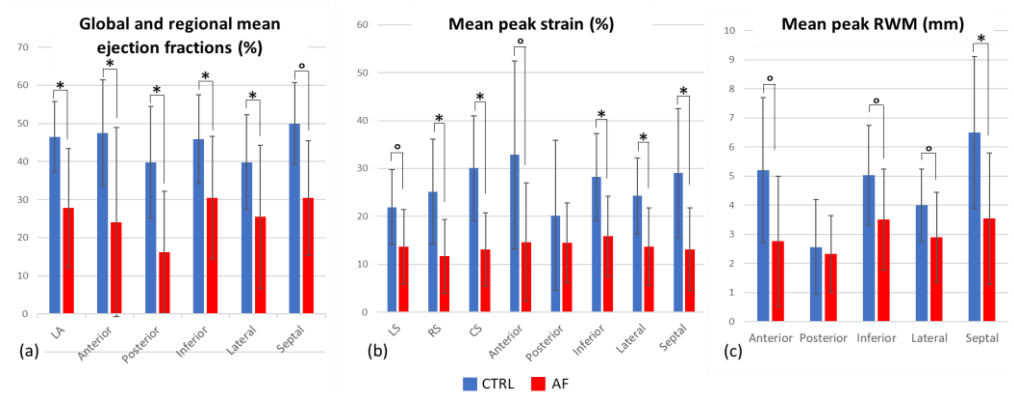

Figure 2-9: Mean EF of LA and defined regions of LA (a), Global and regional mean peak strains (b), Mean peak regional wall motion (c).

Previous works on this topic have been recently published. Most of them [71], [72], [73], [74], [75], [76], [77], [78], [79], [80], [81] are focused on specific clinical objectives that require the subdivision of the LA surface in regions, for example the modelling of muscle fibres [72], [76], [77], [80], atrial fibrosis distribution [74], [81], to determine the electrophysiological relationship between the atria [75], or the existence of sex-based electrophysiological substrate differences to account for worse AF ablation outcomes [73]. In these studies, a different number of LA regions were used; for example, in [82], [74], [76], [77] only PVs, MV and LAA were labelled, and the LA chamber was considered one

region. In [80] and [72] manual seed points are required and affect regionalization results. Importantly, in all these studies, the regionalization approach was not described; and since nowadays guidelines and recommendation are not available, the reproducibility of their results could be affected by this missing information. In [78], a commercial software (ADAS 3D, Galgo Medical, Barcelona, Spain) was applied to divide the LA in 13 regions and allow a 2D atrial mapping for an easy way to visualize and interpret intra-subject information and perform inter-subject comparison; however, such regionalization approach is not open source.

In [81] and [71], the pipeline for LA regionalization has been described in detail. The approach presented in [71], requires some manual inputs and has been optimized to obtain 2D LA flattening maps and then the regionalization was applied to quantitatively assess the correlation

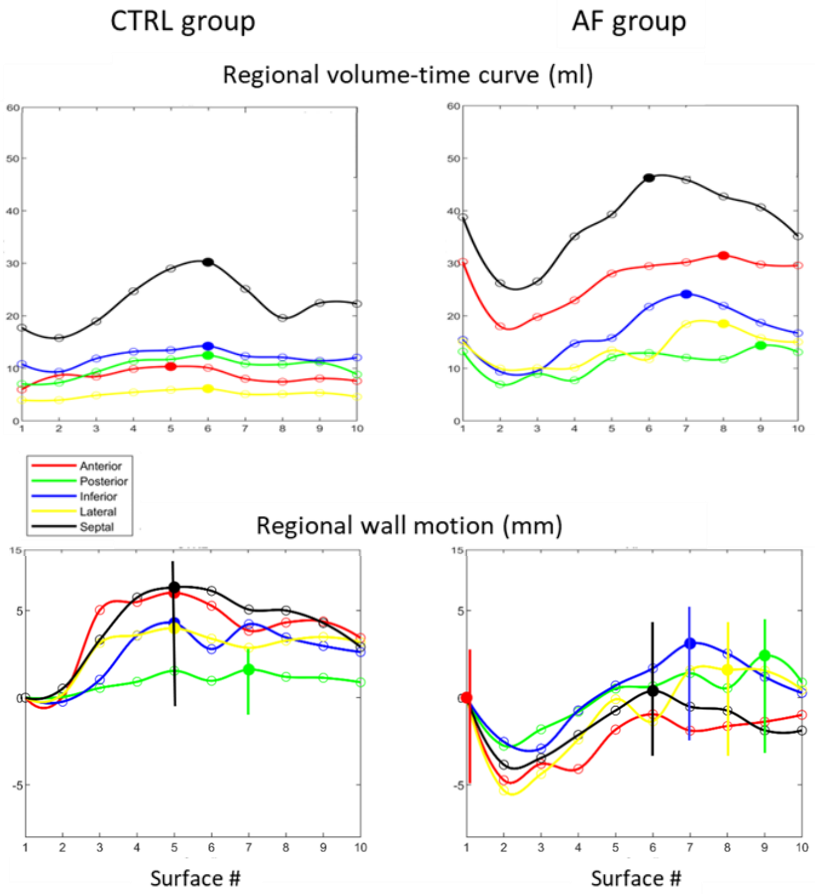

Figure 2-10: RWM and regional volume curves for two subjects.

between the extents of fibrotic tissue from MRI-late gadolinium enhanced scan and low voltage areas measured by electro-anatomical mapping. Unfortunately, no assessment of the regionalization approach is provided and neither the code nor the data are made available to perform a quantitative comparison between our and the proposed approach.

Our LA regionalization approach was tested and demonstrated in most of the LA anatomies reported in literature (Figure 2-5), suggesting that it is able to cover most anatomical variations of LA, regardless of PVs number and size and LAA position. Moreover, our approach was completely automatic minimizing the influence of the operator on regionalization results and allowing a dynamic LA regionalization. Our methodology showed poor results in 10% of the cases (3 patients), presumably due to the presence of bulges and curves on the surface of the LA. To overcome this limitation, we designed a tool for the manual correction of the points P1, P2, P7 and P8 at the PVs, to finalize the regionalization directly on the LA anatomy into the 3D space.

Secondly, we proposed ten parameters to quantify patient-specific LA mechanical contraction. Such parameters had been originally devised for LV regional segmentation [66] and were translated into our regionalization process of LA. Standard EF and REF, LS, RS, and CS at a global level and RRS, RWM, and RSF were computed.

Nowadays in clinical practice LA contraction is assessed by 2D echocardiography. In our study the contraction parameters were made available also in controls and by 3D CT imaging. To assess the reliability of our results they should be compared with other previously published values, mainly derived from echocardiography. Indeed, in [83] longitudinal strain from 3D echocardiography in 105 healthy subjects (median value of age: 42 years) was 23.7±7.6%, which is surprisingly close to the values computed in our CTRL group (21.9 ± 7.9%). In [84], both peak longitudinal and circumferential strain values were reported in a group of healthy subjects (n = 15) and paroxysmal AF patients with and without LA dilation (n = 22 vs n = 9) by 3D speckle tracking echocardiography (3DSTE) and compared the corresponding values obtained by 2D speckle tracking echocardiography (2DSTE). Strain values appear slightly different compared to our results (CTRL group - LS: 25.7 ± 7.2% by 3DSTE vs 21.9 ± 7.9%; CS: 37.1 ± 10.2% by 3DSTE vs 30.07 ± 10.96); AF group - LS: 16.0 ± 6.6% by 3DSTE vs 13.7 ± 7.8%,

CS: 21.2 ± 13.4% by 3DSTE vs 13.1 ± 7.6%). Such differences are probably due to the different imaging modalities and methods applied to compute the strains and might be also due to gender and age differences in the selected population [84]. Unfortunately, the low number of subjects in CTRL group did not allow any deeper investigation; however, our CTRL cohort was slightly older (60.7±10.1 yrs vs 57.9±5.4 yrs), included more males (12 vs 10) and showed higher LA volumes in comparison with [84]. In addition, as previously reported in [85], we should take into account longitudinal strain values might have a wide variability (range: 23.0–67.6%). Of note, our peak longitudinal strain values in AF patients were closer to 3DSTE which is considered more sensitive for the detection of LA dysfunction in AF patients as compared to 2DSTE (13.7 ± 7.8% vs 16.0 ± 6.6% (3DSTE) vs 21.2 ± 13.4% (2DSTE)). Taken together, these considerations rebound our results important for considering the proposed approach usable in clinical practice.

Importantly, in addition to strains, several contraction parameters were proposed for patients with AF. As far as we know, this is the first study in which a quantitative description of the LA contraction alterations associated with a history of AF is presented, not only considering the entire chamber but also at a regional level. Unfortunately, since CT imaging data were acquired in SR in all patients, the cause/effect relationship between functional modifications and occurrence of AF cannot be addressed, and we are able to only describe a significant association. On these premises, results in our 17 AF patients highlighted relevant differences in comparison with CTRL as regards: (1) impaired global and regional contraction, the latter being evident in REF and regional volume as well as in strain values; (2) significantly lower circumferential and radial strain values and (3) worsening of regional contraction parameters in all regions, with the most prominent reduction at the septal region, followed by anterior, inferior, and lateral regions.

Overall, our results showed that: (1) the global impairment of LA contraction associated with AF appears more pronounced along radial and circumferential direction; (2) the more pronounced regional impairment of radial strain in septal, inferior, and lateral regions could point to a more considerable reduction in mechanical efficiency in these regions in comparison to the posterior and anterior ones.

The reduction of mechanical efficiency is also associated with asynchronous contraction underlined by time occurrence of the peaks of the RWM curves in AF patients; in addition, the RWM curves in CTRL and AF groups showed interesting differences in shape, showing a time delay in the beginning of atrial diastole. It seems that at the start of ventricular diastole, the entire process of atrial systole is delayed. Although this observation might be slightly inaccurate due to CT frame rate acquisition, we cannot exclude a slowing down of atrial relaxation in AF condition. This observation needs further investigation in a larger and selected population.

For research purposes, the computed contraction parameters provide patient-specific boundary conditions for computational fluid-dynamic simulations to investigate thrombogenic events within LA. Indeed, in most of the LA computational fluid dynamic simulation studies, rigid LA surfaces are considered. This approach is somehow correct in case of permanent AF patients where the normal atrial contraction is totally compromised. However, in case of paroxysmal AF patients, this approach is prone to errors. Our computed contraction parameters can provide patient-specific boundary conditions to convert a rigid domain into a moving domain and support more realistic simulations.

Our study shows several limitations. Regarding the methodological approach, measurements of RWM may also be influenced by the definition of long axis of LA. In most of the cases, the endpoint of long axis lies on the posterior region which consequently evaluates minimum RWM for posterior region among all other regions and ultimately represents the least contribution in the global LA contraction. Nonetheless, a similar result exists in previous research where posterior region was identified as one of the least contributing regions in terms of regional velocity and regional ejection fraction [45]. Unfortunately, exact comparison is not possible due to differently defined regional boundaries. In the above-mentioned study, regional volume was defined by projecting boundary points of each region towards the geometrical centre of LA, located inside the LA surface and then, by tracing the regional volumetric changes at each point of the cycle, the relative contribution of each region in global volume was measured. However, with this strategy, the cumulative sum of the regional volumes at any time frame may escalate from the global LA volume as an overlapping between regional volumes

may exist. Instead, in our approach, regional volumes were defined using long axis which is a straight line. With this, each region occupied explicit volume without superimposing with other regions and the total sum of regional volume at specific time never exceeded the actual LA volume.

In addition, although the regionalization algorithm is automatic, manual cut of the PVs and LAA is required in the current implementation. A possible approach to overcome this limitation was presented in [86] where a shape diameter function was applied which could be easily integrated into the proposed workflow.

To conduct this study, we acquired CT images for each subject at ventricular end diastole throughout the cardiac cycle. In dynamic CT acquisition, low temporal resolution is a critical factor that may have affected precise detection of end diastolic and end systolic phases and consequently our asynchrony indices which indeed resulted non significantly different between the CTRL and AF groups.

2.6 Conclusion

This study proposes an approach to regionalize LA chamber and assess the region based mechanical function of LA in controls and AF patients. The regionalization method has been proved to be robust with several LA anatomical variations and able to characterize contraction changes associated with AF. Testing on larger dataset may help to evaluate the clinical potential of this methodology.

3 Assessment of LA Appendage Dysfunctional Contractility in Atrial Fibrillation Patients

In this chapter, the dysfunctional contraction of left atrial appendage in atrial fibrillation has been assessed which ultimately gives rise to thrombogenic events within the appendage. To perform this analysis, a semi-automatic approach has been formulated to define left atrial appendage centerline and validated on patient-specific variable morphologies of appendage. Using centerline as a reference frame, left atrial regions have been defined and global and regional contraction parameters have been computed in healthy subjects and atrial fibrillation patients. Eventually, statistical analysis has been conducted to assess the notable disparities between healthy subjects and patients with atrial fibrillation, and subsequently, the obtained outcomes have been analyzed and discussed.

3.1 Abstract

The left atrial appendage (LAA) is a tiny structure, attached to the left atrium (LA). Although it is a small structure, it carries complex and highly variable morphologies. In atrial fibrillation (AF), it has significant importance because the majority of the thrombogenic events happen within it. A compromised LAA mechanical contraction might give rise to blood clot formation and may cause stroke. To date, the effect of AF on the mechanical contraction of LAA is not yet fully explored. In this study, a novel approach to assess the effect of AF on LAA contractility has been proposed and applied to thirteen healthy subjects and seventeen AF patients. LAA ejection fraction, strains, and wall motion parameters were computed on a global and regional basis and compared between the two groups. Results concluded statistically significant differences in LAA orifice, centerline length and tortuosity to evaluate global contractility and in terms of regions, proximal and distal regions presented disturbed contraction between two groups in terms of regional wall motion and shortening fraction.

Keywords: left atrial appendage, atrial fibrillation, LAA centerline, LAA contraction, global and regional assessment.

This chapter has been adapted from: S. Hussain, M. Falanga, A. Chiaravalloti, C. Tomasi, C. Corsi, Assessment of Left Atrial Appendage Dysfunctional Contractility in Atrial Fibrillation Patients, 2024 [Submitted to 'Computers in Biology and Medicine']

3.2 Introduction

Left atrial appendage (LAA) is a complex tubular structure, having a narrow orifice which connects it with the left atrium (LA) body [48], [49] and carries unique anatomical and physiological properties [87]. Previously, it was considered as a relatively insignificant structure of cardiac anatomy; more recently, thanks to a continued in-depth analysis of several investigators, LAA is now acknowledged as a predominant location for thrombus development in individuals afflicted with non-valvular atrial fibrillation (AF) [88]. In fact, in AF patients, around 90% of the thrombi takes place within the LAA [89]: indeed, disturbed, and reduced LAA contractility due to the presence of AF might cause stagnant blood flow within the LAA and consequently increases the risk of thrombus formation which ultimately could lead to stroke [86], [90], [91].

Several efforts have been made to investigate the relationship between the LAA morphology and the thrombogenic events [92], [93], [94], [95]. Among these, the most recognized classification approach categorized the LAA into four different morphologies: cactus, chicken wing, cauliflower, and windsock [51], [90], [96]. Independent investigations conclusively established chicken wing as the 'safe' LAA type [97] and considered to be least likely to result in stroke. However, the above-mentioned classification is highly subjective to the observer and impact of AF on LAA contractility was merely considered when the association between LAA shape and the occurrence of thrombogenic event was performed.

In previous studies, LAA mechanical contraction was indirectly derived by assessing LAA volumes and ejection fraction, LAA orifice area and diameter [98], [99], [100], also considering a floating LAA centerline-based dynamic reference system [101], [102]. Recently, regional assessment of LAA was also considered using idealized models [52]. Although, significant efforts have been made to explore the effects of AF on LAA in terms of contraction, there still exists a lack of well-defined and well tested approach to evaluate the relationship between AF and LAA global and regional contractility.

In this study we designed a novel workflow to quantify LAA global and regional contraction, irrespective of the variability in the LAA morphology. The developed workflow was tested on data from AF patients and healthy subjects to point out differences in contractility

which could potentially explain the increased risk of clot formation in AF patients.

3.3 Materials and methods

3.3.1 Selection of patients and CT imaging

Data used in this study were acquired within the FATA project, approved by the Ethics IRST, IRCCS AVR Committee (CEIIAV n. 1456 prot.6076/2015 I.5/220). All subjects gave written informed consent in accordance with the Declaration of Helsinki.

To conduct this study, seventeen patients with AF (13 males, mean age: 59.65 ± 7.25 yrs and 4 females, mean age: 73.75 ± 2.25 yrs) were retrospectively enrolled with a control (CTRL) group of thirteen healthy subjects (10 males, mean age: 60 ± 10.2 yrs and 3 females, mean age: 61.5 ± 0.5 yrs) having normal size of heart structures and no previous history of AF.

CT dynamic acquisitions of the heart after injection of contrast medium were obtained applying retrospective ECG gating during normal sinus rhythm using a 64-slice multi-detector CT scanner (Philips Brilliance 64 CT scanner) in each patient.

Volumetric CT images were reconstructed for a total of 10 phases from ventricular end diastole (from 0%RR to 90%RR, where RR indicates the interval between two consecutive electrocardiographic R wave peaks). Each reconstructed CT volume was 512x512x200 pixels. The voxel resolution was not isotropic: in-plane resolution was 0.39 mm, and through-plane resolution was 1 mm, resulting in a voxel size of 0.39x0.39x1 mm^3.

3.3.2 Data analysis

The workflow of the performed analysis using CT data is shown in Figure 3-1 and requires several steps detailed in the following subsections.

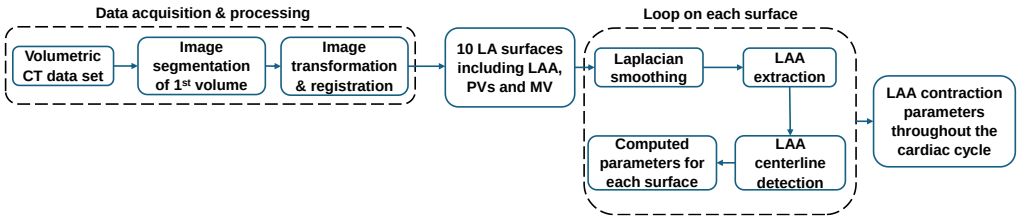

Figure 3-1: Flow chart of the proposed approach, implemented throughout the cardiac cycle.

3.3.2.1 Image segmentation and post-processing

For each dataset, the first acquired volume along cardiac cycle corresponding to end diastole (ED) was segmented applying an active contour algorithm previously developed in MATLAB (MATLAB R2023a, The Mathworks Inc.) [63]. This is the same algorithm which was discussed in section 2.3.2.1. In this algorithm, the segmentation was first restricted to LA and LAA by defining a 3D region of interest and the algorithm was initialized with a manually selected seed; the initial surface grew towards the wall of the LA and enclosed the whole LA anatomy including LAA. This algorithm was manually supervised and corrected in case of inclusion of neighboring structures. The resulting LA surface was saved in stereolithography format.

Following the segmentation, a rigid transformation between the ten CT volumes acquired throughout the cardiac cycle was applied. The 3D mapping function resulting from the rigid transformation was further refined by applying a 3D non-rigid registration based on a B-spline transformation model [103], using the mean square difference as a similarity measure. Once performed the registration procedure, the inter-frame displacements were applied to the segmented ED LA surface including the LAA, the pulmonary veins (PVs) and the mitral valve (MV) to reconstruct the LA surfaces throughout the cardiac cycle [104].

In the post-processing step, a Laplacian smoothing was applied to the surfaces and then, the LAA orifice was manually cut by taking into account the curvature of each surface and including the ridge within the LA chamber. For this purpose, open-source Autodesk Meshmixer software [64] was utilized.

3.3.2.2 LAA centerline extraction approach

To define global and regional LAA contraction parameters, a reference dynamic system was required along which the parameters can be evaluated. For this purpose, a semi-automatic LAA centerline extraction algorithm was designed to generate a piecewise linear line that starts from

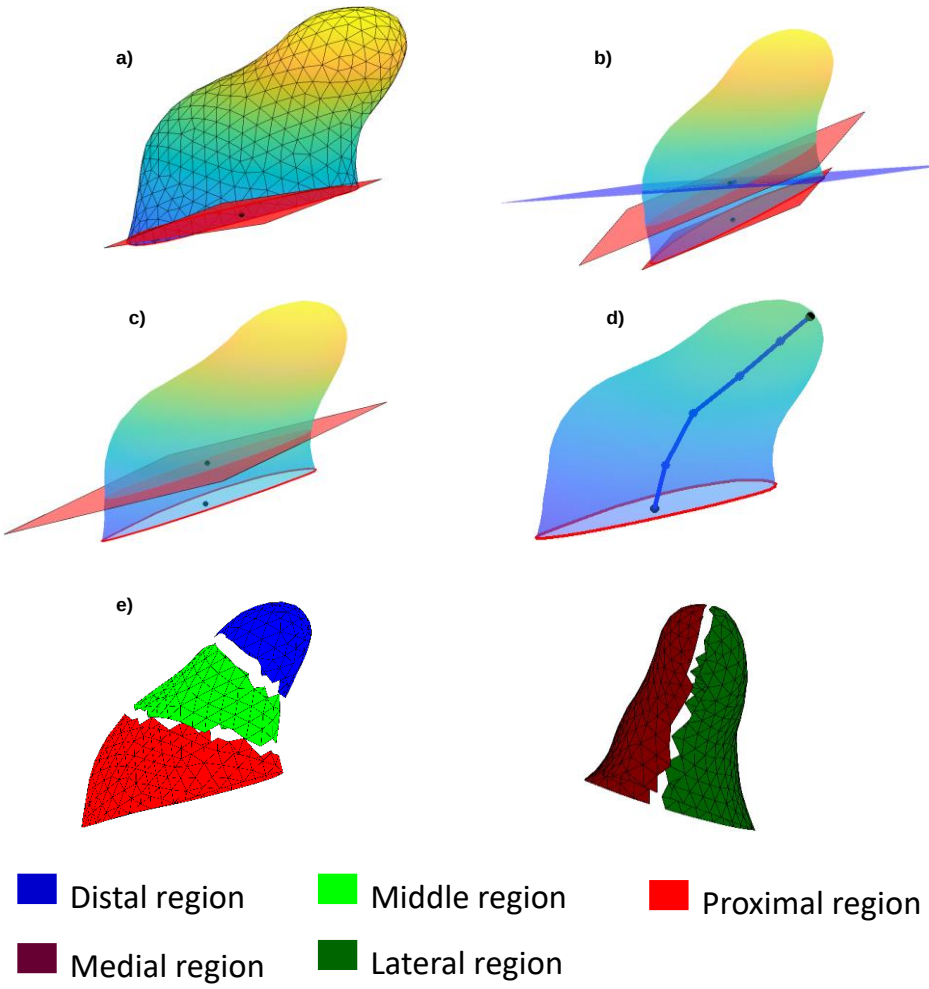

Figure 3-2: Several steps of LAA centerline extraction approach.
a) LAA surface with best fitting ostium plane (red) and barycenter of ostium (black dot). **b)** LAA surface with translated ostium plane (red) and newly generated intersecting plane (blue). **c)** LAA surface with newly generated rotated intersecting plane along with the barycenter of the ostium and the intersecting points (black dots). **d)** LAA surface with piecewise linear centerline, starting from the ostium barycenter till the tip of the LAA surface. **e)** (left) subdivision of LAA into 03 regions, (right) subdivision of LAA into 02 regions.

the center of LAA orifice and reaches the tip of LAA while following the shape of LAA (Figure 3-2).

The best fitting LAA orifice plane was first computed (Figure 3-2.a). Then, this plane was translated towards the tip of LAA. As the translated plane intersected the LAA surface, the intersecting points were considered to compute their barycenter. By joining this barycenter with the barycenter of the plane before translation, a segment was drawn which was used to detect the normal direction of a new plane, containing the new barycenter. In the next step, the intersection between the new plane and the LAA surface was evaluated. In case of incomplete intersection with the LAA, a manual rotation was applied to reach a complete intersection (Figure 3-2.c). Afterwards, the new barycenter was computed and used to build the centerline of LAA. These steps were repeated till the tip of the LAA was reached. By connecting all the barycenters, the LAA centerline was generated (Figure 3-2.d).

After the extraction of LAA centerline, LAA regionalization was performed. The LAA surface was divided into three regions by splitting LAA centerline into three equidistant sections. The region in closest proximity to the LA body was named as the proximal region whereas the region located farthest from the LA body was referred as the distal region; the region between these two was defined as middle region. Additional two regions were obtained by computing the centerline best fitting plane which cut the LAA in a medial region, the one towards the LA body, and a lateral region, the one towards the mitral annulus (Figure 3-2.e).

3.3.2.3 LAA contraction parameters computation

To describe global LAA function, the following parameters were computed throughout the cardiac cycle: LAA volumes, LAA orifice area (LAAOA), LAA centerline length (LAA_{len}), LAA ejection fraction (EF) and LAA tortuosity (LAA_{tort}).

To analyze regional changes, for each region, regional radial dimension (RRD) was evaluated as the average of Euclidean distance of each vertex of that specific LAA region from the centerline for each time point x. Regional radial strain (RRS) was calculated as:

$$\mathrm{RRS(x)} = \frac{\mathrm{RRD(x)} - \min(\mathrm{RRD})}{\min(\mathrm{RRD})} \cdot 100$$

where RRS is the regional radial strain at the time point x, RRD(x) is the regional radial dimension at the time point x and min(RRD) is the minimum value of the regional radial dimension throughout the cardiac cycle.

Once RRS was computed for each region (proximal, middle, and distal; lateral and medial), the global radial strain (RS) was calculated as the average RRS value of medial and lateral regions at each time frame. To compute longitudinal strain (LS), the variation in the length of LAA centerline was traced out throughout the cardiac cycle with reference to the minimum of LAA centerline length, using this formula:

$$\mathrm{LS(x)}=\frac{\mathrm{LAA_{len}(x)\text{-}min(LAA_{len})}}{\mathrm{min(LAA_{len})}}\cdot 100$$

where $LAA_{len}(x)$ is the LAA centerline length at the time frame x and $min(LAA_{len})$ is the minimum LAA centerline length throughout the cardiac cycle.

Contraction of each LAA region was assessed in terms of regional wall motion (RWM), calculated as the difference between current RRD and minimum RRD for each LAA region:

$$\mathrm{RWM(x)} = \mathrm{RRD(x)} - \mathrm{min(RRD)}$$

Two indices of LAA asynchrony (IA_{RWM}) were computed as the standard deviation of the time points in which the RWM curve is maximum, for the proximal, middle, and distal regions and for the medial and lateral regions.

For each surface region, regional peak wall motion was divided by peak regional radial dimension to obtain regional shortening fraction (RSF).

All the computed parameters are reported in Table 3-1.

3.3.2.4 Testing and Statistical analysis

To verify that the proposed LAA centerline extraction approach has the capability to work on different LAA morphologies, the algorithm was tested on the four classical LAA shapes [92].

Global average LAA volume-time curves were compared between AF and CTRL groups, as well as LAA ejection fraction (EF). For the region-

based analysis, the comparison between CTRL and AF groups was performed in terms of peak RRS, peak RWM and peak RSF, peak IA_{RWM} computed for the three axial regions and the two longitudinal regions. The same comparison was made between peak LS, peak RS, peak LAAOA, peak LAA_{len} and peak LAA_{tort}.

Data are reported as median and interquartile range (IQR). T-test with $p<0.05$ was applied to assess if the parameters differ significantly between the two groups.

3.4 Results

The centerline extraction algorithm was tested on patient-specific standard variable LAA shapes. The computation of the centerline was feasible irrespective of the geometrical variation of the LAA morphology throughout the cardiac cycle. Examples of the obtained centerlines on different LAA morphologies are illustrated in Figure 3-3.

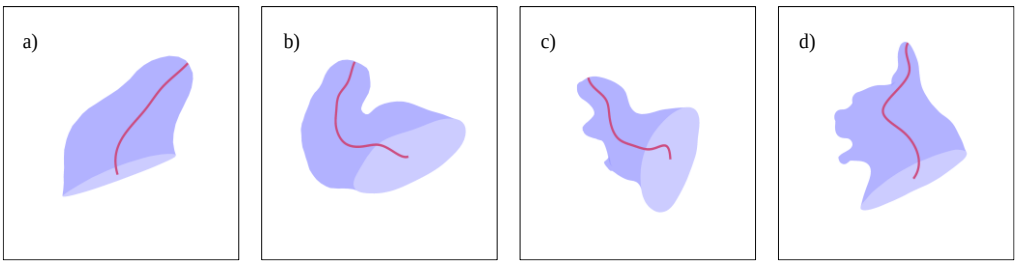

Figure 3-3: Centerline extraction of variable morphological anatomies of LAA. **a)** Windsock. **b)** Chicken Wing. **c)** Cactus. **d)** Cauliflower.

Average LAA volume-time curves for CTRL and AF groups are presented in Figure 3-4. Apparently, AF group has dilated LAA as compared to CTRL group and this phenomenon is evident in terms of LAA volume and LAA surface area ($p<0.005$). No significant difference was reported for LAA EF ($p=0.25$) (Table 3-2).

Significant differences existed between CTRL and AF group in LAA contraction parameters including LAAOA variation, peak LAAOA, peak LAA_{len} and peak LAA_{tort} (Table 3-2). In CTRL group, LAAOA variation was considerably higher as compared to the LAAOA variation in AF

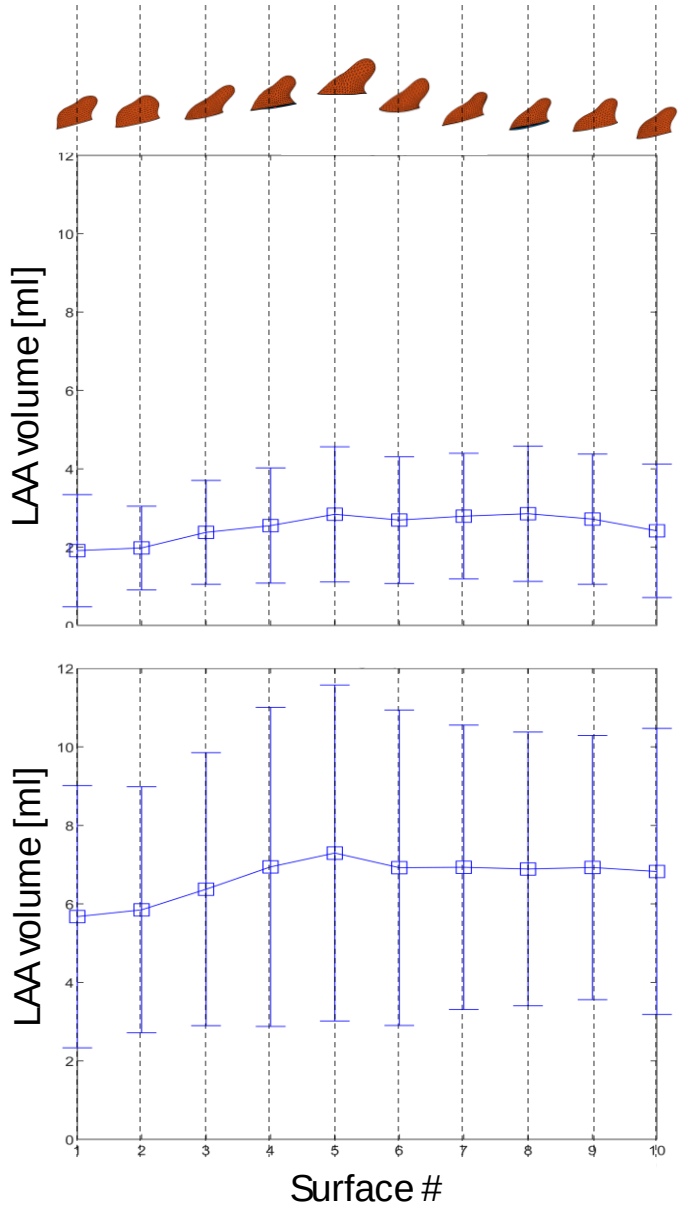

Figure 3-4: LAA average volume-time curves in CTRL (upper panel) and AF (bottom panel) groups.

group showing disturbed ostium contractility. Peak LAAOA, peak LAA_{len} and peak LAA_{tort} were significantly higher in AF group when compared with CTRL group (Table 3-2 and Figure 3-5, top row) which pointed out dilated and more complex LAAs in AF group. No significant variation was found for LS (p=0.4) and RS (p=0.9) between the two groups (Table 3-2 and Figure 3-5, bottom row).

In region-based analysis (Table 3-2 and Figure 3-6), peak RWM in the distal region and RSF in the proximal region were the only parameters which exhibited significant differences between CTRL and AF groups, together.

No significant differences in synchronicity among the two groups was detected when considering the three axial regions and the two longitudinal ones (Table 3-2).

Table 3-1: Description of computed LAA contraction parameters.

Contraction parameters	Description	Equation/Formula
LAA Ejection Fraction (LAA EF) [%]	Amount of blood ejected out from LAA	$\frac{\max(\text{LAA Volume}) - \min(\text{LAA Volume})}{\max(\text{LAA Volume})} \cdot 100$
LAA Orifice Area variation (LAAOA) [%]	Percentage changes in the area of LAA orifice during the cardiac cycle.	$\frac{\max(\text{LAAOA}) - \min(\text{LAAOA})}{\max(\text{LAAOA})} \cdot 100$
LAA tortuosity	Ratio between the LAA centerline length (LAA_{len}) and the Euclidean distance between the endpoints of LAA centerline (L).	$\frac{LAA_{len}}{L}$
Longitudinal Strain (LS) [%]	Measure of the LAA deformation along the LAA centerline, from orifice to apex during the cardiac cycle.	$\frac{LAA_{len}(x)\text{-}\min(LAA_{len})}{\min(LAA_{len})} \cdot 100$
Regional Radial Dimension (RRD) [mm]	Average Euclidean distance of each vertex *i* of that specific LAA region from the centerline for each time point x	$\text{Mean} \sum_{i=1}^{n} \frac{dist(i,centerline)}{n}$
Regional Radial Strain (RRS) [%]	Measure of the deformation along radial direction in a specific LAA region during the cardiac cycle.	$\frac{RRD(x) - \min(RRD)}{\min(RRD)} \cdot 100$
Radial Strain (RS) [%]	Average of the LAA deformation along radial direction during the cardiac cycle.	$\text{Mean}(RRS_{med}(x), RRS_{lat}(x))$
RWM [mm]	Motion of the specific region of LAA during the cardiac cycle.	$RRD(x) - \min(RRD)$

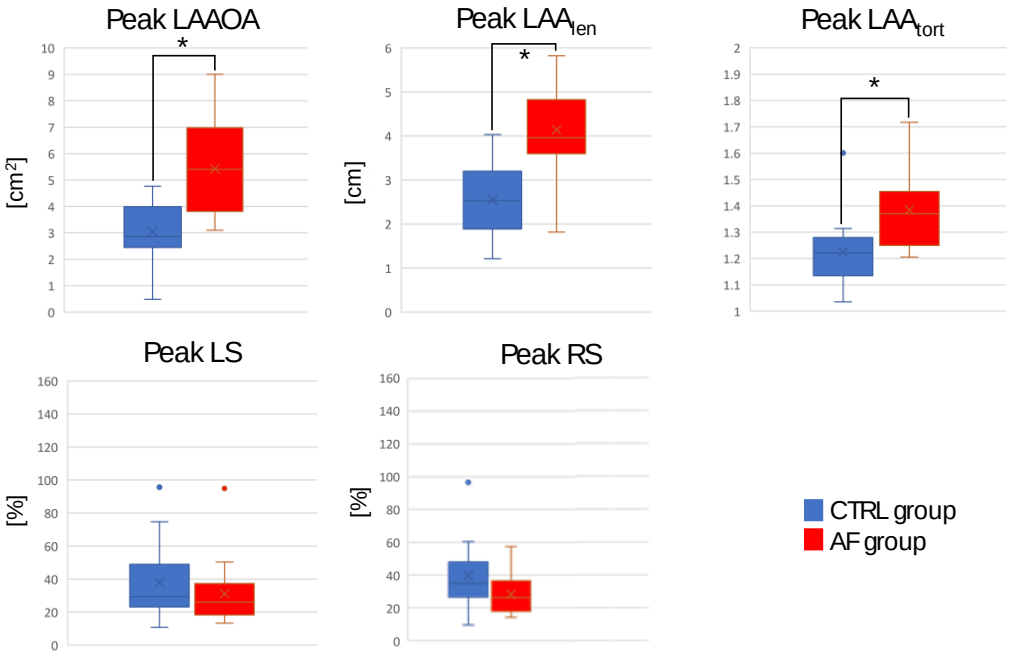

Figure 3-5: Boxplots of peak LAA orifice area (LAAOA), peak length of the LAA centerline (LAA$_{len}$),peak tortuosity of the LAA (LAA$_{tort}$), peak longitudinal and radial strains (LS and RS respectively) in the CTRL (blue) and AF (red) groups.

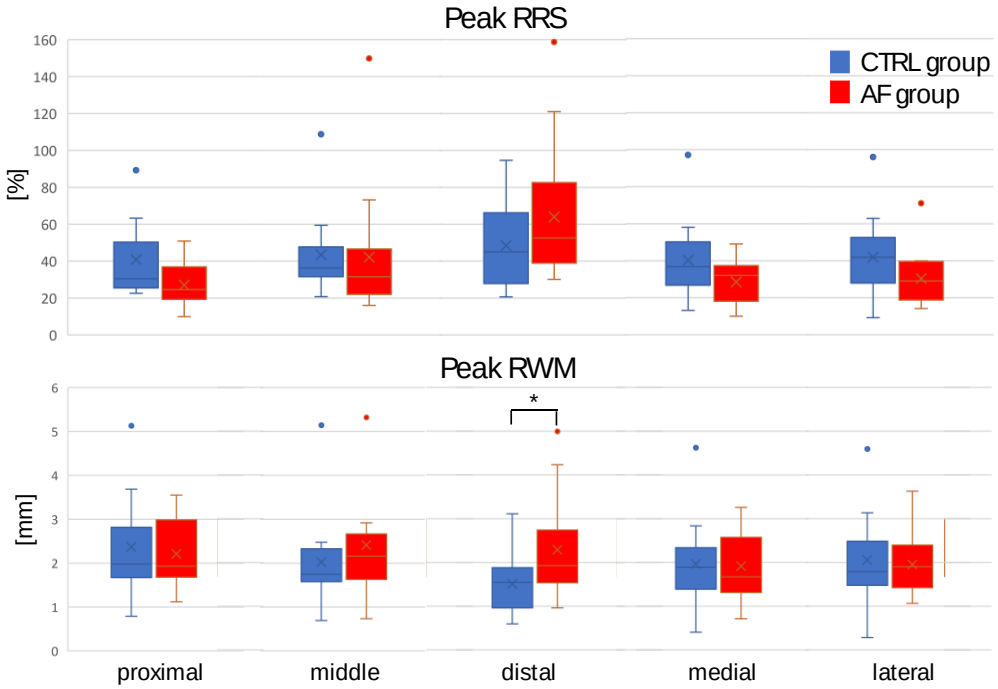

Figure 3-6: Boxplots of peak regional radial strain (RRS) (top row) and regional wall motion (RWM) (bottom row) in the five LAA regions (proximal, middle, distal and medial and lateral) in the CTRL (blue) and AF (red) groups.

Table 3-2: Comparison of LAA contraction parameters between CTRL and AF groups.

Parameters		CTRL group (n=13) Median [Q1, Q3]	AF group (n=17) Median [Q1, Q3]	p-value
LA EF (%)		44 [40, 50.5]	33 [14.5, 42.5]	$p < 0.005$
LAA EF (%)		42.2 [31.4, 58.3]	39.4 [29.9, 46.3]	$p = 0.25$
Left atrial appendage volume index (ml/m²)		1.17 [0.76, 2.04]	3.02 [1.79, 4.9]	$p < 0.005$
LAA surface area (cm²)		8.3 [6.1, 11.9]	15.4 [12.4, 23.5]	$p < 0.005$
LAAOA variation (%)		44.2 [40.9, 57.2]	41.0 [32.0, 45.3]	$p < 0.05$
Peak LAAOA (cm²)		2.9 [2.4, 4.0]	5.4 [3.8, 7.0]	$p < 0.005$
Peak LAA_{len} (cm)		2.5 [1.9, 3.2]	4.0 [3.6, 4.8]	$p < 0.005$
Peak LAA_{tort}		1.2 [1.1, 1.3]	1.4 [1.2, 1.5]	$p < 0.005$
Peak LS (%)		29.4 [23.1, 49]	26 [18.2, 37.5]	$p = 0.4$
Peak RS (%)		35.1 [26.6, 48]	26.3 [17.8, 36.6]	$p = 0.09$
Peak RRS (%)	Proximal	30.5 [25.4, 50.3]	24.6 [19.3, 36.9]	$p = 0.05$
	Middle	36.3 [31.5, 47.7]	31.6 [22, 46.6]	$p = 0.9$
	Distal	45 [27.8, 66.2]	52.6 [38.9, 82.5]	$p = 0.15$
	Medial	36.8 [26.8, 50.2]	32.1 [18.1, 37.4]	$p = 0.08$
	lateral	41.9 [21.9, 52.6]	29 [18.9, 39.6]	$p = 0.11$
Peak RWM (mm)	Proximal	2 [1.7, 2.8]	1.9 [1.7, 3]	$p = 0.6$
	Middle	1.7 [1.6, 2.3]	2.2 [1.6, 2.7]	$p = 0.3$
	Distal	1.5 [1, 1.9]	1.9 [1.5, 2.7]	$p < 0.05$
	Medial	1.9 [1.4, 2.3]	1.7 [1.3, 2.6]	$p = 0.8$
	Lateral	1.8 [1.5, 2.5]	1.9 [1.4, 2.4]	$p = 0.7$
RSF	Proximal	0.23 [0.2, 0.33]	0.2 [0.16, 0.27]	$p < 0.05$
	Middle	0.27 [0.24, 0.32]	0.24 [0.18, 0.32]	$p = 0.63$
	Distal	0.31 [0.22, 0.4]	0.34 [0.28, 0.45]	$p = 0.15$
	Medial	0.27 [0.21, 0.33]	0.24 [0.15, 0.27]	$p = 0.07$
	Lateral	0.3 [0.22,0.34]	0.23 [0.16, 0.28]	$p = 0.12$
IA_{RWM}	03 regions	1.7 [1.1, 2.3]	1.7 [1.1, 2]	$p = 0.4$
	02regions	1.4 [0.7, 2.1]	0 [0, 1.8]	$p = 0.7$

3.5 Discussion

In this study, we propose a new approach for the assessment of LAA contractility on a patient-specific basis. The analysis was performed on models derived from CT imaging and several parameters describing global and regional contraction of the LAA were evaluated in a control group and in an AF group. Our results suggested that globally there exists significant differences between healthy and AF affected pathological LAA anatomies in terms of contraction. Moreover, these differences were also observed in certain LAA regions.

Although, we have proposed several parameters to quantify the LAA mechanical contraction. But few of these parameters have confirmed that there is a significant difference in the contractility of LAA between CTRL and AF group. Apparently, LAA volume, LAA surface area, LAA ostium measurements (i.e, LAAOA variation, peak LAAOA), peak LAA_{len} and peak LAA_{tort} have the capability to identify the global contraction differences between healthy and pathological LAA.

The results of our study have revealed that the patients with AF not only have larger LAAOA as compared to CTRL group but the contractility at LAAOA is significantly disturbed in AF group. Similarly, it is noted that AF group has longer centerline as compared to the CTRL group, and they also carry higher peak LAA_{tort} as compared to the CTRL group which shows that the complex LAA morphologies are more prone to dysfunctional contractility due to AF. These obtained results are in line with previous studies which demonstrated similar findings where dilated LAA, elevated LAA orifice area and increased LAA centerline length are closely associated with high stroke risk [99], [105]. In another study, which was conducted between LAA thrombolic and non-thrombolic group and concluded that thrombolic group carries longer LAA centerline length and bigger ostium in terms of diameter [102].

In our regional analysis, it has been noticed that proximal region and distal region are the only regions which pronounced the significant differences in terms of peak RSF and peak RWM respectively between CTRL and AF groups. For proximal region, peak RSF in CTRL group is observed as 0.23 but in AF group, the evaluated value is 0.2 ($p < 0.05$). This assessment somehow strengthens our previous revelation where contraction dysfunctionality at the LAA orifice was detected as the orifice is a part of proximal region. Then, our investigation concluded significant differences in RWM only for distal region of LAA while such alterations were not reported in any other region. In our characterization of LAA regions, distal region is the farthest part of LAA which includes the apex of LAA and apparently, it is considered as a complex and highly variable part of LAA. Additionally, this part is merely smooth, especially in the case of cactus and cauliflower morphologies and the probability of the occurrence of multiple lobes is high here, which seemingly can disturb the calculation.

In terms of peak RRS, both CTRL and AF groups reported same contraction pattern in case of 03 LAA regions (proximal, middle, distal), which is low in proximal region and high in distal region. However, when 02 LAA regions (lateral, medial) were analyzed, the pattern was altered in both groups. In the CTRL group, the RRS values exhibited a higher magnitude in the lateral region in comparison to the medial region. But in AF group, medial region depicted higher RRS values in comparison of lateral region. Furthermore, it was also noticed that each region presented reduced RRS values in AF group in comparison of CTRL group apart from distal region.

Previously, doppler tissue imaging has been employed for the assessment of both global and regional function of the LV and LA [53], [106]. Later, the same technique was applied on LAA to study the LAA regional contraction disparities [54]. However, in this approach, the identification of LAA regions was performed manually by placing region of interest on images, without defining and standardizing LAA regions which may introduce errors in the analysis. In another study, in which the regional division of LAA was considered and implemented to study the alterations in the contractility of LAA, but on idealized LAA anatomy [52] which does not represent the actual morphology of LAA. Therefore, in our approach, it was considered that the regional division should be executed on patient-specific geometries as well as tested on standard variable morphologies of LAA to verify that the suggested approach is robust and has the potential to cover the different shapes of LAA.

To develop and conduct LAA contraction analysis, we used LAA centerline as a reference frame to define and compute contraction parameters. The centerline of a 3D object can be specified as a central path through that object and potentially define the shape and curvature of the object. In medical imaging, the process of extracting and identifying centerline has already been tested to analyze organs such as blood vessels, the lung, bronchia, and colon [107]. In literature, there are different studies in which LAA centerline methodology has been applied and used to define LAA morphological parameters [101], [102]. However, it was noticed that those approaches are either manual or tested on only single LAA surface during the cardiac cycle but in our study, we tested our defined LAA centerline extraction approach at variable instances to capture the whole cardiac cycle and in this way we were able to trace out

the variability in the centerline length throughout the cardiac cycle which ultimately explains the contractility in the longitudinal direction. .

Our approach has certain limitations as well, one of the constraints is the complex, curvy shape of LAA and the existence of high variability in the morphology of the LAA. In some cases, when there exist multiple lobes, the identification of primary lobe to define centerline can be misleading which can possibly generate incorrect centerline and can eventually include error in the quantification of contractility. In such cases, there is a possibility to manually identify the main lobe and re-generate the centerline, which makes this method semi-automatic.

These computed contraction parameters may play a vital role in computational fluid dynamic simulations when used as boundary conditions to perform patient-specific realistic simulations to study clot formation within LAA.

3.6 Conclusion

In summary, this investigation proposes a new method to evaluate the contractility of LAA by computing LAA centerline and by defining LAA mechanical contraction parameters using patient-specific dynamic dataset. Moreover, region-based analysis has also been implemented to quantify regional contraction differences. The proposed approach has been verified on anatomically variable LAA morphologies and was able to associate dysfunctional LAA contraction with AF. However, a larger cohort of patients may give more convincing results as the sample size of dataset was relatively small and future prospective studies are required to confirm whether the proposed quantitative approach has sufficient accuracy for clinical application.

4 Conclusions

This thesis has been a part of the MSCA PersonalizeAF project. The primary aim has been to investigate the impact of atrial fibrillation (AF) on the mechanical functionality of the left atrium (LA) and left atrial appendage (LAA). Indeed, the research proposed in this thesis was designed for providing a new tool to improve clinical knowledge and the methods applied to satisfy this clinical need are well known in the medical imaging community.

In the context of AF, LA is particularly important as AF causes irregular and ineffective contraction to atria, leading to blood stasis and increases the risk of thromboembolism. A tool for the assessment of LA global and regional contractility in AF condition is not available. Therefore, in this thesis we focused on the quantitative assessment and understanding of global and regional contraction of LA in AF patients. In addition, differently from the left ventricle [68] no approach has been proposed for LA regional segmentation standardization and a clinical expert consensus is not available.

The increasing interest for this cardiac chamber is mainly due to the spread of atrial dysfunctionalities such as AF that is considered the epidemic of the future; therefore, a deeper understanding of LA structural and functional remodeling also at a regional level is of great interest. To the best of our knowledge no other approach has been proposed to standardize LA regional segmentation. Due to this reason, a direct comparison with the state of the art was not possible.

To evaluate our approach, we carefully studied all the papers showing LA regions without presenting any rationale to reach such results since the main objectives of their studies was different. in addition, we evaluated our approach by comparing its performance with the opinion of an expert electrophysiologist. Subsequently, the proposed approach has been tested and validated on variable LA anatomies to confirm the robustness of the proposed methodology.

Furthermore, to assess and quantify the global and regional mechanical functionality of LA in AF patients, several contraction parameters have been computed which have been able to signify LA dilation, dysfunctional global and regional contraction as well as heterogeneous contraction between LA regions when compared with healthy subjects.

As LAA is the primary site of the thrombus formation in AF. Therefore, to analyze the contractility of LAA, separate LAA contraction parameters have been defined and computed using patient-specific LAA anatomies. However, to define LAA contraction parameters, we have formulated a semi-automatic approach to define the LAA centerline which has been tested on standard LAA morphologies and served as a dynamic reference frame to define contraction parameters. Furthermore, this proposed centerline extraction approach can also be helpful to identify the landing zone in the occlusion procedure and to perform LAA analysis before the surgery.

The computed LAA contraction parameters have been able to identify the significance enlargment at the orifice of LAA and along longitudinal direction as well as it has signified dysfunctional contractility at the ostium of LAA in AF patients. In terms of regional analysis, it has demonstrated significant differences between healthy subjects and AF patients in certain regions, especially the regions which are closest and farthest from LA chamber.

For future persepective, these evaluated LA and LAA contraction parameters can play vital role to explore and understand the probability of clot formation within LA when used as boundary conditions to perform patient-specific realistic computational fluid dynamic simulations.

5 References

[1] L. E. Henault *et al.*, “Prevalence of Diagnosed Atrial Fibrillation in Adults,” *Jama*, vol. 285, no. 18, p. 2370, 2003.

[2] J. Andrade, P. Khairy, D. Dobrev, and S. Nattel, “The clinical profile and pathophysiology of atrial fibrillation: Relationships among clinical features, epidemiology, and mechanisms,” *Circ. Res.*, vol. 114, no. 9, pp. 1453–1468, 2014, doi: 10.1161/CIRCRESAHA.114.303211.

[3] A. J. Camm *et al.*, “Guidelines for the management of atrial fibrillation,” *Eur. Heart J.*, vol. 31, no. 19, pp. 2369–2429, 2010, doi: 10.1093/eurheartj/ehq278.

[4] D. D. McManus, M. Rienstra, and E. J. Benjamin, “An update on the prognosis of patients with atrial fibrillation,” *Circulation*, vol. 126, no. 10, 2012, doi: 10.1161/CIRCULATIONAHA.112.129759.

[5] F. Pistoia, S. Sacco, C. Tiseo, D. Degan, R. Ornello, and A. Carolei, “The Epidemiology of Atrial Fibrillation and Stroke,” *Cardiol. Clin.*, vol. 34, no. 2, pp. 255–268, 2016, doi: 10.1016/j.ccl.2015.12.002.

[6] T. Wilke *et al.*, “Incidence and prevalence of atrial fibrillation: An analysis based on 8.3 million patients,” *Europace*, vol. 15, no. 4, pp. 486–493, 2013, doi: 10.1093/europace/eus333.

[7] L. Staerk, J. A. Sherer, D. Ko, E. J. Benjamin, and R. H. Helm, “Atrial Fibrillation: Epidemiology, Pathophysiology, Clinical Outcomes,” *Circ. Res.*, vol. 120, no. 9, pp. 1501–1517, 2017, doi: 10.1161/CIRCRESAHA.117.309732.

[8] P. A. Wolf, R. D. Abbott, and W. B. Kannel, “Atrial fibrillation as an independent risk factor for stroke: The framingham study,” *Stroke*, vol. 22, no. 8, pp. 983–988, 1991, doi: 10.1161/01.STR.22.8.983.

[9] J. L. Dieleman *et al.*, “US Health Care Spending by Payer and Health Condition, 1996-2016,” *JAMA - J. Am. Med. Assoc.*, vol. 323, no. 9, pp. 863–884, 2020, doi: 10.1001/jama.2020.0734.

[10] N. F. Murphy *et al.*, “A national survey of the prevalence, incidence, primary care burden and treatment of atrial fibrillation in Scotland,” *Heart*, vol. 93, no. 5, pp. 606–612, 2007, doi: 10.1136/hrt.2006.107573.

[11] J. N. Ruskin and J. P. Singh, “Atrial fibrillation endpoints:

Hospitalization," *Hear. Rhythm*, vol. 1, no. 2 SUPPL., pp. 31–35, 2004, doi: 10.1016/j.hrthm.2004.04.004.

[12] M. Santini *et al.*, "Atrial fibrillation requiring urgent medical care. Approach and outcome in the various departments of admission. Data from the atrial Fibrillation/flutter Italian REgistry (FIRE)," *Ital. Hear. J.*, vol. 5, no. 3, pp. 205–213, 2004.

[13] V. Fuster and E. Al., *ACC/AHA/ESC guidelines for the management of patients with atrial fibrillation31This document was approved by the American College of Cardiology Board of Trustees in August 2001, the American Heart Association Science Advisory and Coordinating Committee i*, vol. 38, no. 4. 2001. doi: 10.1016/s0735-1097(01)01586-8.

[14] S. Y. Ho, K. P. McCarthy, and F. F. Faletra, "Anatomy of the left atrium for interventional echocardiography," *Eur. J. Echocardiogr.*, vol. 12, no. 10, pp. 11–15, 2011, doi: 10.1093/ejechocard/jer093.

[15] A. V. Mattioli, S. Sansoni, and G. R. Lucchi, "Serial evaluation of left atrial dimension after cardioversion for atrial fibrillation and relation to atrial function," *Am. J. Cardiol.*, vol. 85, no. 7, pp. 832–836, 2000, doi: 10.1016/S0002-9149(99)00876-0.

[16] M. Chard and R. Tabrizchi, "The role of pulmonary veins in atrial fibrillation: A complex yet simple story," *Pharmacol. Ther.*, vol. 124, no. 2, pp. 207–218, 2009, doi: 10.1016/j.pharmthera.2009.07.002.

[17] P. Sanders *et al.*, "Frequency mapping of the pulmonary veins in paroxysmal versus permanent atrial fibrillation," *J. Cardiovasc. Electrophysiol.*, vol. 17, no. 9, pp. 965–972, 2006, doi: 10.1111/j.1540-8167.2006.00546.x.

[18] A. Bittner *et al.*, "Pulmonary vein variants predispose to atrial fibrillation: A case-control study using multislice contrast-enhanced computed tomography," *Europace*, vol. 13, no. 10, pp. 1394–1400, 2011, doi: 10.1093/europace/eur145.

[19] R. J. Hunter *et al.*, "Impact of variant pulmonary vein anatomy and image integration on long-term outcome after catheter ablation for atrial fibrillation," *Europace*, vol. 12, no. 12, pp. 1691–1697, 2010, doi: 10.1093/europace/euq322.

[20] W. Wang, D. Buehler, A. Hamzei, X. Wang, and X. Yuan,

"Comprehensive surgical approach to treat atrial fibrillation in patients with variant pulmonary venous anatomy," *J. Thorac. Cardiovasc. Surg.*, vol. 145, no. 3, pp. 790–795, 2013, doi: 10.1016/j.jtcvs.2012.03.019.

[21] W. A. McAlpine, "Heart and Coronary Arteries," *Heart and Coronary Arteries*. 1975. doi: 10.1007/978-3-642-65983-6.

[22] H. M. Tsao *et al.*, "Quantitative analysis of quantity and distribution of epicardial adipose tissue surrounding the left atrium in patients with atrial fibrillation and effect of recurrence after ablation," *Am. J. Cardiol.*, vol. 107, no. 10, pp. 1498–1503, 2011, doi: 10.1016/j.amjcard.2011.01.027.

[23] G. M. Marcus *et al.*, "Regional left atrial voltage in patients with atrial fibrillation," *Hear. Rhythm*, vol. 4, no. 2, pp. 138–144, 2007, doi: 10.1016/j.hrthm.2006.10.017.

[24] G. Ndrepepa *et al.*, "Impact of atrial fibrillation on the voltage of bipolar signals acquired from the left and right atria," *PACE - Pacing Clin. Electrophysiol.*, vol. 26, no. 4, pp. 862–869, 2003, doi: 10.1046/j.1460-9592.2003.t01-1-00151.x.

[25] Y. Takahashi *et al.*, "Effects of Stepwise Ablation of Chronic Atrial Fibrillation on Atrial Electrical and Mechanical Properties," *J. Am. Coll. Cardiol.*, vol. 49, no. 12, pp. 1306–1314, 2007, doi: 10.1016/j.jacc.2006.11.033.

[26] Y. Lin *et al.*, "Comparison of left atrial electrophysiologic abnormalities during sinus rhythm in patients with different type of atrial fibrillation," *J. Interv. Card. Electrophysiol.*, vol. 39, no. 1, pp. 57–67, 2014, doi: 10.1007/s10840-013-9838-y.

[27] R. Starreveld, L. J. M. E. Van Der Does, and N. M. S. De Groot, "Anatomical hotspots of fractionated electrograms in the left and right atrium: Do they exist?," *Eur. Soc. Cardiol.*, vol. 21, no. 1, pp. 60–72, 2019, doi: 10.1093/europace/euy059.

[28] C. Tobon-Gomez *et al.*, "Standardised unfold map of the left atrium: regional definition for multimodal image analysis," *J. Cardiovasc. Magn. Reson.*, vol. 17, no. S1, pp. 1–3, 2015, doi: 10.1186/1532-429x-17-s1-p41.

[29] Y. L. Chen, J. E. Ban, Y. M. Park, J. Il Choi, S. W. Park, and Y. H. Kim, "The spatial distribution of atrial fibrillation termination sites in the right atrium during complex fractionated atrial electrograms-

guided ablation in patients with persistent atrial fibrillation," *J. Cardiovasc. Electrophysiol.*, vol. 24, no. 9, pp. 949–957, 2013, doi: 10.1111/jce.12187.

[30] R. Kogawa *et al.*, "Left atrial remodeling: Regional differences between paroxysmal and persistent atrial fibrillation," *J. Arrhythmia*, vol. 33, no. 5, pp. 483–487, 2017, doi: 10.1016/j.joa.2017.06.001.

[31] F. Alarco *et al.*, "Preferential regional distribution of atrial fibrosis in posterior wall around left inferior pulmonary vein as identified by late gadolinium enhancement cardiac magnetic resonance in patients with atrial fibrillation," pp. 1–7, 2018, doi: 10.1093/europace/euy095.

[32] S. Kapa, B. Desjardins, D. J. Callans, F. E. Marchlinski, and S. Dixit, "Contact electroanatomic mapping derived voltage criteria for characterizing left atrial scar in patients undergoing ablation for atrial fibrillation," *J. Cardiovasc. Electrophysiol.*, vol. 25, no. 10, pp. 1044–1052, 2014, doi: 10.1111/jce.12452.

[33] K. Kumagai, K. Minami, D. Kutsuzawa, and S. Oshima, "Evaluation of the characteristics of rotational activation at high-dominant frequency and complex fractionated atrial electrogram sites during atrial fibrillation," *J. Arrhythmia*, vol. 33, no. 1, pp. 49–55, 2017, doi: 10.1016/j.joa.2016.05.008.

[34] Y. Nakatani, T. Sakamoto, Y. Yamaguchi, Y. Tsujino, N. Kataoka, and K. Kinugawa, "P-wave vector magnitude predicts the left atrial low-voltage area in patients with paroxysmal atrial fibrillation," *J. Electrocardiol.*, vol. 59, pp. 35–40, 2020, doi: 10.1016/j.jelectrocard.2019.12.015.

[35] R. J. Hunter *et al.*, "Characterization of fractionated atrial electrograms critical for maintenance of atrial fibrillation a randomized, controlled trial of ablation strategies (the CFAE AF trial)," *Circ. Arrhythmia Electrophysiol.*, vol. 4, no. 5, pp. 622–629, 2011, doi: 10.1161/CIRCEP.111.962928.

[36] M. Haissaguerre *et al.*, "Driver domains in persistent atrial fibrillation," *Circulation*, vol. 130, no. 7, pp. 530–538, 2014, doi: 10.1161/CIRCULATIONAHA.113.005421.

[37] R. Karim *et al.*, "Surface flattening of the human left atrium and proof-of-concept clinical applications," *Comput. Med. Imaging*

Graph., vol. 38, no. 4, pp. 251–266, 2014, doi: 10.1016/j.compmedimag.2014.01.004.

[38] A. Yagishita *et al.*, "Correlation of Left Atrial Voltage Distribution Between Sinus Rhythm and Atrial Fibrillation: Identifying Structural Remodeling by 3-D Electroanatomic Mapping Irrespective of the Rhythm," *J. Cardiovasc. Electrophysiol.*, vol. 27, no. 8, pp. 905–912, 2016, doi: 10.1111/jce.13002.

[39] A. W. Teh *et al.*, "Electroanatomic remodeling of the left atrium in paroxysmal and persistent atrial fibrillation patients without structural heart disease," *J. Cardiovasc. Electrophysiol.*, vol. 23, no. 3, pp. 232–238, 2012, doi: 10.1111/j.1540-8167.2011.02178.x.

[40] C. B. Moyer *et al.*, "Wall-motion based analysis of global and regional left atrial mechanics," *IEEE Trans. Med. Imaging*, vol. 32, no. 10, pp. 1765–1776, 2013, doi: 10.1109/TMI.2013.2264062.

[41] M. Nunez-Garcia *et al.*, "Fast Quasi-Conformal Regional Flattening of the Left Atrium," *IEEE Trans. Vis. Comput. Graph.*, vol. 26, no. 8, pp. 2591–2602, 2020, doi: 10.1109/TVCG.2020.2966702.

[42] A. Marui *et al.*, "Impact of left atrial volume reduction concomitant with atrial fibrillation surgery on left atrial geometry and mechanical function," *J. Thorac. Cardiovasc. Surg.*, vol. 135, no. 6, pp. 1297–1305, 2008, doi: 10.1016/j.jtcvs.2008.02.026.

[43] O. Rodevand, R. Bjornerheim, M. Ljosland, J. Maehle, H. J. Smith, and H. Ihlen, "Left atrial volumes assessed by three- and two-dimensional echocardiography compared to MRI estimates," *Int. J. Card. Imaging*, vol. 15, no. 5, pp. 397–410, 1999, doi: 10.1023/A:1006276513186.

[44] L. Thomas, K. Levett, A. Boyd, D. Y. C. Leung, N. B. Schiller, and D. L. Ross, "Changes in regional left atrial function with aging: Evaluation by doppler tissue imaging," *Eur. J. Echocardiogr.*, vol. 4, no. 2, pp. 92–100, 2003, doi: 10.1053/euje.2002.0622.

[45] P. Kuklik *et al.*, "Quantitative description of the 3D regional mechanics of the left atrium using cardiac magnetic resonance imaging," *Physiol. Meas.*, vol. 35, no. 5, pp. 763–775, 2014, doi: 10.1088/0967-3334/35/5/763.

[46] P. Kuklik, P. Molaee, A. G. Brooks, B. John, S. G. Worthley, and P. Sanders, "Quantitative description of the regional mechanics of

the left atria by electroanatomical mapping," *Physiol. Meas.*, vol. 31, no. 4, pp. 555–564, 2010, doi: 10.1088/0967-3334/31/4/007.

[47] C. B. Moyer, P. T. Norton, J. D. Ferguson, and J. W. Holmes, "Changes in Global and Regional Mechanics Due to Atrial Fibrillation: Insights from a Coupled Finite-Element and Circulation Model," *Ann. Biomed. Eng.*, vol. 43, no. 7, pp. 1600–1613, 2015, doi: 10.1007/s10439-015-1256-0.

[48] N. M. Al-Saady, O. A. Obel, and A. J. Camm, "Left atrial appendage: Structure, function, and role in thromboembolism," *Heart*, vol. 82, no. 5, pp. 547–554, 1999, doi: 10.1136/hrt.82.5.547.

[49] S. Saygi, "Atrial fibrillation and the role of LAA in pathophysiology and clinical outcomes?," *J. Atr. Fibrillation*, vol. 5, no. 3, pp. 153–160, 2012.

[50] R. Mahajan *et al.*, "Importance of the underlying substrate in determining thrombus location in atrial fibrillation: Implications for left atrial appendage closure," *Heart*, vol. 98, no. 15, pp. 1120–1126, 2012, doi: 10.1136/heartjnl-2012-301799.

[51] L. Di Biase *et al.*, "Does the left atrial appendage morphology correlate with the risk of stroke in patients with atrial fibrillation? Results from a multicenter study," *J. Am. Coll. Cardiol.*, vol. 60, no. 6, pp. 531–538, 2012, doi: 10.1016/j.jacc.2012.04.032.

[52] D. Vella, A. Monteleone, G. Musotto, G. M. Bosi, and G. Burriesci, "Effect of the Alterations in Contractility and Morphology Produced by Atrial Fibrillation on the Thrombosis Potential of the Left Atrial Appendage," *Front. Bioeng. Biotechnol.*, vol. 9, no. February, pp. 1–11, 2021, doi: 10.3389/fbioe.2021.586041.

[53] D. Y. Leung, A. Boyd, and B. M. S. Hons, "Echocardiographic evaluation of left atrial size and function : Current understanding , pathophysiologic correlates , and prognostic implications," *Am. Heart J.*, vol. 156, no. 6, pp. 1056–1064, 2008, doi: 10.1016/j.ahj.2008.07.021.

[54] G. E. Farese, B. Tayal, S. Stöbe, U. Laufs, and A. Hagendorff, "Regional Disparities of Left Atrial Appendage Wall Contraction in Patients With Sinus Rhythm and Atrial Fibrillation," *J. Am. Soc. Echocardiogr.*, vol. 32, no. 6, pp. 755–762, 2019, doi: 10.1016/j.echo.2019.01.016.

[55] B. D. Hoit, "Left Atrial Size and Function Role in Prognosis," *J.*

Am. Coll. Cardiol., vol. 63, no. 6, pp. 493–505, 2014, doi: 10.1016/j.jacc.2013.10.055.

[56] G. Lippi, F. Sanchis-Gomar, and G. Cervellin, "Global epidemiology of atrial fibrillation: An increasing epidemic and public health challenge," *Int. J. Stroke*, vol. 16, no. 2, pp. 217–221, 2021, doi: 10.1177/1747493019897870.

[57] R. S. Phang *et al.*, "Echocardiographic evidence of left atrial abnormality in young patients with lone paroxysmal atrial fibrillation," *Am. J. Cardiol.*, vol. 94, no. 4, pp. 511–513, 2004, doi: 10.1016/j.amjcard.2004.05.009.

[58] D. P. Zipes, "Atrial fibrillation: From cell to bedside," *J. Cardiovasc. Electrophysiol.*, vol. 8, no. 8, pp. 927–938, 1997, doi: 10.1111/j.1540-8167.1997.tb00855.x.

[59] A. Nemes, P. Domsik, A. Kalapos, and T. Forster, "Is three-dimensional speckle-tracking echocardiography able to identify different patterns of left atrial dysfunction in selected disorders?: Short summary of the MAGYAR-Path Study," *Int. J. Cardiol.*, vol. 220, pp. 535–537, 2016, doi: 10.1016/j.ijcard.2016.06.122.

[60] K. Havasi *et al.*, "Left Atrial Deformation Analysis in Patients with Corrected Tetralogy of Fallot by 3D Speckle-Tracking Echocardiography (from the MAGYAR-Path Study)," *Arq. Bras. Cardiol.*, vol. 108, no. 2, pp. 129–134, 2017, doi: 10.5935/abc.20170004.

[61] P. Reant *et al.*, "Reverse remodeling of the left cardiac chambers after catheter ablation after 1 year in a series of patients with isolated atrial fibrillation," *Circulation*, vol. 112, no. 19, pp. 2896–2903, 2005, doi: 10.1161/CIRCULATIONAHA.104.523928.

[62] L. C. Prasanna, R. Praveena, A. S. D'Souza, and K. M. R. Bhat, "Variations in the pulmonary venous ostium in the left atrium and its clinical importance," *J. Clin. Diagnostic Res.*, vol. 8, no. 2, pp. 10–11, 2014, doi: 10.7860/JCDR/2014/7649.3992.

[63] T. F. Chan and L. A. Vese, "Active contours without edges," *IEEE Trans. Image Process.*, vol. 10, no. 2, pp. 266–277, 2001, doi: 10.1109/83.902291.

[64] Autodesk Meshmixer, "Meshmixer 3.5." [Online]. Available: http://www.meshmixer.com

[65] R. Kato *et al.*, “Pulmonary vein anatomy in patients undergoing catheter ablation of atrial fibrillation: Lessons learned by use of magnetic resonance imaging,” *Circulation*, vol. 107, no. 15, pp. 2004–2010, 2003, doi: 10.1161/01.CIR.0000061951.81767.4E.

[66] C. Corsi *et al.*, “Volumetric quantification of global and regional left ventricular function from real-time three-dimensional echocardiographic images,” *Circulation*, vol. 112, no. 8, pp. 1161–1170, 2005, doi: 10.1161/CIRCULATIONAHA.104.513689.

[67] L. Chen *et al.*, “Left atrial strain measured by 4D Auto LAQ echocardiography is significantly correlated with high risk of thromboembolism in patients with non-valvular atrial fibrillation,” *Quant. Imaging Med. Surg.*, vol. 11, no. 9, pp. 3920–3931, 2021, doi: 10.21037/qims-20-1381.

[68] M. D. Cerqueira *et al.*, “Standardized myocardial sementation and nomenclature for tomographic imaging of the heart: A Statement for Healthcare Professionals from the Cardiac Imaging Committee of the Council on Clinical Cardiology of the American Heart Association,” *Circulation*, vol. 105, no. 4, pp. 539–542, 2002, doi: 10.1161/hc0402.102975.

[69] S. E. Williams *et al.*, “Standardized unfold mapping: a technique to permit left atrial regional data display and analysis,” *J. Interv. Card. Electrophysiol.*, vol. 50, no. 1, pp. 125–131, 2017, doi: 10.1007/s10840-017-0281-3.

[70] Y. Hori *et al.*, “Influence of left atrium anatomical contact area in persistent atrial fibrillation - Relationship between low-voltage area and fractionated electrogram,” *Circ. J.*, vol. 78, no. 8, pp. 1851–1857, 2014, doi: 10.1253/circj.CJ-14-0440.

[71] Y. Coudière, V. Ozenne, and D. Hutchison, *Functional Imaging and Modeling of the Heart 2019 Proceedings*, no. June. 2019.

[72] A. Wachter, A. Loewe, M. W. Krueger, O. Dössel, and G. Seemann, “Mesh structure-independent modeling of patient-specific atrial fiber orientation,” *Curr. Dir. Biomed. Eng.*, vol. 1, no. 1, pp. 409–412, 2015, doi: 10.1515/cdbme-2015-0099.

[73] G. R. Wong *et al.*, “Sex-Related Differences in Atrial Remodeling in Patients with Atrial Fibrillation: Relationship to Ablation Outcomes,” *Circ. Arrhythmia Electrophysiol.*, vol. 15, no. 1, p. E009925, 2022, doi: 10.1161/CIRCEP.121.009925.

[74] O. Razeghi *et al.*, “Fully Automatic Atrial Fibrosis Assessment Using a Multilabel Convolutional Neural Network,” *Circ. Cardiovasc. Imaging*, vol. 13, no. 12, p. E011512, 2020, doi: 10.1161/CIRCIMAGING.120.011512.

[75] S. Prabhu *et al.*, “A comparison of the electrophysiologic and electroanatomic characteristics between the right and left atrium in persistent atrial fibrillation: Is the right atrium a window into the left?,” *J. Cardiovasc. Electrophysiol.*, vol. 28, no. 10, pp. 1109–1116, 2017, doi: 10.1111/jce.13297.

[76] R. Piersanti *et al.*, “Modeling cardiac muscle fibers in ventricular and atrial electrophysiology simulations,” *Comput. Methods Appl. Mech. Eng.*, vol. 373, p. 113468, 2021, doi: 10.1016/j.cma.2020.113468.

[77] J. A. Solís-Lemus *et al.*, “Evaluation of an open-source pipeline to create patient-specific left atrial models: A reproducibility study,” *Comput. Biol. Med.*, vol. 162, no. May, p. 107009, 2023, doi: 10.1016/j.compbiomed.2023.107009.

[78] T. Wang *et al.*, “Standardized 2D atrial mapping and its clinical applications,” *Comput. Biol. Med.*, vol. 168, no. November 2023, p. 107755, 2024, doi: 10.1016/j.compbiomed.2023.107755.

[79] L. Azzolin *et al.*, “AugmentA: Patient-specific augmented atrial model generation tool,” *Comput. Med. Imaging Graph.*, vol. 108, no. September 2022, 2023, doi: 10.1016/j.compmedimag.2023.102265.

[80] T. Zheng, L. Azzolin, J. Sánchez, O. Dössel, and A. Loewe, “An automate pipeline for generating fiber orientation and region annotation in patient specific atrial models,” *Curr. Dir. Biomed. Eng.*, vol. 7, no. 2, pp. 136–139, 2021, doi: 10.1515/cdbme-2021-2035.

[81] C. Goetz *et al.*, “Discrepancy between LGE-MRI and Electro-Anatomical Mapping for Regional Detection of Pathological Atrial Substrate,” *Curr. Dir. Biomed. Eng.*, vol. 9, no. 1, pp. 483–486, 2023, doi: 10.1515/cdbme-2023-1121.

[82] C. H. Roney *et al.*, “Universal atrial coordinates applied to visualisation, registration and construction of patient specific meshes,” *Med. Image Anal.*, vol. 55, pp. 65–75, 2019, doi: 10.1016/j.media.2019.04.004.

[83] Y. Nabeshima, T. Kitano, and M. Takeuchi, “Reliability of left atrial strain reference values: A 3D echocardiographic study,” *PLoS One*, vol. 16, no. 4 April, pp. 1–18, 2021, doi: 10.1371/journal.pone.0250089.

[84] A. Mochizuki *et al.*, “Assessment of left atrial deformation and synchrony by three-dimensional speckle-tracking echocardiography: Comparative studies in healthy subjects and patients with atrial fibrillation,” *J. Am. Soc. Echocardiogr.*, vol. 26, no. 2, pp. 165–174, 2013, doi: 10.1016/j.echo.2012.10.003.

[85] A. B. Nielsen *et al.*, “Normal values and reference ranges for left atrial strain by speckle-tracking echocardiography: the Copenhagen City Heart Study,” *Eur. Heart J. Cardiovasc. Imaging*, vol. 23, no. 1, pp. 42–51, 2022, doi: 10.1093/ehjci/jeab201.

[86] A. Masci, L. Barone, L. Dedè, M. Fedele, C. Tomasi, and C. P. Bradley, “The Impact of Left Atrium Appendage Morphology on Stroke Risk Assessment in Atrial Fibrillation : A Computational Fluid Dynamics Study,” vol. 9, no. January, pp. 1–11, 2019, doi: 10.3389/fphys.2018.01938.

[87] W. Aschenberg, M. Schlüter, P. Kremer, E. Schröder, V. Siglow, and W. Bleifeld, “Transesophageal two-dimensional echocardiography for the detection of left atrial appendage thrombus,” *J. Am. Coll. Cardiol.*, vol. 7, no. 1, pp. 163–166, 1986, doi: 10.1016/S0735-1097(86)80275-3.

[88] J. L. Blackshear, J. A. Odell, and F. Ed, “Appendage Obliteration to Reduce Stroke in Cardiac Surgical Patients With Atrial Fibrillation,” 1996.

[89] W. D. Johnson, A. K. Ganjoo, C. D. Stone, R. C. Srivyas, and M. Howard, “The left atrial appendage: Our most lethal human attachment! Surgical implications,” *Eur. J. Cardio-thoracic Surg.*, vol. 17, no. 6, pp. 718–722, 2000, doi: 10.1016/S1010-7940(00)00419-X.

[90] R. Beigel, N. C. Wunderlich, S. Y. Ho, R. Arsanjani, and R. J. Siegel, “The left atrial appendage: Anatomy, function, and noninvasive evaluation,” *JACC Cardiovasc. Imaging*, vol. 7, no. 12, pp. 1251–1265, 2014, doi: 10.1016/j.jcmg.2014.08.009.

[91] L. Di Biase *et al.*, “Stroke Risk in Patients With Atrial Fibrillation Undergoing Electrical Isolation of the Left Atrial Appendage,” *J.*

Am. Coll. Cardiol., vol. 74, no. 8, pp. 1019–1028, 2019, doi: 10.1016/j.jacc.2019.06.045.

[92] Y. Wang, L. Di Biase, R. P. Horton, T. Nguyen, P. Morhanty, and A. Natale, "Left atrial appendage studied by computed tomography to help planning for appendage closure device placement," *J. Cardiovasc. Electrophysiol.*, vol. 21, no. 9, pp. 973–982, 2010, doi: 10.1111/j.1540-8167.2010.01814.x.

[93] M. Koplay, C. Erol, Y. Paksoy, A. S. Kivrak, and S. Özbek, "An investigation of the anatomical variations of left atrial appendage by multidetector computed tomographic coronary angiography," *Eur. J. Radiol.*, vol. 81, no. 7, pp. 1575–1580, 2012, doi: 10.1016/j.ejrad.2011.04.060.

[94] A. W. Shi, M. L. Chen, B. Yang, K. J. Cao, and X. Q. Kong, "A morphological study of the left atrial appendage in Chinese patients with atrial fibrillation," *J. Int. Med. Res.*, vol. 40, no. 4, pp. 1560–1567, 2012, doi: 10.1177/147323001204000436.

[95] D. S. Beutler, R. D. Gerkin, and A. I. Loli, "The Morphology of Left Atrial Appendage Lobes: A Novel Characteristic Naming Scheme Derived through Three-Dimensional Cardiac Computed Tomography," *World J. Cardiovasc. Surg.*, vol. 04, no. 03, pp. 17–24, 2014, doi: 10.4236/wjcs.2014.43004.

[96] G. Ernst *et al.*, "Morphology of the left atrial appendage," *Anat. Rec.*, vol. 242, no. 4, pp. 553–561, 1995, doi: 10.1002/ar.1092420411.

[97] J. M. Lee *et al.*, "Why is left atrial appendage morphology related to strokes? an analysis of the flow velocity and orifice size of the left atrial appendage," *J. Cardiovasc. Electrophysiol.*, vol. 26, no. 9, pp. 922–927, 2015, doi: 10.1111/jce.12710.

[98] X. Tian, X. J. Zhang, Y. F. Yuan, C. Y. Li, L. X. Zhou, and B. L. Gao, "Morphological and functional parameters of left atrial appendage play a greater role in atrial fibrillation relapse after radiofrequency ablation," *Sci. Rep.*, vol. 10, no. 1, pp. 1–10, 2020, doi: 10.1038/s41598-020-65056-3.

[99] L. Chen, C. Xu, W. Chen, and C. Zhang, "Left atrial appendage orifice area and morphology is closely associated with flow velocity in patients with nonvalvular atrial fibrillation," *BMC Cardiovasc. Disord.*, vol. 21, no. 1, pp. 1–13, 2021, doi:

10.1186/s12872-021-02242-9.

[100] G. Vivoli *et al.*, “Simultaneous Functional and Morphological Assessment of Left Atrial Appendage by 3D Virtual Models,” *J. Healthc. Eng.*, vol. 2019, 2019, doi: 10.1155/2019/7095845.

[101] B. M. Fanni *et al.*, “Correlation between LAA morphological features and computational fluid dynamics analysis for non-valvular atrial fibrillation patients,” *Appl. Sci.*, vol. 10, no. 4, 2020, doi: 10.3390/app10041448.

[102] I. Genua *et al.*, “Centreline-Based Shape Descriptors of the Left Atrial Appendage in Relation with Thrombus Formation,” *Lect. Notes Comput. Sci. (including Subser. Lect. Notes Artif. Intell. Lect. Notes Bioinformatics)*, vol. 11395 LNCS, pp. 200–208, 2019, doi: 10.1007/978-3-030-12029-0_22.

[103] M. Unser, “Splines: A perfect fit for signal and image processing,” *IEEE Signal Process. Mag.*, vol. 16(6), no. NOVEMBER, pp. 22–38, 1999.

[104] A. Masci *et al.*, “A Proof of concept for computational fluid dynamic analysis of the left atrium in atrial fibrillation on a patient-specific basis,” *J. Biomech. Eng.*, vol. 142, no. 1, pp. 1–11, 2020, doi: 10.1115/1.4044583.

[105] G. García-Isla *et al.*, “Sensitivity analysis of geometrical parameters to study haemodynamics and thrombus formation in the left atrial appendage,” *Int. j. numer. method. biomed. eng.*, vol. 34, no. 8, pp. 1–14, 2018, doi: 10.1002/cnm.3100.

[106] K. K. Kadappu and L. Thomas, “Tissue doppler imaging in echocardiography: Value and limitations,” *Hear. Lung Circ.*, vol. 24, no. 3, pp. 224–233, 2015, doi: 10.1016/j.hlc.2014.10.003.

[107] J. Liu and K. Subramanian, “Accurate and Robust Centerline Extraction,” *Advances*, pp. 139–162, 2009.

[108] M. Zoni-Berisso, F. Lercari, T. Carazza, and S. Domenicucci, “Epidemiology of atrial fbrillation: European perspective,” *Clin. Epidemiol.*, vol. 6, no. 1, pp. 213–220, 2014, doi: 10.2147/CLEP.S47385.

6 Conference papers and abstracts

Regional Segmentation of the Left Atrium: A Preliminary Test in Atrial Fibrillation Patients

Sachal Hussain[1], Matteo Falanga[1], Claudio Fabbri[1], Cristiana Corsi[1]

[1] DEI, University of Bologna, Campus of Cesena, Bologna, Italy

Abstract

Differently from the left ventricle, the regional segmentation of the left atrium (LA) is still a matter of investigation, having the LA attracted the interest of the scientific community only recently. In this study, a new automatic approach for LA regional segmentation was proposed. An approach to divide left atrium into well-defined anatomical regions to better evaluate the effects of AF on different regions of left atrium is proposed. Up to now, we have tested this approach on 10 AF patients. Our algorithm rightly divides the LA in all the 10 patients and in future, these anatomical regions can be helpful to assess the deformation of left atrial tissues in different parts of LA.

1. Introduction

Atrial fibrillation (AF) is known to interfere with the normal mechanical functioning of the atrium, and its effects on cardiac function may persist even when patients are in sinus rhythm. Studies have shown that dilatation of the atrium occurs early in AF and is related to cardiovascular morbidity and mortality [1]. Contractile and structural remodeling also occur in AF, leading to significant fibrosis, hypertrophy and myolysis; reduced left atrial (LA) contractility and impaired transport function [2]. Relatively few studies have formally examined the effect of AF on atrial function. Several reports have shown a decreased LA ejection fraction in patients with AF [3].

Moreover, frequent AF episodes damage LA tissue by causing electrical and structural remodeling [4]. This spatial variation in remodeling creates regional heterogeneity in both structure and function. Structural heterogeneity also arises from catheter ablation, which permanently scars atrial tissue. Given the limitations of anti-arrhythmic drugs [5], catheter ablation has become the primary AF therapy [6] and has been proposed as a first-line treatment [7]. Pulmonary vein isolation (PVI) has become an accepted treatment for AF [8]. The efficacy of PVI is sometimes insufficient, and atrial substrate modification of target specific AF signals indicating the substrate responsible for AF perpetuation has been proposed [9,10]. Complex fractionated atrial electrograms (CFAEs), which are electrograms that demonstrate continuous fractionation and very short cycle lengths during AF, may represent the substrate of AF [9,10]. In addition, atrial sites that represent local electrograms with high-dominant frequencies (DFs) may be associated with AF maintenance [11-13].

We hypothesize that, in such scenario, the integration of regional structural and functional information may improve the characterization of AF mechanisms. Unfortunately, the regional segmentation of the LA chamber is still a matter of investigation and no recommendation suggesting a standard approach exists. In this paper, we propose a new approach to automatically divide the LA into seven well defined regions, which are, anterior, posterior, roof, inferior, lateral, septal and LAA, and these regions can be used to evaluate the regional mechanics of the LA in AF patients.

2. Material and Methods

2.1. Image acquisition

CT imaging data of the LA were acquired in sinus rhythm from a Philips Brilliance 64 CT scanner (200 axial slices, 0.4 mm x 0.4 mm pixel size, 1 mm slice thickness).

2.2. Image segmentation

To segment the DICOM data obtained from CT and define the LA anatomical model, we used an active contour algorithm previously developed in Matlab environment. First, we restricted the segmentation to LA only by defining a region of interest (ROI) and then initialized active contour and stopped the evolution

when the LA came inside the contour. At the end, we saved the resulted surface in stereolithography (STL) format.

2.3. Post processing of surfaces

Before starting the regional segmentation, we applied Laplacian smoothing on the LA surfaces and defined cutting planes on all the four pulmonary veins (PVs) and on the mitral valve (MV). For this purpose, we used the open-source Autodesk Meshmixer software. We manually applied cutting planes to exclude tissues from PVs and to get ostium for PVs and MV. Figure 1 shows the output surface resulting from the post-processing in one patient.

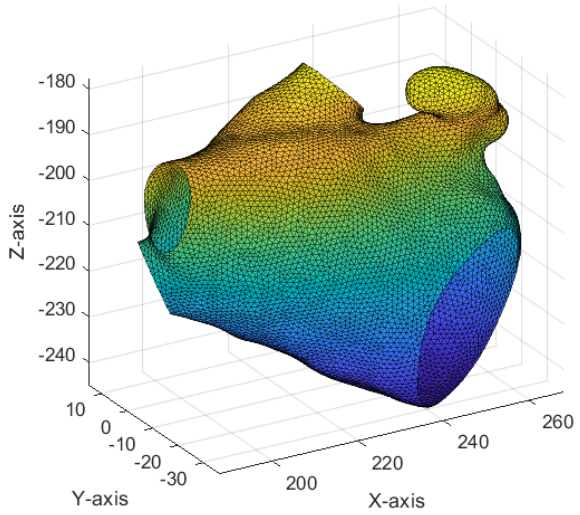

Figure 1. Anterior view of LA anatomical model

2.4. Regional segmentation of Left Atrium

In the first step of the regional segmentation, we excluded the left atrial appendage (LAA) from the LA applying a thresholding approach based on the shape diameter function. [14]. Then the algorithm calculated the barycenter of all the four PVs, the MV and the LAA, and then the weighted barycenter of PVs by considering their area. The latter identified the MV by considering its area as well as its location: we assumed that MV has the biggest area amongst all the openings, and its barycenter is the farthest one.

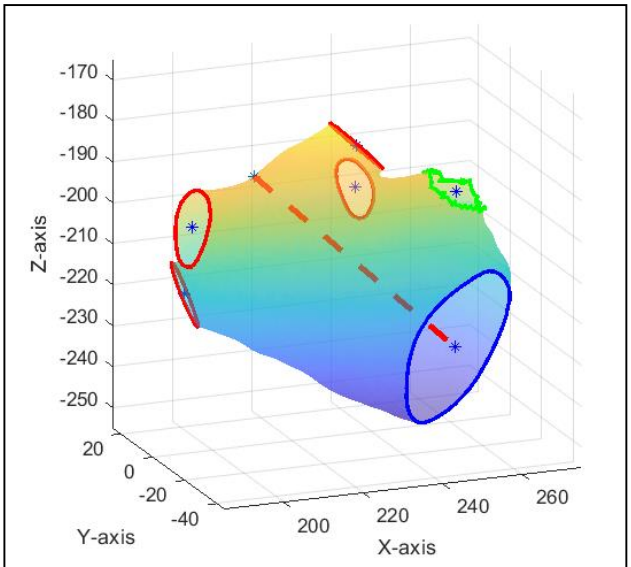

Figure 2. Long axis is represented by the red dotted line which connects MV barycenter with the PVs weighted barycenter. The PVs ostium is in red, the MV ostium is in blue and the LAA ostium is in green.

We drew the long axis of LA by connecting the barycenter of MV and the weighted barycenter of PVs. Long axis is an important parameter because whenever we draw a line in space, we project that line onto the LA in the direction of long axis. The long axis can be

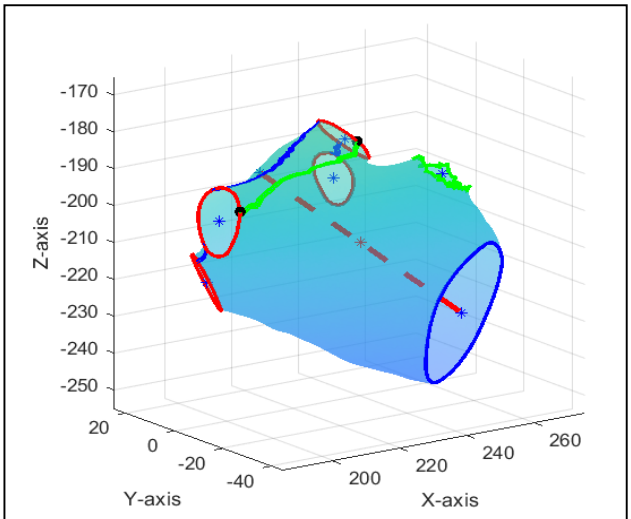

Figure 3. The green line is the new projection line that, together with the blue line above, define the roof.

seen in figure 2 as the red dotted line.

To distinguish the barycenter of each PV, we manually identified the barycenter of the left superior pulmonary vein (LSPV) and with respect to this, our algorithm automatically identified the barycenter of left inferior pulmonary vein (LIPV), right superior pulmonary vein (RSPV) and right inferior pulmonary vein (RIPV).

To initiate regionalization, we connected LSPV and LIPV barycenters, then the barycenters of LSPV and RSPV and finally the barycenter of RSPV to the barycenter of RIPV, these lines (blue lines in figure 3 were projected onto the LA surface in the direction of the midpoint of long axis.

To define the roof region, we drew a line connecting the barycenter of RSPV and the point on the ostium of RSPV generated by the projection of the line connecting the barycenters of RSPV and LSPV. Then we rotated this line 90 degrees in clockwise direction and received a second point on the ostium of RSPV (black points in figure 3). We implemented the same approach on the LSPV but rotated the line by 90 degrees in counterclockwise direction. By doing this, we generated two new points on the ostium of RSPV & LSPV and by connecting them we obtained a new projection line that defines the roof region as shown in figure 3.

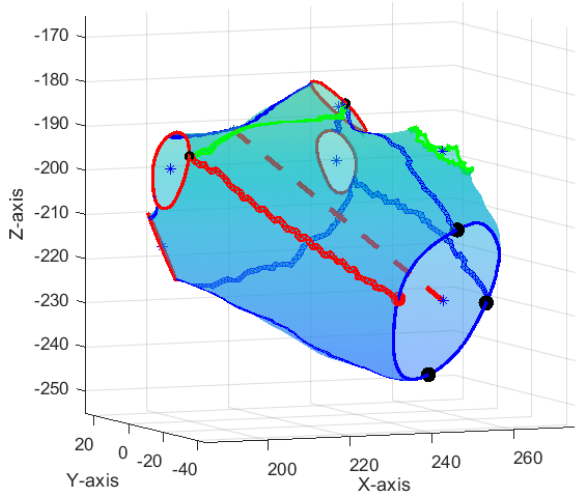

Figure 4. Three new points on the MV ostium in black and the projections in blue to the respective PVs. The red point is generated by connecting the second point on the RSPV ostium with the MV barycenter.

To draw the boundaries between anterior and septal regions (red line in figure 4), we connected the second point on the ostium of RSPV to the barycenter of MV. By doing this, we found one point on the MV ostium (red point) and, by rotating this point in clockwise direction at [90 90 90] angles, we generated three more points on the MV ostium as shown in figure 4. Finally, we connected these three points to the barycenter of LSPV, LIPV and RIPV respectively defining three other regions, which are septal, anterior, and lateral.

To draw the boundaries between posterior and inferior regions, we took the points previously obtained on the ostium of LIPV and RIPV and connected them with a straight line. Then we projected the line onto the LA surface in the direction of midpoint of long axis. Moreover, the LAA was treated as a different region from the rest of LA.

By applying this approach, we labelled seven well defined regions, namely posterior, anterior, roof, inferior, lateral, septal and LAA.

3. Results

In our study, we considered 10 AF patients in which the size and the anatomical structure of the PVs varied as well as the location of the LAA, but still the algorithm ran on all cases and successfully divided the LA into seven regions. Figure 5 shows the final segmentation of LA.
An expert electrophysiologist graded the result of regional segmentation as: unacceptable, poor, fair and good. The grading of the expert was fair and good in 3 and 7 patients, respectively.

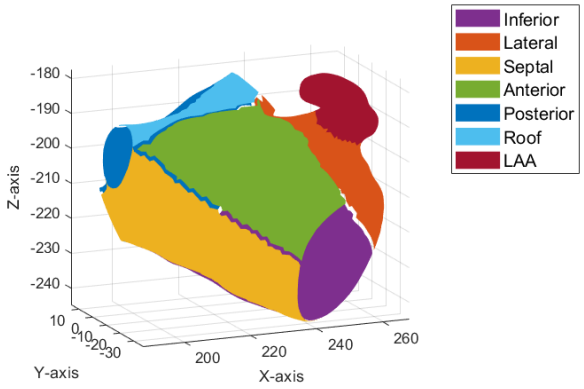

Figure 5. Final regional segmentation of LA.

4. Discussion

This study presents a new approach to automatically divide the LA into seven anatomical regions.

It represents a first step towards the quantification of regional functional and contraction indices of the LA. By considering these regions, different mechanical

functions of LA can be evaluated separately. This approach can also be helpful to monitor regional mechanics during catheter ablation procedures. Also, using this algorithm, it is possible to 3D print individual regions of LA to perform surgical simulation as well as to understand and elaborate structural remodeling of different regions of LA.

Our approach successfully faced the variability in LA anatomy in the 10 patients we enrolled. However further testing is required to confirm these results. We hypothesize the results are dependent on the anatomy, in particular, of PVs. In some cases, we found that left PVs are very close to each other and form a common trunk and, for a very few cases, it also happened for the right PVs. But our algorithm was always able to distinguish each PV and proceeded to calculate their barycenter. Regarding the number of PVs, our algorithm provides well-defined regions when the number is four, which is the most common case but, if the number varies, it may require manual correction to proceed to the identification of different regions.

Localization of the LAA is also one of the crucial tasks since, in AF cases, most of the times blood clots originate in the LAA. The position of the LAA depends on the ostium and the barycenter of LAA. We designed our algorithm so that, if the ostium is totally included in the lateral wall, then the LAA belongs to lateral region. On the other hand, if the ostium is completely on the anterior wall, which is rare, then the LAA will be included in the anterior region. In other cases, if the barycenter of LAA lies on the border of anterior and lateral regions, then it will be partially included in both regions.

5. Conclusion

To conclude, the approach presented in this paper can automatically divide the LA into seven well defined anatomical regions which also includes LAA, PVs and MV and these regions can be used to assess and quantify regional functioning of LA.

Acknowledgments

We would like to thank Dott. Corrado Tomasi for reviewing the regional segmentation results and grading the performance of our automatic approach.

This work was supported by PersonalizeAF project. This project has received funding from the European Union's Horizon 2020 research and innovation program under the Marie Skłodowska-Curie grant agreement No 860974.

References

[1] Phang RS, Isserman SM, Karia D, Pandian NG, Homoud MK, Link MS et al. Echocardiographic evidence of left atrial abnormality in young patients with lone paroxysmal atrial fibrillation. Am J Cardiol 2004; 94:511–3.

[2] De Jong AM, Maass AH, Oberdorf-Maass SU, Van Veldhuisen DJ, Van Gilst WH, Van Gelder IC. Mechanisms of atrial structural changes caused by stretch occurring before and during early atrial fibrillation. Cardiovasc Res 2011; 89:754–65.

[3] Reant P, Lafitte S, Jais P, Serri K,Weerasooriya R, HociniM et al. Reverse remodeling of the left cardiac chambers after catheter ablation after 1 year in a series of patients with isolated atrial fibrillation. Circulation 2005;112: 2896–903.

[4] Allessie M, Ausma J, Schotten U. Electrical, contractile and structural remodeling during atrial fibrillation. Cardiovasc Res. 2002 May; 54(2):230–246.

[5] Van Gelder IC, Hagens VE, Bosker HA, Kingma JH, Kamp O, Kingma T, Said SA, Darmanata JI, Timmermans AJM, Tijssen JGP, Crijns HJGM. A comparison of rate control and rhythm control in patients with recurrent persistent atrial fibrillation. N. Engl. J. Med. 2002 Dec.347(23):1834–1840.

[6] Wann LS, Curtis AB, January CT, Ellenbogen KA, Lowe JE, Estes NAM, Page RL, Ezekowitz MD, Slotwiner DJ, Jackman WM, Stevenson WG, Tracy CM, Jacobs AK. 2011 Writing Group Members. 2011 ACCF/AHA/HRS Focused Update on the Management of Patients with Atrial Fibrillation (Updating the 2006 Guideline): A Report of the American College of Cardiology Foundation/American Heart Association Task Force on Practice Guidelines. Circulation. 2011 Jan.123(1):104–123.

[7] Wazni OM, Marrouche NF, Martin DO, Verma A, Bhargava M, Saliba W, Bash D, Schweikert R, Brachmann J, Gunther J, Gutleben K, Pisano E, Potenza D, Fanelli R, Raviele A, Themistoclakis S, Rossillo A, Bonso A, Natale A. Radiofrequency Ablation vs Antiarrhythmic Drugs as First-line Treatment of Symptomatic Atrial Fibrillation. JAMA: The Journal of the American Medical Association. 2005 Jun.293(21):2634–2640.

[8] Cappato R, Calkins H, ChenSA, et al. Updated worldwide survey on the methods, efficacy, and safety of catheter ablation for human atrial fibrillation. Circ Arrhythm Electrophysiol 2010; 3:32–8.

[9] Nademanee K, McKenzie J, Kosar E, et al. A new approach for catheter ablation of atrial fibrillation: mapping of the electrophysiologic substrate. J Am Coll Cardiol 2004; 43:2044–53.
[10] Verma A, Sanders P, Macle L, et al. Selective CFAE Targeting for Atrial Fibrillation Study (SE-LECTAF): clinical rationale, design, and implementation. J Cardiovasc Electrophysiol 2010; 22:541–7.
[11] Lin YJ, Tai CT, Kao T, et al. Consistency of complex fractionated atrial electrogram during atrial fibrillation. Heart Rhythm 2008; 5:406–12.
[12] Sanders P, Berenfeld O, Hocini M, et al. Spectral analysis identifies sites of high-frequency activity maintaining atrial fibrillation in humans. Circulation 2005; 112:789–97.
[13] Verma A, Lakkireddy D, Wulffhart Z, et al. Relationship between complex fractionated electrograms (CFE) and dominant frequency (DF) sites and prospective assessment of adding DF-guided ablation to pulmonary vein isolation in persistent atrial fibrillation (AF). J Cardiovasc Electrophysiol 2011; 22:1309– 16.
[14] Ilker O. Yaz and Sébastien Loriot. Triangulated Surface Mesh Segmentation. In *CGAL User and Reference Manual*. CGAL Editorial Board, 5.4 edition, 2022.

Address for correspondence:
Cristiana Corsi, PhD
DEI, University of Bologna,
Via dell'Università 50, 47522 Cesena (FC), Italy
cristiana,corsi3@unibo.it

Left Atrial Appendage Contraction Analysis: A Preliminary Test on Atrial Fibrillation Patients

Sachal Hussain[1], Matteo Falanga[1], Alessandro. Dal Monte[2], Corrado Tomasi[2], Cristiana Corsi[1]

[1] DEI, University of Bologna, Campus of Cesena, Bologna, Italy
[2] Santa Maria delle Croci Hospital, AUSL della Romagna, Ravenna, Italy

Abstract

In atrial fibrillation (AF), about 80% of the thrombi originates in left atrial appendage (LAA). However, it is still unclear how and to what extent LAA impaired mechanical contraction and the consequent compromised blood wash-out affects thrombogenesis. In this study, we proposed a novel approach to extract the centerline of LAA and defined different contraction parameters to assess the global impact of AF on LAA. Moreover, we also sub-divided the LAA into different regions and then performed regional contraction analysis. Up to now, we have tested this approach on patient-specific dynamic models of LAA, acquired from 5 normal subjects and 5 AF patients. Our algorithm successfully defined the LAA centerline, irrespective of the existence of variable LAA morphologies and with the help of global and regional contraction parameters, the differences in the contractility of LAA in normal and AF patients were demonstrated.

1. Introduction

The left atrial appendage (LAA) is a complicated tubular structure possessing a narrow orifice that connects it to the left atrium body [1, 2]. Furthermore, it carries unique anatomical and physiological properties [3]. In the past it was considered a relatively insignificant structure of cardiac anatomy; more recently, with continued in-depth analysis, the LAA is now considered a predominant location for thrombus development in individuals afflicted with non-valvular atrial fibrillation (AF) [4]. In fact, approximately 90% of the thrombus in AF occurs within the LAA [5]. Patients affected by AF exhibit improper contractility of the LAA, leading to stagnant blood flow within the LAA and increasing the risk of thrombus blood flow, ultimately resulting in stroke [6-8].

Moreover, the in-depth analysis of the contraction of LAA is still missing. Therefore, in this study, we aim to assess the contractility of LAA and to evaluate the differences in contraction between healthy and pathological LAA anatomies. For this purpose, we are proposing a novel approach of extracting the centerline of LAA and with reference to the centerline, we are defining LAA global contraction parameters. In addition, we are dividing LAA into distinct regions and evaluating regional LAA contraction parameters.

2. Material and Methods

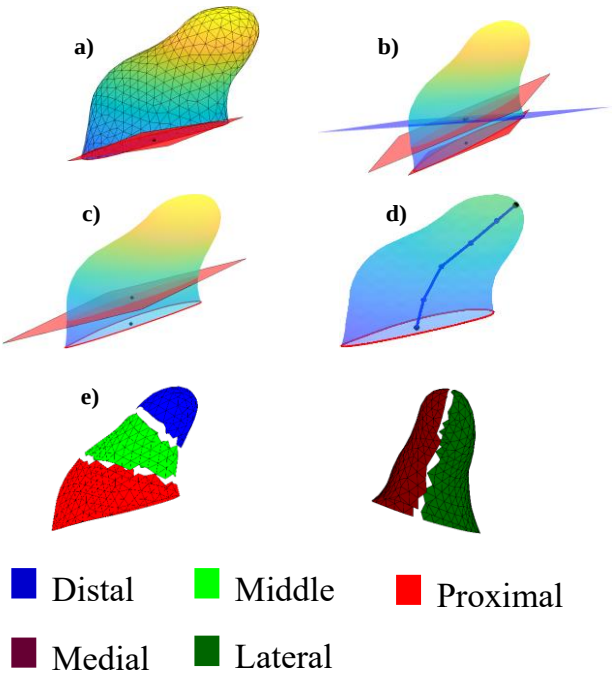

Figure 1: a) LAA surface with best fitting ostium plane (red) and barycenter of ostium (black dot). b) LAA surface with translated ostium plane (red) and newly generated intersecting plane (blue). c) LAA surface with newly generated rotated intersecting plane along with the barycenter of the ostium and the intersecting points (black dots). d) LAA surface with piecewise linear centerline, starting from the ostium barycenter till the tip of the LAA surface. e) (left) subdivision of LAA into 03 regions, (right) subdivision of LAA into 02 regions.

2.1. Dynamic image data acquisition

CT dynamic acquisitions of the heart were obtained for five patients with AF with a control (CTRL) group of five healthy subjects having normal size of heart structures and no previous history of AF.

Volumetric CT images were reconstructed for a total

of 10 phases from ventricular end diastole. Each reconstructed CT volume was 512x512x200 pixels. The voxel resolution was not isotropic: in-plane resolution was 0.39 mm, and through-plane resolution was 1 mm, resulting in a voxel size of 0.39x0.39x1 mm^3.

2.2. Image segmentation

To reconstruct surfaces, the first acquired volume along cardiac cycle was considered. An active contour algorithm was used, which was previously developed in MATLAB environment. For segmentation, an algorithm based on deformable model theory was restricted to LA chamber including LAA only, by defining a region of interest (ROI), and then initialized. Evolution was stopped when deformable surface meets the LA endocardium. The resulted surface in stereolithography format.

In the next step, an affine transformation was applied between ten CT volumes of each dataset. The rigid LA motion was subsequently enhanced by employing a 3D non-rigid registration technique that is founded on the B-spline transformation model [9], utilizing the mean square difference as a measure of similarity. Following the registration procedure, the displacements between frames were implemented on the vertices of the LA surface to reconstruct the LA surfaces along the cardiac cycle [10].

2.3. Post processing of surfaces

Before applying the centreline extraction approach, Laplacian smoothing was implemented on the LA surfaces.

Then the LA appendage, specifically at its orifice, was manually detached from the LA body based on visual observation, taking into consideration the surface's curvature, and incorporating the ridge within the LA chamber (Figure 1a).

2.4. LAA centerline extraction and regionalization

As a first step of LAA centerline extraction method, the best fitting LAA orifice plane was computed (Figure 1(a)). Then this plane was translated in the orthogonal direction to the orifice plane, towards the tip of LAA. As the translated plane intersected the LAA surface, the intersecting points were considered to compute the new barycenter. Using this barycenter and the intersecting points, a new best fitting plane was formulated, having the normal in the direction of previous barycenter and the new barycenter (Figure 1(b)). Then, if the new plane completely intersects the LAA, then the intersection was considered correct and complete. In case of incomplete intersection, a rotation was applied to the plane till the intersection was completed (Figure 1c). Using these intersecting points, the barycenter was computed and considered as one of the points of the centerline of LAA. These steps were repeated till the tip of the LAA was reached and by connecting all the points, LAA centerline was generated (Figure 1d).

After the extraction of LAA centerline, LAA regionalization was applied to explore regional differences. For this step, the LAA surface was partitioned into three regions by splitting LAA centerline into equidistant sections. These regions were named proximal, medial, and distal from the LAA to the tip (Figure 1e, left). Subsequently, LAA was divided into two regions along its longitudinal direction, using the centerline best fitting plane. In this step, the region towards the LA body was identified as the medial region while the region towards the mitral annulus was labeled as the lateral region (figure 1e, right).

To justify that the proposed LAA centerline extraction approach has the capability to work on variable LAA morphologies. This algorithm was tested on the four classical structural morphologies of LAA, presented in the literature [12]. The classification system was based on the shape and structure of LAA and identified them as: “Chicken wing” being the most common (48%), followed by “Cactus” (30%), “Windsock” (19%), and “Cauliflower” being the least common (3%) [13].

2.5. LAA contraction parameters

Standard primary parameters throughout the cardiac cycle were computed to assess LAA function including LAA volume-time curve, LAA ejection fraction (EF), LAA orifice area, LAA centerline length and tortuosity.

To assess regional changes, region-based contraction parameters were defined. For each region, regional radial dimension (RRD) was evaluated, as the average of Euclidean distance of each vertex belonging to a specific region from the centerline; regional radial strain (RRS) was then computed as:

$$\mathrm{RRS(x)} = \frac{\mathrm{RRD(x)} - \mathrm{RRD_{min}}}{\mathrm{RRD_{min}}} \cdot 100$$

where RRD(x) is the current regional radial dimension at the time x and RRD_{min} is the minimum regional radial dimension throughout the cardiac cycle. Once RRS was computed for each region, the global radial strain (RS) was calculated as the average RRS value of medial and lateral at each frame. To compute longitudinal strain, the variation in the length of LAA centerline was traced out throughout the cardiac cycle with reference to the minimum of LAA centerline length, using this formula:

$$\mathrm{LS(x)} = \frac{\mathrm{LAA_{len}(x)\text{-}LAA_{len\_min}}}{\mathrm{LA_{len\_min}}} \cdot 100$$

where $LA_{len}(x)$ is the LAA centerline length at current frame x and LA_{len_min} is the minimum LAA centerline length throughout the cardiac cycle.

Contraction of each region was assessed in terms of regional wall motion (RWM), calculated as the difference between current RRD and minimum RRD for each region.

The index of LAA asynchrony (IA_{RWM}) was computed separately among the three regions and the two regions. Finally, for each surface region, regional peak wall motion was divided by peak regional radial dimension to obtain regional shortening fraction (RSF). RSF was computed for each surface segment and averaged for each subject.

3. Results and Discussion

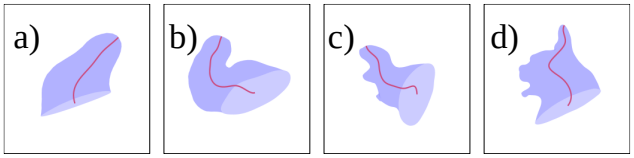

Figure 2: Centerline extraction of variable morphological anatomies of LAA. a) Windsock. b) Chicken wing. c) Cactus. d) Cauliflower.

Anatomical models derived from CT imaging were analysed in 5 healthy subjects and 5 AF patients. The approach was found feasible in all subjects.

Centerline detection in all the four different morphologies of the LAA was successful. In Figure 2 we show an example for each LAA type.

LAA orifice area, RRS and RSF for proximal region demonstrated statistically significant differences ($p<0.05$) between the two groups. However, in this small study, other parameters like global longitudinal strain, global radial strain and IA_{RWM} did not report significant differences. The main findings have been reported in Figure 3.

Among all the parameters, LAA orifice area variation presented statistically significant differences. The median LAA orifice area percentage variation in CTRL group was 59.6% in comparison with 37.1% in AF group ($p < 0.005$) which potentially highlights the disturbed contractility in AF group. It was also seen that the LAA centerline length, LAA orifice area and LAA tortuosity values were higher in the AF group compared to CTRL which showed the existence of dilation and complex morphological behavior of LAAs in AF group. Nevertheless, the differences were found to be not statistically significant.

For region-based analysis, the LAA was subdivided into distinct regions. Nonetheless, only the proximal region showed the significant differences between CTRL and AF groups in terms of RRS and RSF. For proximal region, mean peak RRS in CTRL group was 47.9% while in AF group, it was 20.7% ($p = 0.05$). Similarly, mean peak RSF in the CTRL group was 0.32 and 0.17 in the AF group ($p <0.05$). This assessment strengthens the previous result where dysfunctionality in the contraction of LAA orifice was detected as the orifice is a part of proximal region.

The proposed approach has several limitations, and this is because of the complex, curvy shape of LAA and the existence of high variability in the morphology of the LAA. In some cases, when there exist multiple lobes, the identification of primary lobe can be misleading which generates incorrect centerline and ultimately includes error in the quantification of contractility. In such cases, there is a possibility to manually identify the main lobe and re-generate the centerline, which makes this method semiautomatic.

4. Conclusion

To conclude, the approach presented in this study has

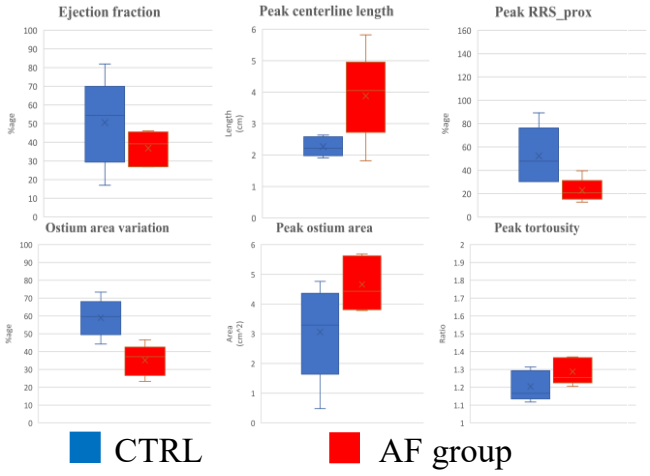

Figure 3: Computed LAA contraction parameters in CTRL and AF group

the potential to extract the centerline of LAA irrespective of the morphological variations in LAA. Furthermore, the proposed LAA contraction parameters have the capability to assess and quantify the global and regional contractility of LAA.

Acknowledgments.

This work was supported by PersonalizeAF project. This project has received funding from the European Union's Horizon 2020 research and innovation program under the Marie Skłodowska-Curie grant agreement No 860974.

References

[1] N. M. Al-Saady, O. A. Obel, and A. J. Camm, "Left atrial appendage: structure, function, and role in thromboembolism," Heart, vol. 82, no. 5, pp. 547–554, 1999, doi: 10.1136/hrt.82.5.547.

[2] S. Saygi, "Atrial fibrillation and the role of laa in pathophysiology and clinical outcomes?," J. Atr. Fibrillation, vol. 5, no. 3, pp. 153–160, 2012.

[3] W. Aschenberg, M. Schlüter, P. Kremer, E. Schröder, V. Siglow, and W. Bleifeld, "Transesophageal two-dimensional echocardiography for the detection of left atrial appendage thrombus," J. Am. Coll. Cardiol., vol. 7,

no. 1, pp. 163–166, 1986, doi: 10.1016/S0735-1097(86)80275-3.
[4] J. L. Blackshear, J. A. Odell, and F. Ed, “Appendage obliteration to reduce stroke in cardiac surgical patients with atrial fibrillation,” 1996.
[5] W. D. Johnson, A. K. Ganjoo, C. D. Stone, R. C. Srivyas, and M. Howard, “The left atrial appendage: our most lethal human attachment! surgical implications,” Eur. J. Cardio-thoracic Surg., vol. 17, no. 6, pp. 718–722, 2000, doi: 10.1016/S1010-7940(00)00419-X.
[6] A. Masci, L. Barone, L. Dedè, M. Fedele, C. Tomasi, and C. P. Bradley, “The impact of left atrium appendage morphology on stroke risk assessment in atrial fibrillation : a computational fluid dynamics study,” vol. 9, no. January, pp. 1–11, 2019, doi: 10.3389/fphys.2018.01938.
[7] R. Beigel, N. C. Wunderlich, S. Y. Ho, R. Arsanjani, and R. J. Siegel, “The left atrial appendage: anatomy, function, and noninvasive evaluation,” JACC Cardiovasc. Imaging, vol. 7, no. 12, pp. 1251–1265, 2014, doi: 10.1016/j.jcmg.2014.08.009.
[8] L. Di Biase et al., “Stroke risk in patients with atrial fibrillation undergoing electrical isolation of the left atrial appendage,” J. Am. Coll. Cardiol., vol. 74, no. 8, pp. 1019–1028, 2019, doi: 10.1016/j.jacc.2019.06.045.
[9] M. Unser, “Splines: a perfect fit for signal and image processing,” IEEE Signal Process. Mag., vol. 16(6), no. NOVEMBER, pp. 22–38, 1999.
[10] A. Masci et al., “A proof of concept for computational fluid dynamic analysis of the left atrium in atrial fibrillation on a patient-specific basis,” J. Biomech. Eng., vol. 142, no. 1, pp. 1–11, 2020, doi: 10.1115/1.4044583.
[11] Autodesk meshmixer, “meshmixer 3.5,” 2018. http://www.meshmixer.com
[12] Y. Wang, L. Di Biase, R. P. Horton, T. Nguyen, P. Morhanty, and A. Natale, “Left atrial appendage studied by computed tomography to help planning for appendage closure device placement,” J. Cardiovasc. Electrophysiol., vol. 21, no. 9, pp. 973–982, 2010, doi: 10.1111/j.1540-8167.2010.01814.x.
[13] L. Di Biase et al., “Does the left atrial appendage morphology correlate with the risk of stroke in patients with atrial fibrillation? Results from a multicenter study,” J. Am. Coll. Cardiol., vol. 60, no. 6, pp. 531–538, 2012, doi: 10.1016/j.jacc.2012.04.032.

Address for correspondence:
Sachal Hussain
DEI, University of Bologna,
Via dell’Università 50, 47522 Cesena (FC), Italy
sachal.hussain3@unibo.it

An Automatic Approach to Define Segmental Regions in Left Atrium in Atrial fibrillation Patients by Including Anatomical Variations in Pulmonary Veins

Sachal Hussain[1], Matteo Falanga[1], Claudio Fabri[1], Cristiana Corsi[1]

[1]DEI, University of Bologna, Campus of Cesena, Bologna, Italy

Background: Unlike the left ventricle, the regions of the left atrium (LA) is still a matter of investigation having the LA attracted the interest of the scientific community only recently. This study sought to define an automatic technique to divide LA into well define standard regions by considering anatomical variations in pulmonary veins (PVs).

Methods and Results: 3D patient-specific anatomical models were derived from CT through an active contour segmentation algorithm. These models represented the domain for segmenting regions. First, the left atrial appendage (LAA) was detected by applying a thresholding approach based on the shape diameter function. Then the algorithm automatically calculated the barycenter of each pulmonary vein and excluded the extra PVs if the number of PVs are greater than four by considering the area of pulmonary vein.
Furthermore, these points were used to detect the roof and the posterior wall. The line connecting the weighted barycenter of the PVs and the center of the mitral valve (MV) was defined as the long axis of the LA. The annulus of the MV was divided into four equal parts allowing to extract four points. The boundaries of the anterior, inferior, lateral, septal regions were detected considering the position of these four points of the mitral valve and of the centers of the PVs. An expert electrophysiologist graded the result of segmented regions as: unacceptable, poor, fair, and good.
We considered 07 atrial fibrillation patients having varied number of PVs (04 -07) and the size and the location of PVs and LAA also varied, but still the algorithm ran on all cases and successfully divided the LA into seven regions. The grading of the expert was fair and good in 3 and 7 patients, respectively.

Conclusions: This proposed approach was effective in dividing the LA into seven standard regions irrespective of the variation in number, size, and location of pulmonary veins. It represents a first step towards the quantification of regional functionality of LA. But further testing is required to confirm these results by including a greater number of atrial fibrillation patients.

Acknowledgment: This work was supported by PersonalizeAF project. This project has received funding from the European Union's Horizon 2020 research and innovation program under the Marie Skłodowska-Curie grant agreement No 860974.

Left Atrial Appendage Contraction Analysis in AF patients.

Sachal Hussain[1], Matteo Falanga[1], Corrado Tomasi[2], Cristiana Corsi[1]

[*] These authors have contributed equally to this work
[1] DEI, University of Bologna, Campus of Cesena, Bologna, Italy
[2] Santa Maria delle Croci Hospital, AUSL della Romagna, Ravenna, Italy

Introduction: Left atrial appendage (LAA) is a small, complex structure connected to left atrium (LA). Irrespective of its size, it keeps significant importance in atrial fibrillation (AF), since about 80% of the thrombi originates within LAA. However, there is a lack of in-depth study of the impact of AF on the LAA contractility and its relationship with the washout effect. In this study, we proposed a method to evaluate the mechanical contraction of LAA on a patient-specific regional basis and correlated it with the blood flow within LAA by performing computational fluid dynamic (CFD) simulations.

Methods: Patient-specific dynamic anatomical models of LA were derived from CT by applying an active contour segmentation algorithm in 5 normal subjects (NL), 5 paroxysmal (PAR) and 5 persistent (PER) AF patients. The LAAs were manually detached from LA chamber (Figure 1(A)). For each LAA, the centerline was automatically extracted (Figure 1(B)) and divided into three equal parts to define proximal, middle, and distal 3D regions (Figure 1(C) – top panel). Furthermore, by considering the position of posterior wall and mitral valve with respect to the centerline, medial and lateral regions were also defined (Figure 1(C) – bottom panel). To evaluate the LAA contractility, we computed changes in LAA ostium area (LAAOA), centerline length (LAA_{len}), LAA tortuosity (LAA_{tort}) as well as several contraction indices including regional strains. Regarding CFD simulations, three cardiac cycles were simulated and only the last one was considered for analysis. To compare velocity values and LAA contraction, the velocity field within the LAA and at its ostium were extracted considering the average of the cardiac cycle.

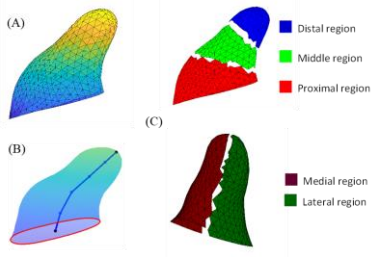

Figure 1: LAA regional division. (A) detached LAA; (B) centerline extraction; (C) automatic detection of 5 volumetric regions.

Results: We found significant differences in peak LAA_{len} ($p=0.01$), and peak LAA_{tort} ($p=0.01$), which were considerably higher in AF patients than in NL. The velocity field at the ostium was significantly higher in NL (average: 0.23m/s) compared to PAR (0.14m/s) and PER (0.13m/s) ($p=0.02$); no significant differences were recorded in the velocity field within the LAA ($p=0.09$). Similarly, the velocity variation at the LAA ostium was higher in the NL group (89%) compared to PAR and PER (74%) ($p=0.02$). The average LAAOA variation was higher in the NL group (57%) compared to PAR (35%) and PER (32%) ($p=0.003$). Importantly, regional radial strain was significantly lower in the proximal region between NL, PAR and PER groups ($p=0.01$).

Conclusions: In this preliminary study, we assessed LAA contraction in NL and AF patients by quantifying global and regional parameters and compared them with blood velocity values within the LAA, obtained from CFD simulations. Compared to NL group, decreased LAA ostium velocities and radial strain values at LAA proximal region together with LAA morphological differences support the hypothesis of a compromised contraction that could explain the increase of thrombogenesis risk in the AF patients. Further analysis in larger groups is required to confirm these results.

7 Appendices

Appendix A: List of submitted papers and attended conferences

A.1: Submitted papers

[1]. **S. Hussain;** M. Falanga; A. Chiaravalloti; C. Tomasi; C. Corsi. Patient-specific Left Atrium Contraction Quantification Associated with Atrial Fibrillation: A Region-based Approach.

[2]. **S. Hussain;** M. Falanga; A. Chiaravalloti; C. Tomasi; C. Corsi. Assessment of Left Atrial Appendage Dysfunctional Contractility in Atrial Fibrillation Patients.

[3]. C. Goetz; L. P. Martinez; E. Invers-Rubio; **S. Hussain;** L. Mont; C. Schmidt; C. Corsi; O. Doessel; A. Climent; B. Rodriguez; U. Schotten; J. Cabrera; A. Loewe; M. Guillem; T. Althoff. Standardized regionalization of the atria for 3D cardiac imaging, electroanatomical mapping and computational modeling – a multidisciplinary consensus of the PersonalizeAF consortium.

A.2: Conference papers and abstracts

[1]. S. Hussain; M. Falanga; C. Tomasi; C. Corsi. Left Atrial Appendage Contraction Analysis in AF patients. CSI Focus LAA 2023.

[2]. S. Hussain; M. Falanga; A. Chiaravalloti; C. Tomasi; C. Corsi. Left Atrial Appendage Contraction Analysis: A Preliminary Test on Atrial Fibrillation Patients. Computing in Cardiology 2023.

[3]. S. Hussain; M. Falanga; C. Fabri; C. Corsi. An Automatic Approach to Define Segmental Regions in Left Atrium in Atrial fibrillation Patients by Including Anatomical Variations in Pulmonary Veins. iHeart MCF 2022.

[4]. S. Hussain; M. Falanga; C. Fabri; C. Corsi. Regional Segmentation of the Left Atrium: A Preliminary Test in Atrial Fibrillation Patients. Computing in Cardiology 2022.

A.3: Award

[1]. Received Best E-poster award for the poster entitled “Left Atrial Appendage Contraction Analysis in AF patients” at CSI Focus LAA 2023.

Appendix B: International research periods

During my PhD, I completed multiple international research periods at different research groups located at the university, hospital, and company. The primary goals of these research works have been shared below.

B.1: IDIBAPS and ADAS3D

At the beginning of April 2022, I started my first research period abroad at IDIBAPS and ADAS3D in Barcelona. One month was spent at IDIBAPS and two months were completed at ADAS3D, which summed up the total duration as three months.

The main aim of this research was to implement atrial regional segmentation on 5 echocardiographic datasets and 5 CT datasets and then to compare the results of regional segmentation in both modalities. After implementing regional segmentation, evaluation, and comparison of the contraction parameters for each region was also planned, as well as comparison between healthy and patient datasets.

However, the primary activities carried out are briefly listed below:

- implementation of atrial regional segmentation methodology
- testing of the developed approach on the data acquired from atrial fibrillation patients
- attended multiple ablation procedures

B.2: Universität Klinikum Freiburg

Starting from December 2022, I spent 02 months at Universität KLINIKUM Freiburg to conduct collaborative research work. During this secondment, the aim was to continue working on the primary goal of my project.

However, the main activities carried out are briefly listed below:

- Testing and validation of atrial regionalization approach.
- Computation of contraction parameters of different regions of the left atrium.
- Establishment of left atrial appendage centerline approach.
- Study of the blood flow velocity and related parameters within the left atrium and left atrial appendage.

B.3: Simula Academy

Near the end of my PhD, I did my last research period abroad at Simula academy, Oslo which lasted for 02 months. During this secondment, the aim was to understand the possibility of integrating the computed left atrium and left atrial appendage contraction parameters in computational fluid dynamic (CFD) model, which was developed at Simula, to perform patient-specific realistic simulation which may further help to understand the thrombogenic events within the left atrium due to atrial fibrillation.

The main activities carried out are briefly listed below:

- CFD simulation of patient-specific aorta model.
- Preprocessing of anatomical models to prepare for simulation.
- CFD simulation of left atrium model using static domain.
- CFD simulation of left atrium model throughout the cardiac cycle using moving domain.

Appendix C: Collaborative research work

Standardized regionalization of the atria for 3D cardiac imaging, electro-anatomical mapping, and computational modeling – a multidisciplinary consensus of the PersonalizeAF consortium

Under the umbrella of MSCA PersonalizeAF project, one collaborative research work was performed to introduce standardized regionalization of atria. The main aim of this study was to establish universal atrial regions which can further be considered for the quantitative regional analysis.

Abstract: 3D imaging and high-resolution electro-anatomical mapping have become an integral part of cardiac electrophysiology and the management of patients with arrythmias. With further technological advances the significance of these modalities continues to grow. Today, the spatial resolution of the various modalities allows for accurate regional characterization of morphological and electrophysiological properties. However, to perform regional quantitative analyses and intra- and inter-individual, as well as cross modality comparisons, a universal definition of atrial regions and their boundaries is required. While for the left ventricle there is already an established standardized regionalization (AHA 18-segment model), albeit not sufficiently precise to allow for reproducible definition of regional borders, there is no consensus for the regionalization of the atria. Here we propose a standardized 15-segment bi-atrial model based on anatomical, electrophysiological, and clinical considerations, with precise definition of regional borders allowing for reproducible and automated regionalization.

Appendix D: Attended workshops and summer schools

D.1: Attended workshops

- “Communicating Scientific Research”, 2021-2022 with 5 credits, Simula Academy, Oslo, Norway.
- “Regulatory Workshop”, January 18-25, 2023, Universita di Bologna, Bologna, Italy.
- “Careers Opportunity Workshop”, May 2-3, 2023, Karlsruhe Institute of Technology, Karlsruhe, Germany, attended remotely.
- “Data Mining and Statistics Workshop” October 26th – November 13th, 2020, Universitat Politecnica De Valencia, Valencia, Spain, attended remotely.
- “Clinical Management of Atrial Fibrillation and Bioengineering Workshop”, January 17th – 25th, 2022, Health Research Institute Hospital La Fe, Valencia, Spain, attended remotely.

D.2: Attended summer schools

- “Cardiac Electrophysiology”, June 27 to July 1, 2022, IHU Liryc, Pessac, France.
- “Fluid mechanics modelling and turbulence”, 2nd to 6th May 2022, Simula Academy, Oslo, Norway.
- “Advanced Signal and Image Processing”, (March – May) 2021, Maastricht University, attended remotely.

D.3: Attended PhD seminar

- "The New Paradigms of soft tissues assessment: medical imaging, machine learning and 3d printing", May 24th, 2021, Universita di Bologna, Cesena campus, Italy.

Appendix E: PersonalizeAF project meetings

- 1st PersonalizeAF meeting, 28th, 29th October 2020, Online.
- 2nd PersonalizeAF meeting, 10th, 11th March 2021, Online.
- 3rd PersonalizeAF meeting, June 28th, 29th 2021, Online.
- 4th PersonalizeAF meeting, January 19th, 20th 2022, Online.
- 5th PersonalizeAF meeting, 4th and 5th July 2022, LIRYC, Pessac, France.
- 6th PersonalizeAF meeting, 16th and 17th January 2023, Universita di Bologna, Bologna, Italy.
- 7th PersonalizeAF meeting, 4th and 5th May 2023, Karlsruhe Institute of Technology, Karlsruhe, Germany, attended remotely.
- 8th PersonalizeAF meeting, 23rd and 24th October 2023, Universitat Politecnica De Valencia, Valencia, Spain.